WILEY-VCH

DOI: 10.1002/ ((please add manuscript number))
Article type: Review

Laser-induced forward transfer: fundamentals and applications

Pere Serra and Alberto Piqué*

Dr. P. Serra
Universitat de Barcelona, Department of Applied Physics, Institute of Nanoscience and Nanotechnology
Martí i Franquès 1, 08028 Barcelona, Spain
E-mail: pserra@ub.edu
Dr. A. Piqué
Materials and Systems Branch, U.S. Naval Research Laboratory, Materials Science & Technology Division
Code 6360, 4555 Overlook Ave, SW, Washington, DC 20375, USA

Keywords: laser-induced forward transfer, laser printing, direct writing, digital manufacturing, additive manufacturing

Laser induced forward transfer (LIFT) is a digital printing technique that uses a pulsed laser beam as driving force to project material from a donor thin film towards the receiving substrate whereon that material will be finally deposited as a voxel. This working principle allows LIFT to operate with both solid and liquid donor films, which provides the technique with an unprecedented broad spectrum of printable materials, and thus makes it very competitive over other digital technologies, like inkjet printing. It is not only that LIFT can access a much wider range of ink viscosities and loading particle sizes; the possibility of printing from solid films allows the single-step printing of multi-layers and entire devices, and even makes possible 3D printing. This versatility translates in turn into a broad field of applications, from graphics production to printed electronics, from the fabrication of chemical sensors to tissue engineering. In this paper an extensive review of the LIFT technique is provided, from its origins to the most recent achievements, focusing on the fundamental aspects of both its working principle and transfer dynamics, as well as on its broad range of applications.

1. Introduction

Around 1439 Johannes Gutenberg developed the first movable type printing press in Europe. The invention represented such a boost in the productivity of written works that it revolutionized the Western World. In a way, we can consider that event as one of the most prominent landmarks in our journey from the discovery of writing to today's knowledge-based economy.

The evolution of the printing industry since the days of Gutenberg is remarkable. In the fifteenth century it took six days for a printing workshop to produce a single copy of a 1,300 pages book (like the famous 42 line Bible), an impressive record compared to the whole year of hard work that a scribe required for the same task before the invention. Today, with techniques such as rotogravure or flexography, we can achieve unprecedented printing speeds of around 500 m/min in an almost completely automatic way. [1] However, it is not all about speed and throughput. One of the most interesting episodes that has taken place in the last decades in relation with printing is its application to commercial areas other than the graphics industry. Since the start of the microelectronics boom in the mid-sixties, [2] until the recent advent of such promising areas as flexible electronics or bioprinting, already existing techniques like photolithography, screen-printing or flexography were successfully adapted to print the materials required by the new applications. [3-10] Ultimately, a device, either electronic or biomedical, comprising a pattern composed of layers of different materials, which in combination provides it with the required functionality can be regarded in essence like a graphic motif, wherein functionality replaces color. We should not be surprised, therefore, that techniques imported from the graphics industry play such a decisive role in the new technological scenario.

The aforementioned printing techniques are well suited for mass production and can operate with flexible substrates, which makes them compatible with roll-to-roll production lines. However, all of them rely on the use of elements like masks, rolls or screens that support the pattern in a permanent way, and which production cost is usually high. This in turn results in high fixed costs prior to the first copy, which makes these techniques impractical for prototyping, low volume orders, and individualization of functional goods. Furthermore, there is a generalized trend today in the manufacturing industry towards the *digital* paradigm, according to which flexible solutions allowing a very fast transition from the idea to the final realization are desired, even for long runs.

Direct-writing techniques, in that they allow printing materials in a serial manner following a pattern previously recorded as a digital file, are much better suited to respond to the requirements of the digital paradigm [11] than the more conventional approaches pointed out above. The list of direct-write techniques is extensive and for further information the reader is directed to several publications including a book on the subject [12] and several more recent review articles. [11, 13] Inkjet printing, though still far from being a serious competitor in terms of market volume before techniques like screen printing, is probably the most widespread direct-writing technique in the manufacture of printed devices. [14] With a long history of development behind, inkjet printing makes patterning possible with high resolution and control in the flexible way pointed out earlier. However, significant constraints concerning the rheological properties of the ink to be used limit the scope of the technique. [15, 16] On one hand, the range of printable viscosities for a given printing head is rather narrow, typically between 1 and 50 mPa·s for most commercial heads, a constraint which usually results in increased costs in the development of new inks. On the other hand, there are also limitations affecting the size of the particles suspended in the ink. It is commonly accepted that $1/100^{th}$ of the output nozzle diameter constitutes the upper limit of the printable particle size, which can easily exclude many functional materials from being printed by inkjet printing. At the same

time, some nanostructured materials, like nanowires, nanofibers, or nanotubes, very promising in many electronic applications, are difficult to process by inkjet printing without altering the aspect-ratios of the dispersed structures that provide them with their unique properties. [17] Aerosol jet printing, one of the strongest competitors of inkjet printing, presents a broader window of printable viscosities (1-1000 mPa·s), but suffers the same restrictions regarding the size of the particles loading the ink. [18] Other direct writing techniques, like dip pen lithography or syringe-based direct writing, [11] offer valuable solutions in particular niches of application, but they seem hardly competitive, especially in terms of speed, at an industrial scale.

Laser-induced forward transfer (LIFT), the aim of the present review, constitutes an additional contribution to the large set of direct writing techniques presented in the previous paragraph. It is a nozzle-free printing technique wherein the driving force for material transfer is laser radiation, and which can achieve printing qualities, resolutions and speeds similar to most of the aforementioned technologies. In contrast to them, though, it presents very few restrictions concerning the rheological properties of the transfer material; in fact, LIFT is capable of printing solid materials and even entire intact devices. The feasibility of the technique has been otherwise extensively proved in a number of applications, ranging from the fabrication of printed electronic devices or chemical sensors, to tissue engineering for regenerative medicine. Although previous revisions on laser direct writing already exist, [19, 20] in this paper we try to provide with a more extensive, comprehensive and updated review of the LIFT technique.

2. Laser-induced forward transfer

Although the first reports on laser printing date back as early as the late 60s, [21, 22] the term LIFT was not coined until 1986, when Bohandy *et al.* investigated the laser transfer of Cu

metal patterns on a silicon substrate. [23] Since then its use and development has grown steadily. LIFT encompasses a broad range of simple yet powerful techniques which employ a pulsed laser to locally transfer material from a source film onto a substrate in close proximity or in contact with the film, thus achieving the laser direct-write of patterns independent of surface type or material form. The source is typically a coated laser-transparent substrate, referred to as the target, donor, or ribbon. Laser pulses propagate through the transparent donor carrier and are absorbed by the film. Above an incident laser energy threshold, material is ejected from the film and propelled toward the acceptor or receiving substrate. Translation of the source and receiving substrate, or scanning and modulation of the laser beam, enables the formation of complex patterns in two- and three-dimensions with speed typically limited by the laser repetition rate. Commercially available, computer-controlled translation stages and/or galvanometric scanning mirrors enable rapid motion and with sufficient precision to generate high-resolution patterns from the individually written voxels that result from the laser transfer process. A schematic showing the basic components of a LIFT system is shown in **Figure 1**. The fact that the laser transfer process does not require the presence of vacuum or use of cleanroom equipment greatly contributes to the technique's great simplicity and compatibility with a wide range of materials and substrates.

From early on, the LIFT technique gained broad acceptance and was used successfully for a wide variety of single element materials, mainly metals such as Cu, [24] V, [25] Au, [24, 26] Al, [27] W, [28, 29] Cr, [30, 31] Ni [32] and Ge/Se thin film structures. [33] Reports of LIFT for oxide compounds such as Al_2O_3, [34] In_2O_3, [31] V_2O_5 [35] and $YBa_2Cu_3O_7$ high temperature superconductors [34, 36] are worth mentioning, although the quality of the transferred ceramics was not as good as those deposited by traditional film growth techniques. In a variation to the basic process, polycrystalline silicon films can be deposited using a hydrogen assisted LIFT technique. [37] More recent examples include transfers of TiO_2-Au nanocomposite films, [38] C

nanotubes for field emitter applications, [39, 40] conducting polymers such as Poly(3,4-ethylenedioxythiophene) (PEDOT) [41] and semiconducting beta-FeSi2 crystalline phases. [42]

The relative simplicity of the laser-induced transfer process has given rise to a large number of variants some of which will be further discussed in this review. One alternative is laser-induced backward transfer (LIBT), wherein the donor film is irradiated directly, either at normal incidence through a transparent receiving substrate [11, 43] or at oblique incidence with flexible receiving substrates, [44] and the irradiated material is propelled in a direction opposite to that of laser beam incidence. This approach is more restrictive and probably more difficult to set up than regular LIFT, but when used for the printing of liquid inks, it has proved very effective for large area and large throughput applications. [44] Another variation from regular LIFT is referred to as film-free laser printing. [45] This approach, which works only with liquid inks transparent to the laser radiation, requires the use of very short laser pulses. However, it allows the transfer to be carried out directly from the ink contained in a reservoir, without the need of having to prepare and then replenish a thin donor film. Film-free laser printing can operate in both forward and backward configurations.

As these works demonstrate, LIFT is able to transfer materials in its solid or liquid phase and this review will cover these variants of LIFT in more detail in the following sections. However, a few variants of LIFT which have been given their own name are worth mentioning. Some of these techniques evolved from the original LIFT concept such as the Matrix-Assisted Pulsed Laser Evaporation-Direct Write or MAPLE-DW. In MAPLE-DW, the material to be transferred is mixed in a laser-absorbent matrix comprising of organic binders or aqueous gels, which are vaporized by the laser during transfer [46] and the laser is used to vaporize the matrix. With MAPLE-DW, the laser printing via LIFT of photolabile materials such as enzymes, proteins, antibodies, cells and bacteria was first reported. [47, 48] For applications in the graphics industry, a process relying on the conversion of absorbed IR pulses into heat by IR-absorbing dyes has been named LAT for Laser Ablative Transfer. [49]

With LAT, the transfer of non-absorbing materials using thermal ablation of an absorbing sacrificial layer (the first demonstration of the use of a dynamic release layer or DRL) was used for the dry, noncontact printing of high-resolution full-color graphics. [50] Another laser-based dry printing technique based on LIFT, known as Laser-Induced Thermal Imaging or LITI was developed for printing conducting polymers for organic electronics. [51] LITI is a thermal transfer process that relies on release/adhesion mechanisms rather than ablation. LITI was further developed by the 3M Corporation for the fabrication of LCD color filters and OLED emitters [52] and beginning in 2000, 3M partnered with Samsung SDI to jointly develop the process for active-matrix OLED (AMOLED) displays. [53] More recently, Sony Corporation developed its own version of LITI, named Laser-Induced Patternwise Sublimation or LIPS, for printing the RGB pixels found in their AMOLED displays. [54]

The implantation of intact polymer molecules using a laser transfer process has been reported by the group of H. Fukumura from Tohuku University. The technique known as laser molecular implantation or LMI is used for the implantation of fluorescent molecules into polymer films at precise locations and depths. [55] In LMI, the laser passes through a transparent polymer serving as the receiving substrate, such as poly(butyl methacrylate) or PBMA, or poly(ethyl methacrylate) or PEMA which is in contact with an absorbing polymer film containing the organic molecules to be implanted, such as pyrene [56] or photochromic molecules. [57] More recently it was reported the laser implantation of coumarin C545 in a process called laser-induced molecular implantation technique (LIMIT) for organic electronics and optical device applications. [58] Both LMI and LIMIT are very similar and their use is limited to applications requiring the implantation of specific molecules on a polymer matrix just below its surface and as such they have not found widespread use.

3. LIFT from solid donor films

3.1 Transfer with phase change

The original work in LIFT by Bohandy et al., used donor films of metals such as Cu subjected to melting and partial vaporization during the transfer process. [24] These early reports relied on a LIFT process based on the phase transformation of the material in the donor layer as it experienced rapid heating prior to ejection and then cooling afterwards. In these cases, the transferred material (typically a metal but also Si and Ge semiconductors) undergoes various changes in phase while its thermal properties drive the LIFT process. For metals, their high thermal diffusivity and short optical absorption depth determines the nature of their interaction with the laser pulse which affects the properties of the resulting transfer. In LIFT of metals, the laser energy is confined at the interface between the donor substrate and the donor film. Above a laser energy threshold, the transfer mechanism can be broken down in four phases: (i) the laser pulse heats the interface of the film at the donor substrate; (ii) a resulting melt front propagates through the film until it reaches the free surface; (iii) at about this time, the material at the interface is superheated beyond its boiling point until, (iv) the resulting vapor induced pressure at the interface propels the molten film forward towards the acceptor substrate. [59] This simple mechanism works well in explaining LIFT of metals with ns laser pulses. For ns and shorter laser pulse-widths, the morphology of the transfers in phase-changing LIFT will vary depending on the donor film thermal diffusion length (L_{th}) and thickness (t) and also on the laser fluence. Two types of ejection mechanisms can be observed: vapor-driven and droplet-mode. [60] Vapor driven LIFT is observed with thicker donor films ($t > L_{th}$) and it results in spreading of the transfer with corresponding degradation in printing resolution at laser fluences higher than the transfer threshold. [27, 61] At fluences near the transfer threshold transfers with resolutions near the size of the laser pulse can be achieved as long as the donor film is not very thick (a micron or less). Droplet-mode LIFT on the other hand can produce transfers with feature sizes smaller than the laser spot, thus

enabling extremely high printing resolutions. [62, 63] Droplet-mode LIFT can be achieved with thin donor films (t ~ L_{th}) and at low fluences and takes place through complete melt-through of the donor film. The surface tension of the molten metal and resulting pressure and temperature gradients result in the formation of a jet of molted material that gives rise to the ejection of droplets. [62, 64] When fs laser pulses are used, the droplet-mode LIFT can be used for printing metal and semiconductor nanoparticles with diameters of a few hundred nanometers. [61, 63] Examples of several transfers illustrating the two types of ejection mechanisms undergoing phase change during LIFT of metal donor films are shown in **Figure 2**a-d. The SEM images illustrate the wide range of morphologies that can be generated by LIFT of metal donor films ranging from explosion-like debris from vapor-driven transfers to single-drop voxels from liquid jet transfers.

It is worth considering the similarities in the evolution of the molten metal jets during LIFT with phase changing materials, i.e. metals, and those observed during LIFT of liquid donor films. Studies of LIFT of 60 nm thick metal donor films using fs laser pulses by Kuznetsov et al., show an expanding bubble of fully molten metal collapsing into two counterjets due to surface tension with a droplet forming at the tip of each jet. [65] At laser fluences below the droplet ejection threshold, the droplet is unable to break away from the jet giving rise to complex 3D structures in the donor substrate as the metal cools down and solidifies as shown in Figure 2e,f. [60, 63, 66] As the laser fluence is increased above this threshold, the droplet from the forward traveling jet breaks free resulting in the transfer of a single spherical particle. [63] If the laser fluence is increased further, multiple molten droplets are generated from the break-up of the bubble. Despite the higher surface tension and lower viscosity of molten metals, as compared to water, the general behavior of LIFT of metals undergoing phase transition is very similar to LIFT of liquid donor films, which will be discussed in more detail in Section 4 of this review.

3.2 LIFT of nanoparticles

In the previous section it has been stated that nanoparticles printing from solid donor films could be achieved in droplet-mode LIFT. Such nanoparticles are in fact nanodroplets from melted donor material that re-solidify upon contact with the receiving substrate. Since droplet-mode LIFT makes possible the transfer of feature sizes smaller than the laser spot, sub-micron resolutions are attained through tight focusing of the laser beam, close to the diffraction limit of the optical focusing system, and through the use of very thin donor films, as already pointed out. The first results on nanoparticles printing through LIFT were obtained by means of femtosecond excimer irradiation and they corresponded to Cr [31] and Pt [43] nanodroplets. Soon after, and through the use of different laser sources and pulse durations, other works on metallic nanodroplets formation followed: Al, [67] Cr, [64] Cu [61] and Au, [68, 69] this last also through LIBT.

The production of metallic nanodroplets has been usually attributed to a capillary-driven phenomenon (droplet-mode LIFT). In fact, the presence of bumps and re-solidified jets found in the donor film after transfer seems consistent with that interpretation (**Figure 3**). [62, 66, 67, 70-72] However, some authors remarked the presence of distinctive craters left on the donor film during nanodroplets printing that rather suggest the occurrence of some vaporization, a situation closer to the vapor driven mode of LIFT described in Section 3.1. [31, 43, 61] Banks *et al.* have noted that both mechanisms are not incompatible with one another: [64] at low laser fluences the droplet-mode would be activated, while at high fluences vaporization would take place. In fact, vaporization is consistent with jetting and droplet ejection, as it has been extensively proved in the LIFT of liquid donor films (Section 4.1-4.3); strong evidence for that was provided by Kuznetsov *et al.*, [65] as mentioned in the previous section (see Section 4.2 for details about the jetting dynamics). Although time-resolved imaging analyses have been carried out, the extremely small dimensions of the ejecta make them hardly conclusive:

at laser fluences just above the threshold for nanodroplet formation a jetting-like dynamics resulting in single droplet emission seems apparent, [73, 74] though this does not allow to discriminate between the two possible mechanisms.

The production of metallic nanoparticles through LIFT is being explored for the fabrication of printed metal circuits [73] and vias, [75] and very especially for micron-scale 3D printing (Section 5.5). [76-78] Through the combination of pre-structured Au films and LIFT the production of large-scale nanoparticle arrays has been proved feasible, [79] very interesting in sensing applications. In addition to metals, semiconductors have also been used for nanoparticles production through laser printing, also with great potential in future applications. Indeed, the electric and magnetic dipole resonances within the visible spectral range of Si nanoparticles, alongside their low optical losses, provide these structures with unique optical properties that make them very interesting for the fabrication of metasurfaces, for example. LIBT has been successfully used to produce Si and Ge nanodroplets from bulk semiconducting targets, [80] and with Si-on-insulator targets it has been possible to attain particle diameters in the range 100-200 nm. [81]

3.3 Transfer without phase change

For certain applications, the donor material must not undergo melting or vaporization during the LIFT process. This is the case for donor films comprised of single domain or single crystal structures or containing oriented pre-structured layers. In these situations, LIFT must be performed without changing or damaging the donor film in order to preserve their structure after transfer. One way to accomplish this is by using intermediate layers between the laser pulse and the material to be transferred. This approach is described in the next section. In some cases, however, it is possible to transfer the donor film intact in its solid phase. For example, by using multiple, sub-threshold fs laser pulses it is possible to cause the

incremental delamination of the solid donor film from the donor substrate. The reproducibility of this technique, named ballistic laser assisted solid transfer or BLAST, improves by using spatially-shaped laser pulses with a higher intensity profile along the perimeter of the transfer [82] or by pre-patterning the edges of the transferred region in the donor substrate. [83] The former approach was used for transferring Cr disks without melting, while the later was applied to the transfer of pre-machined (using focused ion beam milling) 5 and 10 micrometer diameter ZnO disks. In later reports, the BLAST technique has been used to laser transfer other solid ceramics such as Y-Fe garnet. [84]

LIFT of solid donor films has also been reported using fs laser pulses for the transfer of bismuth selenide, lead zirconate titanate and Terfeneol-D, although details on the morphology of the transferred materials were not provided other than sorting them as "intact" versus "molten" or "fragmented" as a function of laser pulse intensity. [85] The same group later reported LIFT of solid films using ns laser pulses of three types of chalcogenides: bismuth selenide (Bi_2Se_3), bismuth telluride (Bi_2Te_3) and bismuth antimony telluride ($Bi_{0.5}Sb_{1.5}Te_3$). The films were LIFTed onto polymer-coated glass substrates to prevent fracture of the soft chalcogenide films upon landing on the receiving surface. [86] The thermoelectric properties of the transferred films were about 25% lower than their initial values, indicative of some damage sustained during the laser transfer process.

LIFT of organic semiconductors such as PEDOT:PSS and photodefinable polymers such as photoresists provide a further example of solid materials whose films are unable to sustain phase change during transfer. In the case of PEDOT:PSS the use of spatially shaped ns laser pulses with higher intensity along the edges of the transferred voxel has been reported. [87] For the transfer of photoresist films (Shipley 1818), a multilayer stack comprising of the photoresist and a layer of dried but not sintered silver nanoparticles was LIFTed successfully without damage as **Figure 4**a shows schematically. [88] The transfer of intact solid multilayers by LIFT, confirmed by cross sectional analysis as shown in Figure 4b, exemplifies the utility

of transfers without phase change or excessive heating, which would damage the interface and integrity of the multilayer. In this example of LIFT of solid multilayers comprising photoresist/silver nanoparticles, the printed voxels were used to fabricate functional capacitors after transferring over a metal coated receiving substrate. In this case the photoresist layer functioned as the dielectric and the silver nanoparticle layer served as the top electrode for planar capacitors as shown in Figure 4c,d.

3.4 LIFT with a dynamic release layer

In the case of carrying out LIFT with transparent materials, or materials sensitive to the laser radiation, the donor substrate is usually pre-coated with an absorbing, sacrificial layer, commonly known as *dynamic release layer* (DRL). The DRL, intermediate between the donor substrate and the donor film, is responsible for absorbing most of the laser intensity, and provide upon vaporization the thrust required to propel a fraction of the donor material towards the receiving substrate. The first use of a DRL did not exactly correspond to LIFT, but rather to LAT (Section 2), aiming at the production of high-resolution color images; [50] the principle of operation is, nevertheless, essentially the same. Now the use of DRLs in LIFT is practically ubiquitous.

The simplest DRL is possibly a metallic thin film. Quartz and glass substrates are easy to metallize with coatings around 50-100 nm thick of different materials: Ti, Au, Pt, Cr. Being metals strongly absorbing to most laser radiations, such thicknesses are usually larger than the radiation penetration depth, and therefore guarantee that practically no radiation reaches the donor film. The first true work on LIFT using a metallic DRL corresponded to the transfer of phosphor powders by means of an Au DRL for the fabrication of phosphor screens. [89] Although the LIFT of solid donor films is feasible with metallic DRLs, these are, however, more commonly used with liquids, as it is described in detail in Section 4.4.

The most common DRL in the LIFT of solid donor films is the photodecomposing triazene polymer (TP). TP is a polymer that contains aryl-triazene chromophores, with high absorption peaks at several common laser wavelengths (Nd:YAG 266 and 355 nm, and XeCl 308 nm). [90-92] Among these, XeCl radiation is probably the most popular in LIFT: TP presents a well-defined ablation threshold at that wavelength, and its surface appears free from carbonization after ablation. [93] Upon irradiation, the TP-DRL (typically a few hundreds of nm thick) decomposes into volatile products that push away the donor material in the irradiated spot, leading to its delamination and further transfer (**Figure 5**a-c). [94-96] According to this ejection mechanism, the voxel (called *flyer* in this context) suffers no phase change during transfer, as it corresponds to the instances described in the previous section. Thus, the DRL protects the donor material from the incident laser radiation while minimizing any contamination issues: in contrast to metallic DRLs, where some ablation debris is always transferred with the voxel, the volatile character of the TP decomposition products allows the spontaneous elimination of the DRL residue. [97] However, the use of TP-DRLs has a side-effect, the formation of a shock wave associated with the vaporization of the polymer. This shock wave, that travels at a faster speed than the flyer, after being reflected back by the receiving substrate can interact with the propagating flyer and destroy it. [98-100] Such detrimental effect can be mitigated through operation with small donor/receiver gaps or in a reduced pressure atmosphere. [101] The influence of the process parameters in the TP ablation behavior and the dynamics of the laser-generated flyer have been investigated in detail. [102-105]

The particular transfer mode of LIFT with a TP-DRL makes this approach especially suited for printing fragile materials or materials with a complex stoichiometry that would be irreversibly altered under a phase change. Thus, complex oxides like $Gd_3Ga_5O_{12}$ [106] or $Ca_3Co_4O_9$ [107] have been successfully transferred through the use of a TP-DRL. Similarly, with the aim of being used in sensing applications, different polymers have also been printed through the same strategy: polyisobutylene, [108, 109] polyethylenimine, [108, 110]

polyepichlorhydrine. [111] Even microarrays of polystyrene microbeads have been deposited by means of a TP-DRL (Figure 5b), showing that through this method no specific immobilization process was required. [112, 113] Yet TP-DRLs are not only interesting for printing complex materials. It has been shown that in some instances the approach can present some advantages over direct LIFT in the printing of simple metals: clear-cut edges, and absence of traces of splashing or debris outside the pixel area. [94, 95] Nevertheless, it is in the printing of multilayer stacks and entire devices where LIFT with a TP-DRL reveals all its power; these instances are described in detail in Section 5.1.

4. LIFT from liquid donor films

4.1 Droplets printing

Since the pioneering works of Bohandy and co-workers [23, 24, 59] it was clear that material transfer was possible in the liquid state. In fact, they proved that the portion of solid donor film irradiated by the laser beam was melted under the action of the laser pulse, and that it was that molten fraction which was ejected towards the receiving substrate, where it was finally deposited as a pixel of re-solidified material (the mechanisms responsible for this transfer mode are described in detail in sections 3.1 and 3.2). However, some years later A. Piqué and co-workers [114] demonstrated that printing was also feasible from liquid donor films, and that under that mode of operation the transferred material remained in the liquid state along all the stages of the process, from its removal from the donor film until its deposition on the receiving substrate. The finding was remarkable in that it paved the way to an even broader range of possibilities for the LIFT technique, making it closer to more conventional printing techniques, like inkjet printing, for example.

The mode of operation for LIFT with liquid films (**Figure 6**) is practically identical to the one with solid films, with the main difference – aside from the physical state of the donor, of course -that the thickness of the donor film is larger, typically between 1 and 100 μm. The laser beam is focused at the interface between the liquid donor film and the transparent donor substrate, and under the action of the laser pulse a tiny fraction of liquid is removed and transferred onto the receiving substrate, where it is deposited as a sessile droplet (**Figure 7**). [115-122] In contrast to the LIFT of solid films, in this case the printing outcome is a 'liquid pixel', not substantially different from that of an inkjet printing event. The strategy to print a pattern of a given material can be, therefore, the same: an ink is prepared by suspending or dissolving the material in an appropriate solvent, to be later transferred by means of LIFT droplet by droplet. Once the ink has been deposited, the drying of the solvent results in a printed pattern of the material of interest. As with inkjet printing, continuous lines and areas can be achieved through proper droplet overlap (**Figure 8**) and, accordingly, any two-dimensional pattern printable with that technique can also be realized through LIFT.

The main advantage of the LIFT of liquids over other more conventional direct writing techniques, like inkjet printing or even aerosol jet printing, is that LIFT is nozzle-free, and therefore presents very few restrictions concerning the viscosity of the ink [123] or the size of the particles suspended in it. [124] In fact, viscosities as high as tens and even hundreds of Pa·s, well above the upper limit of aerosol jet printing, have been successfully printed through LIFT. [125-130] Similarly, inks with loading particle size clearly beyond the limits of the aforementioned techniques are also perfectly printable through LIFT. [131-133] Both instances are extremely interesting from a technological point of view. On one hand, the possibility of printing high viscosities allows working with conductive inks of high solid content, very interesting for printed electronics applications due to the resulting low sheet resistance of interconnects (section 5.1), as well as with alginate-based solutions, essential in tissue engineering applications (section 5.4). On the other hand, the tolerance of LIFT with

relatively large particle sizes allows printing nanostructured materials like nanotubes, nanofibers, nanorods or graphene, all of them of great interest in several applications, like in the manufacturing of printed sensors (section 5.3).

The dimensions of the droplets printed through LIFT can be easily controlled by adjusting the different process parameters (laser fluence, beam diameter, donor film thickness), and strongly depend on the composition of the ink, as well as on the nature of the receiving substrate. For the same ink/substrate combination, LIFT can achieve minimum droplet diameters similar to, and usually smaller than, those attained with inkjet printing. Through the proper tuning of the laser parameters, droplet volumes as small as 10 fL have been obtained, which resulted in diameters below 10 μm. [119, 134] A detailed description of the evolution of the droplets size versus the different process parameters requires, however, some insight on the physical mechanisms responsible for material transfer.

4.2 The jetting dynamics

Time-resolved imaging has been revealed as a powerful instrument for the investigation of the LIFT of liquid donor films since the early days of the technique. [135-137] Through stroboscopic strategies it is possible to easily attain time resolutions of the order of tens or hundreds of nanoseconds, which are enough to track the entire evolution of the ejected liquid, from a few instants after laser pulse absorption in the donor film, to sessile droplet deposition in the receiving substrate is complete.

Although the liquid transfer can proceed through a series of different routes, the most common scenario that leads to the printing of uniform circular droplets is probably the one delineated by Duocastella et al. (**Figure 9**). [138-140] The absorption of the laser pulse energy in the donor film results in the formation of a high-pressure bubble in the liquid, which expansion and further collapse leads to the generation of a thin, long and stable jet that

propagates away, towards the receiving substrate. The contact of the jet with that substrate sets the starting point of droplet formation: the jet feeds continuously the growing droplet until the onset of a Plateau-Rayleigh instability leads to the jet breakup, and thus to the end of the process. Typical jet front speeds range between a few m/s and several hundreds of m/s, and jets can attain significant aspect ratios of around 1000 along their propagation (widths of a few microns versus lengths of a few millimeters). [140-142]

The mechanism responsible for the jetting dynamics is essentially the same as that of the evolution of a bubble generated close to the free surface of a liquid, a typical problem in fluid mechanics which has been analyzed both experimentally [143-145] and through numerical calculation. [143, 146, 147] In the case of LIFT there are a few differences, though, all of them arising from the presence of the rigid donor substrate adjacent to one side of the laser-generated bubble. The donor substrate thus prevents expansion in that direction, so that the bubble only expands laterally and towards the liquid free surface (**Figure 10**a). This results in the onset of a pressure gradient in the liquid surrounding the bubble, between its sides and its pole (it is much easier for the bubble to displace the thin liquid film on top of it than all the liquid around it), that drives liquid along the bubble walls and towards the pole. The induced streamlines converge in a stagnation point in the pole, where the high pressure is released through the ejection of two liquid jets: the jet responsible for droplet deposition, propagating away from the donor film, and a re-entrant jet (the so called counter-jet), propagating towards the donor substrate surface (Figure 10b). [148] While the contact of the jet with the receiving substrate leads to the formation of the sessile droplet that ultimately becomes the printed pixel, the impact of the counter-jet with the donor substrate just results in the fast dissipation of its kinetic energy. [149] Eventually, the re-expansion of the laser-generated bubble after collapse can lead to the formation of a second jet that would also contribute to the printed droplet (see section 4.5 for more details). [141, 144, 150]

The mechanism described in the previous paragraph is not the only one that can result in the printing of well-defined droplets through the LIFT of liquid donor films. For small enough donor-receiver gaps it is possible for the expanding bubble to impact the receiver substrate before the jet can be developed (**Figure 11**). [129, 151, 152] In this case, liquid transfer proceeds during the direct contact of the bubble with the substrate; once in contact, the bubble gradually deflates until a relatively thin neck is formed, which finally breaks up, again through the onset of a Plateau-Rayleigh instability. In fact, the perimeter of the bubble contact line with the receiving substrate is in general larger than the dimensions of the droplet that would result through jetting under identical irradiation conditions. However, the final droplet size is usually not so different: the deposited liquid shrinks during transfer so that the resulting sessile droplet is confined in a smaller area. [151]

4.3 Role of process parameters

The evolution of the droplets diameter versus laser pulse fluence reveals that there always exists a range of fluences leading to the formation of uniform circular droplets. [118, 121, 139, 153] It is also observed that there is a fluence threshold below which no deposition takes place, and that above a certain value satellite droplets and splashing occurs, which compromises the definition of the printing outcome (**Figure 12**). The correlation of the printing results with time-resolved images of the transfer dynamics allows identifying the onset of splash with that instance wherein the pressure inside the laser-generated bubble is so high that it bursts before a jet can be developed. [139] In other words, the internal pressure can no longer be counterbalanced by the external pressure plus the capillary forces, thus leading to the rupture of the bubble wall. However, the correlation of the transfer dynamics with the fluence threshold for deposition is not so straightforward. In fact, that threshold does not exactly correspond to the threshold for bubble formation. It is observed that there are situations

wherein a bubble is generated in the liquid donor film, but there is no deposition of material at all. In those instances, a jet develops and starts to advance towards the receiving substrate, but gradually slows down and recoils pulled back by capillary forces before contact can take place. This threshold is obviously strongly dependent on the gap between donor and receiving substrates.

The size of the printed droplets is always found to increase with laser fluence, which allows the easy tuning of the dimensions of the printed pixels. [118, 121, 139, 153] However, there is no uniform trend (**Figure 13**). Thus, for aqueous solutions of glycerol printed on glass a linear increase of the droplets volume with laser fluence has been usually encountered. [118, 139, 154-157] However, for Ag nanoparticle inks, the linear evolution versus laser fluence has been found for the droplets diameter (instead of the volume) when printed on SiO_2 on Si, [121] but the behavior becomes clearly non-linear when printed on polyethylene terephthalate. [120] In view of the jetting dynamics characteristic of the LIFT of liquid donor films, it should not be surprising that the amount of transferred material is dependent on the receiving substrate composition: in contrast with other techniques, like inkjet printing, liquid deposition in LIFT proceeds through contact of the emitted jet with the receiving substrate, so that the interaction between both can play a decisive role in the onset of jet breakup that ultimately determines the final amount of deposited material. [158]

Another relevant consequence of the jetting dynamics, and in particular of the extreme stability and aspect ratio of the generated jets, is the relatively large tolerance gaps between donor and receiving substrates (Figure 13). [120, 155] Uniform droplets can be printed at gaps ranging from a few microns up to a few millimeters, with practically no variation in droplet size. This is especially interesting from an industrial point of view, where tolerances as large as possible are required in order to avoid contact between donor and receiver (gaps of some hundreds of micron are usually acceptable); in particular, this issue becomes crucial in roll-to-roll manufacturing, where high winding speeds can be attained.

Printing speed is always an important aspect in the setting up of any direct-writing technique, and LIFT is not an exception. The combination of both laser repetition rate and the speed of relative translation of the donor/receiver system respect to the laser beam determine the resulting printing speed in a LIFT setup. Commercially available lasers can easily deliver pulses at repetition rates of several MHz, and through galvo-scanners and polygon mirrors it is possible to deflect the laser beam at speeds of hundreds and even thousands of m/s. [44, 159, 160] These characteristics make LIFT a really competitive direct-writing technique in terms of speed. There is, however, one issue related with the jetting dynamics that requires some attention here. At laser repetition rates higher than some tens of kHz the time delay between two consecutive laser pulses can be shorter than the lifetime of the liquid jet, which on average is around 100 μs. Depending on the separation between the adjacent jets (determined by the scanning speed) these can interact with each other, which can compromise the printing outcome. [44, 161] Two different mechanisms of jet-jet interaction have been identified. The mildest one corresponds to the tilting of the jet propagation direction induced by the capillary wave generated in the liquid donor film by the preceding neighboring jet. [162] At irradiation conditions leading to the formation of prominent bubbles, though, a second and stronger type of interaction can take place: the collision of the two (or more) adjacent bubbles during their expansion, which results in the total alteration of the jet propagation dynamics and which can lead to completely unpredicted printing outcomes. [161, 163] In consequence, these issues need to be taken into account in the preparation of the printing layout under very high speed operation.

4.4 LIFT with an absorbing layer and Blister-actuated LIFT

In the preceding paragraphs it has been implicitly assumed that laser radiation absorption took place in the liquid donor film, in a thin layer adjacent to the donor substrate-film interface

(**Figure 14**a). However, not all of the inks of interest for printing purposes are absorbing to the applied laser radiation, and it is not always possible to find a laser wavelength that matches the absorbing properties of the ink. Furthermore, in many instances it can be interesting to use the same laser for printing very different materials, with different absorbing properties each. In order to overcome those difficulties, a DRL can be used in the same way as described for solid donor films in Section 3.4. The sacrificial DRL, usually a solid film that coats the donor substrate, absorbs the laser radiation, which results in the vaporization of the irradiated fraction of the layer, and which in turn provides the donor liquid with the thrust required for transfer (Figure 14b). [164] From this moment on, liquid ejection proceeds as described in Section 4.2, through bubble expansion and jet formation, until the contact of the jet with the receiving substrate leads to the formation of the sessile droplet. Several different materials have been used as DRLs since the early days of the LIFT of liquid donor films, from gelatin [116] to different metals (the most common option), like titanium [165-167] or Ag. [168] Although the removal of the DRL inevitably results in some residue on the receiving substrate, [169] this usually constitutes a minute fraction of the printed material, and in most instances no detrimental effects have been observed on the functionality of the deposits. Explosive polymers, like TP (Section 3.4), have also been used as DRLs for liquid films, [94, 170, 171] although not so extensively as metals.

Aside from its use with non-absorbing liquids, it has also been claimed that using DRLs could be beneficial even for absorbing inks. Remarkable differences in the transfer of conductive inks have been observed when comparing LIFT performed with and without a metallic DRL. [120, 121, 142] Results from different studies demonstrate that the use of a DRL allows a better control of the printing process: the range of laser fluences leading to circular droplets without splashing or satellites is sensibly wider than when LIFT is carried out directly, without a DRL. In addition to the described performances, DRLs are useful to shield sensitive materials in the ink from laser radiation. However, they cannot completely protect those materials from heat:

though for most inks this is not an issue, the vaporization of the absorbing layer has the potential to damage very delicate materials. In this regard, *blister-actuated LIFT* (BA-LIFT) emerges as an alternative approach to LIFT with conventional DRLs that allows mitigating any thermal or optical effect on the transferred ink. [153, 172] BA-LIFT uses a much thicker (~1-10 μm) polymer layer than most conventional metallic DRLs (usually tens on nm thick) for transfer. Though apparently insignificant, the difference is remarkable, since the liquid ejection mechanism in this approach is substantially altered compared to the previous case. Upon ablation of the irradiated portion of the polymer film, the expansion of trapped gasses results in a blister on the polymer layer that converts the chemical energy released during laser ablation into a mechanical impulse that propels the ink (Figure 14c). Since there is no material from the polymer layer released into the ink, there is no contamination by ablation products, and the DRL in turn fully shields the ink from laser light and heat.

Time-resolved imaging has revealed that no cavitation bubble is generated in the liquid donor film during BA-LIFT. [148, 173] The absorption of the laser pulse energy in the polymeric DRL results in the decomposition of the polymer into diverse gaseous species. These remain confined between the intact portion of the film and the glass substrate, which leads to the buildup of the pressure at the interface, and finally to the release of that pressure though the deformation of the DRL into a blister. For the correct operation of BA-LIFT it is essential that only a fraction of the DRL is ablated, while the remaining layer stays intact. In order to achieve this, the penetration depth of the laser into the polymeric DRL must be smaller than the total thickness of the film. In spite of the obvious differences between BA-LIFT and conventional LIFT (either with or without DRL), the following stages of liquid transfer are surprisingly similar. The expansion of the laser-produced blister displaces the ink away from the donor film, following a jetting dynamics almost identical to that found in the conventional LIFT of liquid films, so that droplets printing again proceeds through the contact of the jet with the receiving substrate.

BA-LIFT is not only interesting for printing delicate materials, as it has been demonstrated, [153, 172] but also for more fundamental reasons. The absence of cavitation bubble in the donor liquid substantially simplifies the analysis of the liquid transfer dynamics during LIFT. The deformation of the blister can be modelled from empirical data in a quite straightforward way, and that information can be introduced in a finite element code that allows reproducing the jetting process with very good agreement with the experimental results. [174-176]

4.5 Film-free laser printing

Film-free laser printing (FF-LIFT) consists in a LIFT-based approach to liquids printing which allows eliminating the need for the preparation of the donor material in thin film form. Although there exist a number of well-established technologies for the preparation of liquid donor films (blade, bar, spin coating), in some instances this task can result substantially challenging due to the inherent instabilities of liquid films. FF-LIFT is capable of depositing liquid directly from a reservoir. [45, 177-181] This is achieved through the tight focusing of a laser beam underneath the free surface of the liquid, so that the absorption of the laser pulse energy inside the ink provides the thrust required for material ejection. The receiving substrate must then be placed in close proximity to the donor free surface, in such a way that allows collecting the propelled liquid as an individual sessile droplet. Two different configurations can make this possible: inverted or forward configuration (**Figure 15**a) and upright or backward configuration (Figure 15b). For this approach to work, though, the laser pulse energy needs to be absorbed just in a tiny volume around the beam focus, with no significant absorption in the rest of the liquid. This imposes certain restrictions on the optical properties of the liquid to be printed and/or on the laser to be used which need to be carefully addressed.

FF-LIFT relies on the generation of a cavitation bubble by laser irradiation at the appropriate depth beneath the free surface of the donor liquid. For this to occur, the ink needs to be highly

transmissive at the applied laser wavelength, otherwise the laser pulse energy is absorbed all along the beam path inside the liquid, and not just at the chosen position below the free surface. Provided that the laser intensity around the focal point is high enough, the threshold for optical breakdown can be overcome at that position, resulting in the formation of a confined hot plasma whose expansion induces the generation of a cavitation bubble. [182-185] This requires attaining very high radiation intensities in the focal point, usually well above 10^{12} W/cm^2, which can be achieved through the tight focusing of the laser beam and through the use of very short laser pulses (subpicosecond). This last condition allows promoting the onset of non-linear absorption mechanisms in the ink (multiphoton absorption and impact ionization), [45, 185] which result in the sharp threshold necessary to grant absorption just at the desired position within the liquid. The further evolution of the as-formed cavitation bubble, including its initial growth and final collapse, induces fluid flows that can ultimately lead to the generation of the outward propagating jets required for printing. Indeed, it has been shown that for standoff distances (non-dimensional parameter corresponding to the depth below the free surface at which the bubble is generated over the maximum radius that it attains along its expansion) between 0.3 and 0.8, liquid is ejected in a jetting dynamics almost identical to that of conventional LIFT (Figure 15c). [143, 144, 146, 180] The two configurations described in the preceding paragraph, forward and backward, allow collecting the liquid displaced by the laser-induced jet.

It is worth asking which configuration is the most suitable to implement, forward or backward? There is no definitive answer, though; each of them has its own advantages and drawbacks. The forward configuration, closer to the traditional scheme of LIFT, can operate with opaque and patterned receiving substrates, while the use of the backward configuration is restricted to flat transparent substrates. However, in that the optical path inside the liquid is usually much longer in the forward mode, this is more prone than the backward configuration

to spherical and chromatic aberrations that can result in 'longer' focal points and pulse durations, and which can make the process more difficult to control.

The need to operate with transparent and weakly absorbing liquids also imposes certain restrictions on the materials which can be printed through FF-LIFT. For example, the most widely used ink in printed electronics applications, Ag conductive ink, cannot be printed with this technique. Similarly, other inorganic inks of diverse functional materials, either conductive or dielectric, are not printable through FF-LIFT. However, there are other applications which FF-LIFT is especially suited for. One potential niche market is the printing of biological materials, which are usually found in aqueous solutions and suspensions, and which are therefore transparent to most popular laser wavelengths. Thus, it has been proved that the technique is feasible for printing biomolecules like DNA and some proteins, [177, 178] and therefore for biosensors fabrication (Sections 5.2 and 5.3), and more recently it has been shown that FF-LIFT is especially suited for printing living cells for tissue engineering applications [186] (Section 5.4). Another set of materials very attractive to be printed with the film-free approach are optical grade adhesives, normally used in the fabrication of micro-optical components. [158, 187]

4.6 Congruent LIFT

LIFT of donor films comprising suspensions with a wide range of viscosities enables extending the capabilities of the technique beyond the printing of low viscosity fluids and/or suspensions, as already pointed out in Section 4.1. This means that LIFT can be used to print suspensions with a wide range of medium (~ 0.01 Pa·s) to very high (> 100 Pa·s) viscosities (designed for applications such as screen printing or stenciling) and do so with higher voxel resolution than these techniques can achieve. [188] Furthermore, by using higher viscosity suspensions, the size range of laser transferable particles is significantly broadened from

nanometers to tens of microns. [189] The ability to print high viscosity suspensions allows LIFT to be used to print commercially available screen printable pastes, [190, 191] as well as custom prepared and highly inhomogeneous mixtures of various materials in solid form with polymer binders suspended in an organic electrolyte as those found in Li-ion battery electrodes. [192]

When LIFT is used to transfer high-viscosity nanopastes, it is possible for the printed voxel to match congruently the illuminating laser pulse, a process referred to as laser decal transfer or LDT. [193, 194] This LIFT mode offers a unique approach to direct-writing techniques in which voxel shape and size become controllable parameters, allowing the non-lithographic generation of thin film-like structures. The ability to adjust or entirely change the size and shape of a voxel according to the desired final pattern allows for the formation of complex structures in one single transfer step, reducing the processing time as well as avoiding problems related to the merging of multiple voxels, which is prevalent with inkjet. [195] Nanopastes tailored for screen-printing have been used to achieve congruent LIFT, as reported by various groups. [196, 197] These results were obtained using a silver nanopaste manufactured by Harima Chemicals (NPS Series). [198]

It is useful to compare features produced by LIFT of low-viscosity (0.01 Pa·s) silver nanoink and high-viscosity (100 Pa·s) silver nanopaste using square, rectangular, and gridded beam spatial profiles (**Figure 16**). [199] As the figure illustrates, only the high-viscosity paste produces a square-shaped voxel from a square beam profile (Figure 16d) and a sharp-edged line from a rectangular beam profile (Figure 16e). In Figure 16c, a grid feature was laser-printed with multiple voxels of low-viscosity nanoink, while a single (gridded) voxel of nanopaste was used in Figure 16f to print the entire grid with one laser shot. The clean and sharp overlap at the line intersections in Figure 16f, compared to Figure 16c, demonstrates the advantages of using high-viscosity nanopastes for the transfer of arbitrarily shaped voxels.

Time-resolved analysis of LIFT of high viscosity silver nanopastes have shown the transfer mechanism to be very distinct than that of low viscosity inks and fluids. Using still frames

obtained from a high-speed (10^5 frames/sec) video of individual voxels as they are launched from the donor layer indicates that they travel away with velocities near 1 m/s. [200] This is an order of magnitude slower than velocities observed with other types of LIFT processes, including low viscosity silver nanoinks, [201] ceramic films transferred using fs laser pulses, [85] ceramic films propelled by a DRL [202] and BA- LIFT of thin liquid films. [148, 203] The videos reported by Mathews et al. also reveal that the voxel forms without a bubble, shock wave or other associated plastic deformation, while the voxel perimeter appears early in the release process without debris. Furthermore, the kinetic energy carried by the released voxel is almost negligible compared to the total energy of the laser pulse. [200] These slowly traveling voxels experience a "soft landing" on the receiving substrate, which helps minimize their deformation and fragmentation upon impact with the receiving substrate. By virtue of its extremely low release velocity and subsequent soft landing, congruent LIFT is uniquely suited for the fabrication of free-standing structures, such as interconnects, [204] cantilevers, [205] and membranes [206] without the need for sacrificial support layers.

In order to achieve congruent LIFT, certain conditions involving donor layer preparation, and proper choice of laser and transfer parameters must be satisfied. Starting with the donor material, the paste not only has to exhibit sufficiently high viscosity, but it also has to contain well dispersed suspensions of particles with sizes of the order of 100 nanometers or less. The paste must also be stable in terms of solvent content and viscosity during the time it takes to prepare the donor substrate and complete the transfer process. Once ready for transfer, the spatial intensity profile of the laser beam must be uniform across the transfer area in order to avoid "hot spots" and the pulse-to-pulse energy stability within less than 5% to avoid damage of the voxel. Finally, the thickness of the donor layer, the area of the voxel and the appropriate range of laser fluences must be optimized in order to achieve reproducible congruent transfers. In general, the higher the laser spatial uniformity is, i.e. non-Gaussian, the better the congruent transfers. Given the strong dependence for size, shape and thickness

of the transferred voxel to the laser fluence threshold, the use of custom spatial laser beam profiles (as those produced with spatial light modulators) for transferring patterns of arbitrary shape and size at various resolutions have met with great success and are expected to streamline the implementation of congruent LIFT. [207, 208]

5. Applications

5.1 Laser printing of electronic materials

As we have already stated in the Introduction, printed electronics is one of the broadest and most promising fields of application for digital printing techniques like LIFT. In this context, a very small feature size is not necessarily the most coveted aim; the typical feature dimensions usually range between 10 and 100 µm. Instead, aspects like flexibility, low cost, large area, or roll-to-roll compatibility are of paramount importance. In this scenario a new range of materials, practically absent in conventional electronic devices, come to light: organic materials. Polymers are widely used not only as flexible substrates, but also as semiconductors in organic electronic devices like organic thin-film transistors (OTFTs) or organic light-emitting diodes (OLEDs).

Printing OTFTs and OLEDs requires stacking the different conducting, semiconducting and insulating layers that constitute the device in a particular configuration. The realization of multilayer structures from organic inks, although possible, can be cumbersome due to problems of solvent compatibility between adjacent layers. LIFT, in that it allows printing materials from solid donor films on both rigid and flexible substrates, can be a very interesting choice to overcome those difficulties. Furthermore, it also makes possible to transfer multilayer stacks in a single step.

In the fabrication of OTFTs through LIFT the deposition of the organic semiconducting layer is usually the most challenging step. The technique has proved to be feasible for printing a number of different polymers from solid donor films, like copper phthalocyanine (CuPc), [209] distyryl-quaterthiophene (DS4T), [210] or the diPhAc-3T (bis(2-phenylethynyl) end-substituted terthiophene) compound. [211, 212] For the correct performance of the resulting devices it is essential to preserve the structural and electrical properties of the films, which also applies to the laser transfer of the dielectric layer in the transistor gate. [213] To this aim, the use of a polymer DRL is helpful: it prevents the direct exposure of the film to laser irradiation and therefore the generation of light and thermally induced defects in the material. The transfer of organic semiconductors has also been proved feasible from liquid inks, [214, 215] although in these cases especial care needs to be taken with the compatibility between the ink solvents and those of the other layers in the OTFT. For the conducting layers (source and drain electrodes) both Ag nanoparticle inks in liquid phase [216, 217] and conducting polymers in solid phase [218] have been successfully transferred. The Ag inks, however, require a sintering step after printing that can thermally damage the semiconducting or dielectric layer adjacent to the electrode. Finally, the possibility of transferring multilayer structures pointed out above has also been exploited for the fabrication of OTFTs through LIFT in a single step, with performances very similar to those of devices fabricated by sequential evaporation processes. [219] For the transfer of very thick structures the process can clearly benefit from beam shaping strategies (Section 4.6). [87, 208]

In a similar way to OTFTs, LIFT can be a very interesting choice for OLED fabrication. In fact, in the early 2000s laser-induced thermal imaging (LITI), closely related to LIFT (Section 2), was already used by Samsung SDI to print a full-color active-matrix OLED display prototype. [53, 52, 220] Most research on OLED fabrication through LIFT has focused on multilayer transfer in a single step with TP-DRL; most light-emitting polymers (LEP) are very sensitive to laser radiation, so that a DRL can help prevent damaging the active material. The

basic architecture corresponds to a multilayer donor film composed of DRL/metal/LEP and indium tin oxide (ITO) coated glass as receiving substrate, eventually covered with an organic conducting polymer (**Figure 17**). Following this scheme, several works have proved that LIFT is feasible for printing OLEDs with good light emitting performance. [95, 172, 221-223] Best results are obtained if the transfer process is carried out at a reduced pressure of the order of 1 mbar: [98, 101] a low pressure allows eliminating the laser-induced shock-wave in air that can easily damage the flying voxel (Section 3.4), while at the same time reducing the voxel transfer speed compared to vacuum conditions. Transfer in liquid phase has also been assayed, though not so extensively as transfer from solid donor films. [224] In this case, in order to prevent damage to the sensitive electroluminescent material, BA-LIFT has been used to successfully print the active layer. [153] Finally, though not corresponding to organic materials, we must note here that LIFT has also been proved feasible for printing quantum-dots LEDs, a very attractive application given their high color purity and stability. [96]

In spite of the clear interest in printing organic semiconductors and active devices, like OTFTs and OLEDs, it is simple metals, like Ag or Cu, which tend to be the most abundant materials found in printed electronic devices. Indeed, these materials are essential in the fabrication of interconnects, electrodes and capacitor plates, and therefore constitute the basis of any printed circuit. Thus, it is not surprising to find those elements among the first printed through LIFT in actual electronic devices. [46, 225] The most common approach to printing conductive lines through LIFT, though, is by using metallic nanoparticle inks and pastes. [120, 121, 152, 216, 226] In order to produce conductive lines, it is required to print consecutive droplets with an appropriate overlap that results in continuous, uniform and stable lines. Line stability is one of the major issues to address when printing by accumulation of droplets. [227] For example, bulging, a phenomenon common to other printing techniques, like inkjet printing, [228] can seriously compromise the functionality of the printed element. Several strategies have been investigated to mitigate this effect, like overlapping sets of droplets with an intermediate

drying step, [229] or printing within fluidic guides previously generated by laser ablation. [230] At high laser scan speeds (tens of m/s) and repetition rates (1 MHz), the interaction between jets described in Section 4.3 can surprisingly also help suppress bulging as well. [163] After transfer, the inks must be dried and sintered, a step that can be also carried out by laser irradiation. [121, 231, 232]

LIFT allows printing higher viscosities than almost any other digital printing technique. This is particularly relevant for the printing of conductive inks since, as described in Section 4.1, it is possible to attain much lower sheet resistances than with typical inkjet printing inks, for example. [129, 191] Another attractive field of application of the LIFT of conductive pastes is the printing of isotropic conductive adhesives for device bonding. [233] In addition, through congruent transfer of inks with and extremely high viscosity (Section 4.6), single step transfer of entire conductive elements can be achieved. [88, 193, 208, 234, 235]

Printing inks and pastes is not the only approach to the transfer of conductive elements. In fact, the LIFT of solid donor films, in this case metallic films, appears to be also convenient in certain applications. Thus, LIFT has been used, for example, to bond vertical-cavity surface-emitting lasers to silicon grating couplers [236, 237] and single dies to Au contact pads on glass. [238] A hybrid approach combining solid metal films with conductive inks and pastes has also proved feasible in the fabrication of microcapacitors. [239-241] Also, by means of applying very short laser pulses, and according to the mechanisms described in Sections 3.1 and 3.2, it is possible to print very small metallic features [63, 77, 81, 242] that can be used as interconnects. Conducting lines of Cu, Al, and Au with minimum widths down to 2 μm and with good electrical properties have been successfully printed through this approach. [243-246]

5.2 Laser printing of biomolecules

Biomolecules are the essential sensing element in biosensors, microarray chips, point-of-care diagnostic kits, and even in some chemical sensors aimed at the detection of non-biological analytes. Irrespective of their particular principle of operation, all these devices rely on the deposition and immobilization of one or more different types of biomolecules in specific locations. As with the electronic devices described in the previous section, there is also a clear interest in miniaturization here: reduction of device size, use of small sample volumes, waste reduction, high throughput, and batch processing. [247] Many microfabrication techniques commonly used for such a purpose, like dot-blotting, micro-contact printing, photolithography or inkjet printing, present important drawbacks, though: low speed, contamination, protein denaturation or nozzle clogging. Being LIFT a nozzle-free and non-contact direct-writing technique with few restrictions concerning the materials that can be printed, it can represent an interesting alternative for biomolecules printing.

Although the LIFT of biomolecules has been sometimes carried out from solid donor films through the use of ultrafast pulsed lasers, [248, 249] the most common way of printing them is through LIFT in liquid phase (biomolecules are usually found and handled in aqueous solution). In spite of the fragile nature of most biomolecules, the use of lasers for printing is not an issue in general. The laser pulse just vaporizes an extremely small volume of donor solution, much smaller than the transferred amount of liquid, which acts as transport vector for the biomolecules contained in it. Once the sessile droplet is deposited, the solvent evaporates and the biomolecules remain adhered on the substrate. For their correct immobilization special substrates are required, like poly-L-lysine coated glass slides, a typical support for a wide range of biomolecules. Furthermore, since aqueous solutions are transparent to most conventional laser wavelengths, DRLs are commonly used, which provides with an additional element of protection for the fragile molecules.

Different biomolecules have been successfully printed through the LIFT of liquid donor films, in most cases through the use of a metallic DRL. Thus, single-stranded DNA has been shown

to preserve its integrity and capability of selectively hybridizing after transfer (**Figure 18**).[165, 167, 250] Proteins add an additional level of complexity to single-stranded DNA: their three-dimensional structure. This makes them particularly challenging, since the alteration of that structure (denaturing) completely deprives proteins of their functionality. Nevertheless, LIFT has been extensively proved feasible to print a broad range of proteins without altering their selectivity: horseradish peroxidase,[47, 251] bovine serum albumin,[115-117, 252] enzymes,[253] antigens,[166] streptavidin,[254] biotin-avidin,[255, 256] immunoglobulin G,[154, 257] and even the gigantic protein titin.[251, 256] In addition, FF-LIFT (Section 4.5) has also been used to print biomolecules, namely immunoglobulin G [177, 175] and DNA.[177]

LIFT has also been applied to the deposition of other biological compounds which do not correspond exactly to biomolecules, but which are nevertheless of great interest in medicine and biology. Among them peptides,[258] and more specifically amyloid peptides,[252, 259] a useful tool in cell-growth studies. Similarly, liposomes are also very interesting structures with attractive applications as drug carriers and in biological sensing. They are molecular structures consisting of lipid bilayers that enclose an aqueous core. Liposomes can attain diameters of tens of micrometers, a particle size hard to print with conventional direct-writing techniques. As pointed out in Section 4.1, LIFT is specially suited to print large particle sizes and, indeed, it has been proved feasible for printing these biological structures with no damage to the liposomal membrane.[171]

5.3 Laser printing of biological and chemical sensors

In the preceding section we have pointed out the advantages that miniaturization offers in the manufacturing of biological sensors, and how LIFT, thanks to its capability of printing with high resolution a wide range of materials both in solid and liquid state, can contribute to that aim. In this regard, chemical sensors are not any different. In this section we will review the

most representative works addressed at proving the feasibility of LIFT for the fabrication of both biological and chemical sensors. In fact, some of these realizations have implicitly been presented in Section 5.2; the integrity, functionality and selectivity of DNA and most proteins described there was proved through the fabrication and further test of biomolecule microarrays, which are nothing else but biological sensors with optical reading. Nevertheless, LIFT can also be used to fabricate other more complex sensors with alternative working principles and signal recording strategies.

Aside from the already mentioned DNA microarrays produced by LIFT, [167, 250] the technique has also been used with the aim of investigating the possibility of fabricating other types of DNA sensors, for example capacitive sensors. [260] The first biosensor fabricated by LIFT, though, was probably a dopamine electrochemical sensor prepared from a composite of banana tissue-based and graphite. [47] Similarly, an amperometric biosensor for the detection of catechol in aqueous solution was fabricated by depositing through LIFT a solution of the enzyme laccase onto graphite screen-printed electrodes. Thanks to the particular dynamics of the LIFT of liquids, as well as to the rough surface of the electrodes, biomolecules immobilization was possible without the need of any intermediate functionalization step. It is also remarkable the fabrication by means of LIFT of a bio-electronic nose for the detection of volatile odorant molecules to identify the presence of contaminants in food. [261, 262] Solutions containing different types of odorant-binding proteins were printed on surface acoustic wave resonators, which showed a sensitivity and selectivity to the detection of volatile carvone and octenol similar to sensors fabricated with more conventional printing techniques. Although all the reported examples correspond to biomolecule-based sensors (that is, the sensing element is a biomolecule), with practically no restrictions concerning the printable particle size, LIFT also allows printing more complex biological structures. Thus, LIFT has been used to print a suspension of thylakoid membranes on Au electrodes for the realization of a photosynthetic-based biosensor aimed at the detection of herbicides. [263] Finally, biological molecules can

also be used to sense inorganic materials. For instance, deoxyribozymes can selectively detect Pb^{+2} ions, a major environmental contaminant. By printing a solution of DNAzymes on capacitive micromembranes, the fabrication with high spatial resolution of this type of sensors has been shown by LIFT, [264] resulting in a sensor that is biological regarding the sensing element, but chemical regarding the sensed analyte.

LIFT has also been proved feasible to print materials for the fabrication of miniaturized chemical sensors aiming at diverse applications: identification of spilled chemicals, foods and drinks quality, water analysis, air quality monitoring. The first work reporting laser printing for sensing applications was probably the realization of a gas sensor by LIFTing chemoresistive polymer composites. [265] However, as described in Section 4.1, one of the greatest advantages of LIFT over other competitor techniques is the possibility of printing large particle sizes, and this is particularly interesting for sensing applications: nanostructured materials are ideal candidates for sensing materials. Thus, reduced graphene oxide has been printed from aqueous solution on Au electrodes and the resulting sensor successfully tested against water, ethanol and xylene vapors. [132] Similarly, but this time taking advantage of the possibility of printing from solid donor films, composite layers of polymers and carbon nanotubes have been LIFTed on Al microelectrodes for the fabrication of amperometric chemical sensors. [266] Aside from nanostructured materials, [124] other materials like tin oxide [267] or diverse polymers [108, 111, 268-270] have also been printed through LIFT and proved successful in the detection of different gases. Finally, a new approach to LIFT, reactive LIFT (rLIFT), has been used to print SnO_2 for gas sensors fabrication. [271] rLIFT consists in using UV-absorbing metal complex precursors (metal acetylacetonates), which partially decompose to SnO_2 upon absorption of the laser radiation. The as-prepared sensors have been proved feasible for the detection of ethanol and methane.

5.4 Laser printing of cells

The printing of living cells, also known as bioprinting, is of great interest in diverse areas of biotechnology and medicine. On one hand, the possibility of building two and three-dimensional cell constructs allows controlling the spatial organization of cells, which has a clear impact on cell behavior. Thus, bioprinting provides us with a powerful tool for cell biology studies, like cell-cell and cell-environment interactions, or cell growth and differentiation. On the other hand, through the combination of cell printing with other biomaterials we can create structures as close as possible to tissue and organs (*tissue engineering*), which can be used in drug testing and regenerative medicine applications.

Most living cells range between 1 and 100 µm in size, and in bioprinting applications they are usually found in hydrogel suspensions with quite high viscosities, easily of the order of 1 Pa·s (hydrogels like alginate are very convenient due to their resemblance with the natural extracellular matrix and their immunoisolation barrier properties). [272] With these viscosities and loading particle sizes, it is then obvious that the LIFT of donor liquid films constitutes a very interesting choice as cell printing tool. But these are not the only strengths of LIFT for bioprinting. The technique also allows combining different cell types and biological factors that permit to mimic the heterogeneity of tissue. [273-275] In addition, by being a non-contact and nozzle-free printing technique, LIFT mitigates cross-contamination problems and eliminates clogging issues, while avoiding orifice shear-induced stress. [272] Finally, given its unprecedented level of control and accuracy as compared to other more conventional bioprinting techniques, LIFT enables the printing of patterns with high cell densities, thus reducing the maturation culture time of the engineered constructs, [276] while at the same time making possible single cell printing. [273]

Although the first work involving the use of lasers for bioprinting corresponds in fact to a laser guiding technique, [277] the first publication on actual laser cell printing is that of Wu and co-workers, [47] who used the technique to deposit Chinese hamster ovaries on quartz with no

measurable damage to their structures or genotype. After that, many other cell types followed: *Escherichia coli*, [48] rat cardiac cells, [278] human osteosarcoma cells, [273, 279] B35 neuronal cells, [280] bovine aortic endothelial cells, [281] mouse NIH3T3 fibroblast cells, [282] olfactory ensheathing cells, [283] yeast, [284] human endothelial cells, [274] and stem cells, [153, 285] among others. [286-292] Even multicellular microorganisms have been successfully printed through LIFT. [168] In most cases, post-printing tests demonstrated a near 100% viability, with no alteration in the functionality of the cells, in their genotype or in their phenotype; normal cell growth and proliferation was always observed. Eventually, some cell damage can be observed postprinting, mostly attributed to the incident laser radiation, heat stress, and shear stress during acceleration (cell droplet formation) or deceleration (cell droplet landing on collector slide), with negligible UV damage in the case of working with that laser radiation. [288, 284] Nevertheless, the heat and radiation harmful effects are only significant at high laser fluences and can be substantially mitigated through the use of DRLs. [293, 294] On the other hand, the detrimental effect of shear stress can be greatly reduced through increasing the ink viscosity. [295]

Once it was demonstrated that LIFT was perfectly feasible for cell printing, with clear advantages over other competitor techniques, it immediately became a powerful tool for two major applications of bioprinting: cell biology studies and tissue engineering. Indeed, thanks to its high resolution, LIFT is particularly well-suited to investigate cell-cell and cell-microenvironment interactions *in vitro*, and remarkable advances in this field have been achieved. Thus, by printing human adipose-derived stem cells and endothelial colony-forming cells it was shown that stable vascular-like networks were promoted by direct cell-cell interactions. [296] Similarly, it was demonstrated that LIFT allowed building three-dimensional constructs that could reproduce native tissues or organs, with the consequent reduction in animal testing during drug development studies. [276] Finally, laser printing can also play a significant role in one of the fields where cell biology studies are most relevant: cancer

research. Hence, LIFT was used to build three-dimensional structures with human osteosarcoma cells (MG63) and rat cardiac cells, [278, 279] and LIFTed pluripotent embryonic carcinoma cells (P19) proved to maintain cell viability and differentiation capacity post-print. [288]

Tissue engineering also benefits from the capacity of LIFT for printing cells and other biomaterials. The control of the technique in cell positioning at micron scale translates into a precise control in cell organization, essential for the correct functioning of the final tissue. Thus, different kinds of tissues have been successfully engineered through laser printing. Diverse skin cell lines and human mesenchymal stem cells (hMSC) have been LIFTed aiming at the production of skin substitutes for promoting skin tissue repair and regeneration for burned patients; [297, 298] through a layer by layer printing approach (**Figure 19**), LIFT makes possible to mimic the layered architecture of skin (dermis plus epidermis). [299] Once transplanted into skin wounds in mice, the cellularized skin substitutes showed the formation of skin tissue and blood vessels in the direction of the printed cells. [300] Related to this, LIFT has been proved feasible for printing human umbilical vein endothelial cells (HUVEC) for blood vessels generation [301, 302] and also the printing of HUVECs, this time in combination with hMSCs, has allowed addressing heart tissue growth through the same approach. [303] Given that bone tissue regeneration is a major health issue today due to population aging, it is not surprising that LIFT has been assayed for bone tissue engineering as well. Bioceramics and osteoblast-like cells, [304] and also nanohydroxyapatite (nHA) and human osteoprogenitors, [305] have been used to create two- and three-dimensional composite structures through laser printing with good functionality and allowing the vascularization of the bone substitute. Remarkably, nHA particles have been successfully transferred *in situ* onto bone calvaria defect in mice, [306] showing the feasibility of LIFT for *in vivo* operation. Another example of LIFT being carried out *in vivo* corresponds to the printing of three-dimensional constructs of MSCs embedded in a matrix biomaterial (plasma and alginate) that led to autologous bone

and cartilage tissue grafts after culture, opening the possibility to transplants. [307] The last major application example of laser bioprinting considered here corresponds to nervous tissue. Due to the limited healing capacity of this tissue, this application remains particularly challenging. Results obtained after printing neurons and glial cells through LIFT pave the way for the future generation of complex cellular models with unprecedented cellular organization. [308]

The understanding of the dynamics of viscous hydrogels (alginate) transfer during laser printing is of prime interest in cell biology studies and tissue engineering. On one hand, and as stated in the second paragraph of this section, many cells are usually printed in a suspension of these liquids; on the other hand, alginate is a perfect candidate for the generation of three-dimensional structures that can work as scaffolds for tissue growth and development (**Figure 20**). [126, 128, 309] Although alginate laser-induced ejection proceeds through a jetting dynamics very similar to that described in Section 4.2, the visco-elastic properties of those hydrogels present significant particularities that require dedicated studies. [130, 310, 311]

5.5 Laser printing of 3D metal structures

The ability to generate free-standing structures with LIFT has led to its application in the microfabrication of 3D stacks and other types of 3D structures non-lithographically. When LIFT of congruent voxels is repeated over the same location in order to stack each transfer on top of each other the result are out-of-plane or 3D structures useful for interconnect or via applications. [204] LIFT can also be used to generate 3D microstructures that fold along an edge, which allows the printing of interconnects alongside two orthogonal planes on the same substrate. [312] That is, by adjusting the laser energy required to release the voxel from the donor substrate, it is possible to make the voxel fold along the edge of a substrate and thus

make contact on two distinct surfaces perpendicular to each other. This ability has no parallel in lithography and can be used to generate top-to-side interconnects. Moreover, LIFT of congruent voxels has been demonstrated for printing crossover interconnects without using sacrificial layers. [204] This was achieved using LIFT in multiple steps, first generating the vertical posts and then printing a free-standing top metal interconnect connecting the posts. The resulting structure resembles a flattened, low-profile wire bond with the same functionality but occupying a much smaller volume. [204] SEM images corresponding to several of these structures are shown in **Figure 21**. [313]

In order to reliably fabricate 3D structures with LIFT it is necessary to control the spatial placement of individual voxels to a fraction of their size, while their adhesion to each other and to the substrate must be sufficiently strong to withstand mechanical and thermal strains during processing and use. In order to accommodate the printing of 3D structures with LIFT of pastes, accuracy in placement tends to decrease as the distance between the donor and receiving substrates increases. [235] Furthermore, voxel adhesion is hindered when solids or pastes containing large particles (> 0.1 μm) are used rather than nano-suspensions, unless high post-processing temperatures are applied to sinter the material. One solution is to transfer molten metal drops that solidify upon landing. This type of transfer can be achieved with LIFT of metals using ps and fs laser pulses whereupon exposure to the laser pulse, the metal layer in the donor substrate melts and undergoes jet formation leading to the ejection of a highly forward directed metal drop (see Sections 3.1 and 3.2). Even then, achieving mechanically strong attachment between voxels while avoiding oxidation remains a challenge. Previous results indicate that the resulting structures are limited to low aspect ratio pillars when micro-spherical gold metal drops generated by fs-LIFT are stacked on top of each other. [63] These micro-spheres were generated at the transfer threshold fluences of a thin gold film (< 200nm) donor substrate. In contrast, by operating at fluences above threshold, it is possible to control the velocity of the drops forcing them to deform into flattened disks upon landing

on the receiving substrate to achieve the stacking of micrometer-sized metal voxels and form very high aspect ratio pillars as demonstrated by Visser and co-workers [242] and shown in **Figure 22**a,f. This LIFT regime also minimizes oxidation and enhances adhesion of the molten metal voxels through the use of a metal coated receiving substrate, which speeds the solidification of the drops so they stick to each other with less oxidation than during ns-LIFT. Figure 22b displays a high-aspect ratio copper pillar generated by ps-LIFT of copper drops which exhibit very homogenous cross section along their entire length as shown by the SEM images in Figures 22c-e. It is worth noting how the shape of the printed voxel can be controlled from deformation of the molten metal from spherical (low fluences) to spraying (high fluences) as shown in Figure 22f. [242] Similar results have been reported by Zenou and co-workers for other metals such as gold and aluminum [77] and copper/silver alloys. [78]

These results show how LIFT can be used as an additive micro-manufacture technique to generate 3D metal structures. These examples are significant since they demonstrate a 3D micro-manufacturing capability with metals difficult to obtain with other direct-write techniques and impossible to achieve with photolithography.

5.6 Laser printing of materials for power storage

One of the advantages of LIFT is that the deposited materials typically show porous structures with high surface areas. These porous structures are very important features for electrochemical devices due to an increased contact area between the electrodes and the electrolyte, leading to improved charge transfer and accordingly a more complete utilization of the electrode materials. Thus, the LIFT technique can be used to print fully functional electrodes for micro-scale energy storage systems, such as ultracapacitors and microbatteries. [189] LIFT can also be used to print energy harvesting structures such as photovoltaics [189] and thermoelectric junctions. [86]

Electrochemical ultracapacitors can be used for load leveling and applications where a short burst of power is needed. These energy storage devices are comprised of two identical electrodes composed for example of a hydrous metal oxide. [314] Arnold et al. was the first to demonstrate the fabrication of planar hydrous ruthenium oxide ultracapacitors using LIFT with significantly improved discharge behavior. [315] The electrochemically active ink used in the LIFT of these devices was prepared by mixing hydrous ruthenium oxide powder with a sulfuric acid electrolyte solution. The cells based on the laser-printed ruthenium oxide electrodes exhibited a linear charge/discharge response at constant current, indicating ideal capacitor behavior, and when connected in series and parallel configurations, they could be discharged at currents above 50 mA. [316]

The LIFT technique has been successfully employed to print thick-film electrodes for both alkaline and Li-ion microbatteries with much higher capacities per electrode area than those made by sputter-deposited thin-film electrodes. [189] The intrinsically porous structures produced by LIFT facilitate the diffusion of ions across the electrodes with minimum loss due to internal resistance. For example, LIFT has been used to print thick-film electrodes comprising of lithium cobalt oxide ($LiCoO_2$) cathodes and carbon anodes with a laser-cut porous membrane soaked in a gel-polymer electrolyte (GPE) as separator to fabricate functional Li-ion microbatteries. [317] A diagram illustrating the cross-section of the LIFT printed microbatteries together with an SEM micrograph of one such structure is provided in **Figure 23**. With LIFT, the thickness of the printed films can easily be adjusted by changing the number of printing passes, thus allowing the discharge capacity of the LIFT microbatteries to be adjusted during fabrication to accomodate a particular load.

The electrochemical properties of Li-ion microbatteries based on laser-printed $LiCoO_2$ cathode thick films are highly dependent on the cathode thicknesses. As demonstrated by Kim *et al.*, the discharge capacity per active electrode area increases linearly with the cathode film thickness (up to ~ 100 μm). [317] The Li-ion microbatteries exhibit excellent cycling

performance of over 200 cycles with a slow fade rate and retain about 80% of their initial capacity after 200 cycles. Based on discharge capacity per active electrode area, standard microbatteries made by sputter-deposited 2.5 µm thick $LiCoO_2$ cathodes (active area = 1 cm^2) exhibit a capacity of 160 mAh/cm^2 (or ~64 mAh/µm cm^2) at a current density of 100 mA/cm^2. [318] On the other hand, laser-printed 115 µm thick $LiCoO_2$ cathodes (active area = 0.49 cm^2) achieve a capacity of 2586 mAh/cm^2 (or ~22.5 mAh/µm cm^2) at the same current rate. [317] Despite a three times smaller volumetric capacity than that of the sputter-deposited thin-film cells, the laser-printed thick-film microbatteries can produce orders of magnitude higher capacities per unit area. Overall, laser-printed thick-film microbatteries are well suited for applications where limited space is available for the power source, such as embedded microelectronic systems and distributed sensors.

LIFT has also been applied to the printing of porous nanocrystalline TiO_2 (nc-TiO_2) layers used in dye-sensitized solar cells (DSCs). [319, 320] In these devices, the anode consists of a light-absorbing dye molecule attached to the surface of electrically connected nc-TiO_2 particles assembled as a porous structure and filled with a liquid electrolyte (typically a iodine-based redox couple). In this type of cell, the electrons generated by oxidation of the dye molecules are injected into the conduction band of the nc-TiO_2 film and transported to the external circuit through a transparent conducting oxide layer, i.e. fluorine-doped tin oxide. On the cathode side, a metal catalyst enables the direct reduction of the electrolyte itself, which subsequently reduces the dye molecules to their initial state. The schematic structure and operating principle of such a dye-sensitized solar cell is illustrated in **Figure 24**a,b. In the DSC system, the porous nanocrystalline microstructure of the TiO_2 layer with a high surface area is essential for achieving high efficiency since it increases the dye absorption which results in increased solar light collection per unit area. A cross-section of this TiO_2 layer, the result of multiple printing passes, is shown in Figure 24c. Note the lack of interfacial gaps between printed layers demonstrating the uniformity of the laser printed structure, which upon

sintering in air at 450 °C gives rise to a 3-D network of interconnected TiO_2 nanoparticles improving electron conduction (Figure 24d). Both properties of the porous TiO_2 layers made by LIFT, high surface area and interconnected particles are essential for the fabrication of efficient dye-sensitized solar cells.

A final example illustrating the use of LIFT in energy harvesting applications can be found in the work of Feinaeugle *et al.* aimed at the fabrication of thermoelectric generators. [86] There LIFT was used to print p-n junctions comprised of p-type bismuth antimony telluride and n-type bismuth telluride layers, each about 1 µm thick, onto polymer-coated glass substrates. A planar assembly of multiple junctions designed to increase output voltage was later demonstrated onto a polydimethylsiloxane (PDMS) coated substrate. [321] The resulting assembly showed a Seebeck coefficient of 0.17 mV/K per junction which was lower than the expected output for this type of p-n junction (0.19 mV/K) and an overall efficiency factor of 1.3×10^{-4} µW K^{-2} cm^{-2}, which is comparable to thermoelectric devices fabricated on flexible substrates by other techniques. [321]

5.7 Laser transfer of intact structures and functional devices

LIFT can also be applied to the placement of entire functional components and devices onto a specified location on any given surface. The first results on the use of LIFT processes for the transfer and placement of prefabricated parts or components onto a receiving substrate was reported by Holmes *et al.* [322] In their work, the authors describe the laser-driven release of Si-based microstructures from a UV-transparent substrate with an intermediate polymer sacrificial layer. Upon irradiation with an excimer laser pulse, a thin fraction of the sacrificial layer is vaporized, releasing the microstructure. This technique was later used to demonstrate the laser-assisted assembly of microelectromechanical devices from parts fabricated on separate substrates. [323] These initial results showed how to use the laser transfer process as an

alternative to conventional pick-and-place approaches for the placement of electronic components such as passives and semiconductor bare dies. The basic concept relies in the use of a laser absorbing sacrificial release layer. In essence, it requires a sacrificial layer such as the polymer film used by Holmes to attach the individual components to a UV-transparent support. As the laser pulse ablates the sacrificial layer, the vaporized material releases and propels the component towards a receiving substrate placed in close proximity. This laser device-transfer process is contact-less thus allowing the transfer of very small and very thin components, which could easily be damaged by pick-and-place tools.

A few years later, this concept was applied to the laser transfer of semiconductor bare dies by a group from the University of Twente in the Netherlands. In this work, Karlitskaya and coworkers developed a simple model that predicts the fluence threshold for the release of 200×200 μm^2 by 150 µm thick Si dies held with a polyvinyl chloride (PVC) sacrificial layer. [324, 325] The model shows that the release threshold is below the thermal damage threshold for the reverse side of the die (< 673 K), based on heat diffusion of the absorbed laser pulse through the Si substrate. In this case the authors applied the laser transfer process to devices with the active region facing opposite to the laser pulse to minimize thermal damage. However, this configuration is rather unpractical since it requires extremely precise alignment to establish the electrical connections between the transferred die and the acceptor substrate. A better solution is to transfer the die with its active surface facing up enabling wire bonding or direct-write printing to generate the connecting lines between device and acceptor substrate. The challenge however, is to be able to strike the die's active region with the transfer laser pulse and trigger its release without damaging it.

About a year later, this capability was demonstrated for the laser forward transfer of individual InGaN LED semiconductor substrates (250×350 μm^2) in bare die form, i.e. unpackaged, using a series of low fluence (~150 - 200 mJ/cm^2) 10 ns pulses from either excimer (248 nm) or YAG (355 nm) lasers by Mathews et al.. [326, 327] Once laser transferred,

the LED's were electrically tested and their operation verified. This laser-driven pick-and-place of electronic devices has been named "lase-and-place" [328] and is shown schematically in **Figure 25**a. [313] Diagram (ii) in the schematic illustrates how a specially constructed donor substrate containing the devices to be transferred instead of an ink or paste can be used in the lase-and-place process, as part of the steps required to embed and interconnect an electronic device inside a substrate. The fact that the devices are not damaged upon laser illumination of their active surface and subsequent transfer demonstrates that both laser-based component placement and interconnecting processes are possible via LIFT by combining lase-and-place with laser printing of metallic inks. Figure 25b,c show examples of embedded devices, LEDs in (b) and integrated ciruits (ICs) together with capacitors and resistors in (c) subsequently interconnected by laser printed silver inks to form working circuits (as illustrated by the inset in Figure 25b showing the LEDs turned on).

The lase-and-place technique has been used successfully to laser transfer a wide variety of components such as surface mount devices and semiconductor integrated circuits ranging in size from 0.1 to over 6 mm^2 in area. [329] Studies by other groups have shown the viability of this technique to achieve device placement precision and speeds competitive with well-established pick-and-place tools [330] and the use of magnetic self-assembly for the trapping and alignment of the individual chips to improve device orientation, thus minimizing rotation during placement. [331] Finally, the lase-and-place technique has also been shown to be compatible with the transfer of ultra-thin (≈10 μm) silicon substrates up to 1 mm^2, which despite their fragility can be placed with extreme precision without damage or fracture after transfer onto the acceptor substrate. [327]

Lase-and-place can also be applied to structures ranging in size from a few microns to millimeters as shown by the images in **Figure 26**. The displayed examples do not represent the lower or upper limit of transferable sizes and shapes for lase-and-place but rather illustrate how versatile this LIFT technique is. As shown in Figure 26a, a 10 μm long, 200 nm diameter

nickel nanorod can be laser transferred without deformation or fracture above two posts etched on a silicon substrate. This capability offers great potential for the precise placement of discrete nanoscale structures, which would otherwise require handling via more complex and time-consuming techniques such as AFM-tips or laser tweezers. [333] Patterned thin films can also be laser transferred as shown in Figure 26b, where a pre-patterned 500 nm thick copper film 50 μm long by 10 μm wide was placed to form a bridge between two SU-8 pads. Alternatives for placing these two sample structures at a given location on a substrate without damage are limited to self-assembly techniques. However, self-assembly is best suited for fabricating large arrays of identical elements, and becomes impractical when applied to a few components of varying size requiring placement at arbitrary locations.

Lase-and-place can also handle larger metal structures like those shown in Figures 26c,d. The copper foils are 1 mm long and are attached with silver paste to the contact pads at the edges of the two devices for the purpose of serving as electrical interconnects. LIFT of copper foils allows the fabrication of low-profile interconnects as well as 3D laser-shaped interconnects shown in Figures 26c,d, respectively. In both cases, the laser transferred interconnects are much more robust and durable than those produced with printed inks or pastes. [333] The ability to shape and print metal foils accross the contacts of existing devices allows for low-profile interconnects of greater cross section, while minimizing the volume taken by the interconnects themselves. Overall, the use of flat or shaped metal beams or foils enables the printing of low-profile, low-resistance, and mechanically compliant interconnects. Such features are very important towards the development of next-generation flexible hybrid electronics comprising different types of electronic components, interconnects, and printed structures.

5.8 LIFT in industry

As highlighted in the previous sections, the applications of LIFT span across a wide-range of industries. However, most of the efforts to date have focused on proof-of-principle demonstrations and process development at the laboratory level employing setups designed for experimentation rather than production environments. Nevertheless, numerous multidisciplinary teams involving academic and commercial groups have emerged in the past few years, with the aim of adapting LIFT techniques to various industrial applications. So far, these teams have focused in applications aimed to emerging markets in the electronics, biomedical and graphics printing industries.

Since its early development, the use of LIFT for printing electrically conductive materials for electronic applications has garnered much attention. Applications requiring the printing of electrically conductive patterns over large areas such as electrodes for solar cells, heating elements for automotive glass windshields and conformal antennas for autonomous systems call for direct-write technologies capable of generating electrically conductive patterns. Some early adopters reported on the use of laser-induced transfer techniques for applications in the flat panel display industry with the goal of laser printing conducting polymers [51] and light emitting organic semiconductors. [52] Blanchet's process led to several commercial applications, as mentioned in Section 2, that illustrate the use of laser transfer processes for the digital printing of electronic materials. It is important to note that digital printing systems based on inkjet processes are rather limited for the transfer of conductive inks. On the other hand, LIFT with conductive inks and pastes has successfully demonstrated its applicability to a wide range of commercially available silver suspensions. Among these reports, a few of them have systematically studied and evaluated LIFT's printing conditions with the goal of process scale-up and commercialization. For example, results from analysis performed with LIFT of various commercial silver nanoink inkjet formulations are provided by the works of Duocastella *et al.* [226] and Rapp *et al.*; [120] while analysis of LIFT of silver nanopastes formulated for screen printing can be found in the works of Mathews *et al.* [200] and Auyeung

et al.; [208] and LIFT of micron-sized metal pastes has been studied by Muñoz-Martín *et al.* [129] Incorporation of these studies into specific applications in the electronics industry can be found in the repair of interconnect defects in flat panel displays, [194] which is being commercialized by Orbotech, Ltd.. [334] Finally, interest in LIFT for electronics is now benefiting from its combination with additive manufacturing techniques and roll-to-roll processes for the printing of RFID antennas and fingerprint sensors, as exemplified by the recently established European consortium of companies, research labs and academia named HiperLAM (for High Performance Laser Additive Manufacturing).[335]

Biomedical applications utilizing printed bio-compatible scaffolds and printed biomaterials make up another area where LIFT is poised to have a great commercial impact. Despite the fact that the first reports of the use of LIFT with biomaterials such as proteins and live organisms such as bacteria and cells date from the early 2000's, [47, 48] the commercialization of the technique in the biomedical field has only recently taken off. Here again, the attention generated by additive manufacturing and its promise of going from a design to a printed construct comprised of biomaterials, i.e. tissue engineering, has provided new opportunities for LIFT's commercialization. LIFT of cells is competitive with other more traditional biomaterial printing techniques such as dispensing, given its reproducibility, speed, material placement precision and single-cell resolution. Combine this with LIFT's ability to transfer cells viably over two- and three-dimension arrangements without the need of a printing head or nozzle and it is no surprise that its commercialization for *in vitro* and *in vivo* cell biology studies and tissue printing applications is currently being pursued by several companies. One company working on commercial LIFT systems for bioprinting applications is Poietis, in France. Their printing platform designed for the production of 3D tissue models for cosmetics and pharmaceutical laboratories is designed to achieve 20 µm drop resolution at printing speeds of 10,000 drops/s. [336] Poietis calls their process laser-assisted bio-printing or LAB and

is working in preclinical evaluation of human tissue-engineered grafts comprised of fibroblast cells embedded in a collagen matrix each printed by LIFT.

Finally, the use of LIFT for industrial graphics applications has also been demonstrated successfully. Perhaps earlier than most, the graphics industry investigated and adopted digital printing processes with the result that a broad range of digital printing techniques are in use today. That explains why perhaps the first application of laser transfer phenomena was for laser-based paper printers, back in the late 1970's and early 1980's, before the term LIFT had been coined. Back then, the high cost and size of lasers made this idea impractical and later on, with the development of toner-based printers, the laser transfer itself was no longer pursued. However, recent applications requiring printing of special inks (for packaging or decorative applications) and markets with very small numbers of runs or individual customization, which cannot be handled by traditional printing techniques, have offered new opportunities. In some cases, inkjet is not a solution, as in the food and pharmaceuticals industry, where the inks used contain chemicals not compatible with food or drugs, or in ceramics decoration, where the inks contain ceramic pigments which clog the inkjet nozzles. In these and other applications LIFT offers advantages if it can be scaled to be cost-effective against industrial printing processes such as rotogravure. A LIFT technique specially designed for these applications was developed by Aurentum GmbH, in Germany, and given the commercial name Lasersonic®.[44] The scale-up of the Lasersonic® process to a four-color reel-to-reel system capable of printing at a rate of 1.3 m^2/minute with a resolution of 600 dpi was demonstrated under the DI Project AG by a team from Daetwyler AG, Switzerland, and Interprint GmbH, Germany.[44] **Figure 27** shows the four-color printing machine that was developed under this project.

6. Summary and Future Perspective

LIFT is a direct writing technique that allows printing materials both in solid and liquid phase through the use of a laser beam as driving force. This dual nature, alongside other advantages like being non-contact and nozzle-free, place this relatively unconventional technology in a certainly competitive position in the digital manufacturing scenario. Indeed, its pixel by pixel mode of operation makes LIFT truly digital, thus avoiding the need for masks, screens and rolls so characteristic of most typical printing techniques, and providing the flexibility required by the new digital paradigm. And since depositing a wide range of materials through a number of different working modes and printing strategies becomes possible with the same technique, this means that an unprecedented spectrum of applications ranging from printed electronics to regenerative medicine can now be accesed using LIFT.

LIFT from solid donor films through melting of the transfer material is especially suited for printing metals, and therefore adequate for the realization of electrical contacts and vias; the resolidification of the melted material upon deposition on the receiving substrate leads to compact features that present electrical properties close to those of bulk material. On the other hand, this mode of operation allows depositing droplets of nanometric size, which results in extraordinary printing resolutions and makes possible true micron-scale 3D printing. However, transfer through melting is not the only option: it is also feasible to remove a portion of the solid donor film without any phase change taking place in the donor material. This approach is particularly appropriate for materials that would irreversibly decompose or change their structure upon melting or vaporization, namely ceramics and many polymers. Thus, LIFT has proved viable for printing chalcogenides for the fabrication of thermoelectric devices or conducting polymers for sensing and printed electronics applications, for example. In this context - transfer in solid state - the use of a TP-DRL is remarkably beneficial. On one hand, the photodecomposing DRL polymer protects the donor sensitive materials from potentially damaging effects of the laser radiation and, on the other hand, the volatile nature of the decomposition products mitigates undesired contamination in the printed features.

Nevertheless, one of the aspects that makes the LIFT from solid donor films most unique is probably the possibility to print multi-stacks and entire devices. Indeed, both with and without DRL, the technique has been proved feasible for printing functional OTFTs and OLEDs from multi-layer donor films, and even pre-fabricated components through the lase-and-place process, the photonic version of conventional pick-and-place.

Laser printing can also be carried out from liquid donor films, an approach probably easier to associate with the commonly accepted meaning for the word 'printing'. In most conventional printing techniques, either digital (inkjet printing) or not (screen-printing, rotogravure, flexography), the donor material is an ink, that is, a solution or suspension of the material to be printed in a solvent. In the LIFT from liquid donor films, the driving laser pulse is responsible for the onset of a particular jetting dynamics that results in the ejection of a fraction of the ink towards the receiving substrate. There the liquid is deposited as a sessile droplet that ultimately results in the printed pixel. In this regard, the operation mode of LIFT is not essentially different from inkjet printing, its main digital competitor. However, by allowing the printed liquid to be unconstrained by a nozzle, LIFT presents two remarkable advantages: a substantially broader range of printable viscosities and very few restrictions concerning the size of the particles loading the ink. The impact of these advantages on the applications is clear. Thus, the possibility of printing high viscosities translates into printing conducting inks with high solid content, essential for the production of interconnects with low sheet resistance in printed electronic devices, and truly compatible with flexible substrates. LIFT can even operate with such high viscosities that make possible congruent transfer in the LDT mode, thus achieving the transfer of complex shapes in a single laser pulse. On the other hand, printing large particle sizes allows LIFT depositing nanostructured materials, so interesting in sensing applications, for example. Finally, since most biological materials (biomolecules, cells) are handled and stored in liquid media, the LIFT from liquid donor films is also suited for bioprinting applications. In this regard, the aforementioned advantages

especially impact the printing of living cells, usually with relatively large sizes and contained in viscous media, which can be printed through LIFT without harm even in 3D arrangements. Tissue engineering for cellular studies and regenerative medicine thus becomes a really promising field for the technique.

Since the term LIFT was first used over 30 years ago, the technique and its numerous derivatives have been investigated extensively for numerous classes of materials and demonstrated for a wide range of applications. In the process, an extensive body of work has been generated paving the way for LIFT's transition to industry. And for the first time, as these findings are translated from the laboratory into commercial applications, industry is embracing the potential brought by LIFT as an additive manufacturing technique for meso- and microscale fabrication. LIFT offers benefits in cost reduction for prototyping and production, manufacture simplification (through the reduction of production steps), and greater design freedom due to the inherent geometrical versatility allowed by the laser transfer processes. LIFT of structures and functional devices is ideally suited for applications ranging from product prototyping to high-throughput production. For applications in electronics, the ability to print conformal electronic assemblies on any surface and its combination with existing additive manufacturing tools is actively being pursued by both small and large companies. For biomedical applications, the feasibility of using LIFT for 3D printing tissue and organs has been embraced by several new companies with the aim of developing turn-key laser-based bioprinting tools. There are plenty of challenges before LIFT-based electronic circuit or tissue engineered printers become common. Examples of those challenegs include the establishment of design rules, such as process modeling and optimization, integration of many types of structures (either devices or cells), process control, metrology and evaluation of the printed assemblies (either electrically or biologically), and long-term reliability or viability of the LIFT-printed constructs. Solving these challenges will require a considerable effort but as applications develop and industries ranging from aerospace to biomedical

embrace laser-based additive microfabrication processes, these issues will find solutions. With increasing development and opportunities in the development of hybrid systems, some combining electronics, photonics, and fluidics, and others combining cells in a biocompatible matrix, LIFT will play a significant role in the new paradigm offered by digital microfabrication.

Acknowledgements
P.Serra acknowledges the AEI of the Spanish Government (under Projects TEC2014-54544-C2-1-P and TEC2015-72425-EXP) for its support, and thanks P.Sopeña for his assistance with the edition of the figures. A.Piqué would like to acknowledge the support of the Office of Naval Research (ONR) through the Naval Research Laboratory Basic Research Program.

Received: ((will be filled in by the editorial staff))
Revised: ((will be filled in by the editorial staff))
Published online: ((will be filled in by the editorial staff))

References

[1] K. Chen , W. Gao , S. Emaminejad , D. Kiriya , H. Ota , H.Y.Y. Nyein ,K. Takei , A. Javey, *Adv. Mater*. **2016**, *28*, 4397.

[2] G. E. Moore, (Reprinted in:). *Proc. IEEE* **1998**, *86*, 82.

[3] M. Tudorache, C. Bala, *Anal. Bioanal. Chem.* **2007**, *388*, 565.

[4] A. Carlson, A.M. Bowen, Y. Huang, R.G. Nuzzo, J.A. Rogers, *Adv. Mater.* **2012**, *24*, 5284.

[5] B. Kang, W.H. Lee, K. Cho, *ACS Appl. Mater. Interfaces* **2013**, 5, 2302.

[6] S.H. Kim, K. Hong, W. Xie, K.H. Lee, S. Zhang, T.P. Lodge, C.D. Frisbie, *Adv. Mater.* **2013**, 25, 1822.

[7] H.W. Choi, T. Zhou, M. Singh, G.E. Jabbour, *Nanoscale* **2014**, 1 3338.

[8] Y. Aleeva, B. Pignataro, *J. Mater. Chem. C* **2014**, *2*, 6436.

[9] W.J. Hyun, E.B. Secor, M.C. Hersam, C.D. Frisbie, L.F. Francis, *Adv. Mater.* **2015** *27*, 109.

[10] S. Khan, L. Lorenzelli, R.S. Dahiya, *IEEE Sens. J.* **2015**, 15, 3164.

[11] K.K.B. Hon, L. Li, I.M. Hutchings, *CIRP Ann. Manuf. Technol.*, **2008**, *57*, 601.

[12] A. Piqué, D.B. Chrisey, *Direct-Write Technologies for Rapid Prototyping Applications*, Academic Press, San Diego, CA, USA **2001**.

[13] S. Roy, *J. Phys. D: Appl. Phys.* **2007**, *40*, R413.

[14] R. Abbel, P. Teunissen, E. Rubingh, T. van Lammeren, R. Cauchois, M. Everaars, J. Valeton, S. van de Geijn, P. Groen, *Transl. Mater. Res.* **2014**, *1*, 015002.

[15] T.H.J. van Osch, J. Perelaer, A.W.M. de Laat, U.S. Schubert, *Adv. Mater.* **2008**, *20*, 343.

[16] F. Bonaccorso, A. Bartolotta, J.N. Coleman, C. Backes, *Adv. Mater.* **2016**, *28*, 6136.

[17] D. J. Finn, M. Lotya, J. N. Coleman, *ACS Appl. Mater. Interfaces* **2015**, *7*, 9254.

[18] L.J. Deiner, T.L. Reitz, *Adv. Eng. Mater.* **2017**, *19*, 1600878.

[19] C.B. Arnold, P. Serra, A. Piqué, *MRS Bulletin* **2007**, *32*, 23.

[20] P. Delaporte, A.P. Alloncle, *Opt. Laser Technol.* **2016**, *78*, 33.

[21] R.S. Braudy, *Proc. IEEE* **1969**, *57*, 1771.

[22] M.L. Levene, R.D. Scott, B.W. Siryj, *Appl. Opt.* **1970**, *9*, 2260.

[23] J. Bohandy, B.F. Kim, F.J. Adrian, *J. Appl. Phys.* **1986**, *60*, 1538.

[24] J. Bohandy, B.F. Kim, F.J. Adrian, A.N. Jette, *J. Appl. Phys.* **1988**, *63*, 1158.

[25] P. Mogyorósi, T. Szörényi, K. Bali, Z. Tóth, I. Hevesi, *Appl. Surf. Sci.* **1989**, *36*, 157.

[26] R. J. Baseman, N. M. Froberg, J. C. Andreshak, Z. Schlesinger, *Appl. Phys. Lett.* **1990**, *56*, 1412.

[27] V. Schultze, M. Wagner, *Appl. Phys. A* **1991**, *53*, 241.

[28] Z. Tóth, T. Szörényi, A. L. Tóth, *Appl. Surf. Sci.* **1993**, *69*, 317.

[29] Z. Kántor, Z. Tóth, T. Szörényi, A. L. Tóth, *Appl. Phys. Lett.* **1994**, *64*, 3506.

[30] I. Zergioti, S. Mailis, N.A. Vainos, C. Fotakis, S. Chen, C.P. Grigoropoulos, *Appl. Surf. Sci.* **1998**, *127–129*, 601.

[31] I. Zergioti, S. Mailis, N.A. Vainos, P. Papakonstantinou, C. Kalpouzos, C.P. Grigoropoulos, C. Fotakis, *Appl. Phys. A* **1998**, *66*, 579.

[32] T. Sano, H. Yamada, T. Nakayama, I. Miyamoto, *Appl. Surf. Sci.* **2002**, *186*, 221.

[33] Z. Tóth, T. Szörényi, *Appl. Phys. A* **1991**, *52*, 273.

[34] J.A. Greer, T.E. Parker, *SPIE Proc.* **1988**, *998*, 113.

[35] S. Chakraborty, H. Sakata, E. Yokoyama, M. Wakaki, D. Chakravorty, *Appl. Surf. Sci.* **2007**, *254*, 638.

[36] E. Fogarassy, C. Fuchs, F. Kerherve, G. Hauchecorne, J. Perriere, *J. Appl. Phys.* **1989**, *66*, 457.

[37] D. Toet, M. O. Thompson, P. M. Smith, T. W. Sigmon, *Appl. Phys. Lett.* **1999**, *74*, 2170.

[38] H. Sakata, S. Chakraborty, E. Yokoyama, M. Wakaki, D. Chakravorty, *Appl. Phys. Lett.* **2005**, *86*, 114104.

[39] S. K. Chang-Jian, J. R. Ho, J. W. J. Cheng, C. K. Sung, *Nanotechnology* **2006**, *17*, 1184.

[40] C.W. Cheng, S.C. Liao, H.T. Chen, J.R. Ho, J.W.J. Cheng, H.Y. Liao, L.E. Chou, *SPIE Proc.* **2007**, *6459*, 645910.

[41] B. Thomas, A.P. Alloncle, P. Delaporte, M. Sentis, S. Sanaur, M. Barret, P. Collot, *Appl. Surf. Sci.* **2007**, *254*, 1206.

[42] A. Narazaki, T. Sato, R. Kurosaki, Y. Kawaguchi, H. Niino, *Appl. Phys. Express* **2008**, *1*, 057001.

[43] P. Papakonstantinou, N.A. Vainos, C. Fotakis, *Appl. Surf. Sci.* **1999**, *151*, 159.

[44] G. Hennig, T. Baldermann, C. Nussbaum, M. Rossier, A. Brockelt, L. Schuler, G. Hochstein, *J. Laser Micro/Nanoeng.* **2012**, *7*, 299.

[45] M. Duocastella, A. Patrascioiu, J. M. Fernández-Pradas, J. L. Morenza, P. Serra, *Opt. Express* **2010**, *18*, 21815.

[46] A. Piqué, D.B. Chrisey, R.C.Y. Auyeung, J. Fitz-Gerald, H.D. Wu, R.A. McGill, S. Lakeou, P.K. Wu, V. Nguyen, M. Duignan, *Appl. Phys. A* **1999**, *69*, S279.

[47] P.K. Wu, B.R. Ringeisen, J. Callahan, M. Brooks, D.M. Bubb, H.D. Wu, A. Piqué, B. Spargo, R.A. McGill, D.B. Chrisey *Thin Solid Films* **2001**, *398–399*, 607.

[48] B.R. Ringeisen, D.B. Chrisey, A. Piqué, H.D. Young, R. Modi, M. Bucaro, J. Jones-Meehan, B.J. Spargo, *Biomaterials* **2002**, *23*, 161.

[49] I.Y.S. Lee, X. Wen, W.A. Tolbert, D.D. Dlott, M. Doxtader, D.R. Arnold, *J. Appl. Phys.* **1992**, *72*, 2440.

[50] W.A. Tolbert, I.Y.S. Lee, M.M. Doxtader, E.W. Ellis, D.D. Dlott, *J. Imaging Sci. Technol.* **1993**, *37*, 411.

[51] G.B. Blanchet, Y.L. Loo, J.A. Rogers, F. Gao, C.R. Fincher, *Appl. Phys. Lett.* **2003**, *82*, 463.

[52] M.B. Wolk, J. Baetzold, E. Bellmann, T.R. Hoffend, S. Lamansky, Y. Li, R.R. Roberts, V. Savvateev, J.S. Staral, W.A. Tolbert, *Proc. SPIE* **2004**, *5519*, 12.

[53] B.D. Chin, M.C. Suh, M.H. Kim, T.M. Kang, N.C. Yang, M.W. Song, S.T. Lee, H.H. Kwon, H.K. Chung, *J. Inform. Display* **2003**, *4*, 1.

[54] T. Hirano, K. Matsuo, K. Kohinata, K. Hanawa, T. Matsumi, E. Matsuda, R. Matsuura, T. Ishibashi, A. Yoshida, T. Sasaoka, *SID International Symposium* **2007**, *38*, 1592.

[55] H. Fukumura, Y. Kohji, H. Masuhara, *Appl. Surf. Sci.* **1996**, *96-98*, 569.

[56] H. Fukumura, Y. Kohji, K.I. Nagasawa, H. Masuhara, *J. Am. Chem. Soc.* **1994**, *116*, 10304.

[57] H. Fukumura, H. Uji-i, H. Banjo, H. Masuhara, D.M. Karnakis, N. Ichinose, S. Kawanishi, K. Uchida, M. Irie, *Appl. Surf. Sci.* **1998**, *127-129*, 761.

[58] M. Kishimoto, J. Hobley, M. Goto, H. Fukumura, *Adv. Mat.* **2001**, *13*, 1155.

[59] F.J. Adrian, J. Bohandy, B.F. Kim, A.N. Jette, P. Thompson, *J. Vac. Sci. Technol. B* **1987**, *5*, 1490.

[60] D.A. Willis, "Laser-induced Forward Transfer of Metals," Chapter 7 in Laser Printing of Functional Materials: Electronics, 3D Microfabrication and Biomedicine, Edited by A. Piqué and P. Serra, Wiley-VCH Verlag GmbH & Co., Weinheim, **2018**. ISBN 9783527342129.

[61] L. Yang, C.Y. Yang, X.C. Ni, Z.J. Wang, W. Jia, L. Chai, *Appl. Phys. Lett.* **2006**, *89*, 161110.

[62] D.A. Willis, V. Grosu, *Appl. Phys. Lett.* **2005**, *86*, 244103.

[63] A.I. Kuznetsov, R. Kiyan, B.N. Chichkov, *Opt. Express* **2010**, *18*, 21198.

[64] D.P. Banks, C. Grivas, J.D. Mills, R.W. Eason, I. Zergioti, *Appl. Phys. Lett.* **2006**, *89*, 193107.

[65] A.I. Kuznetsov, C. Unger, J. Koch, B.N. Chichkov, *Appl. Phys. A* **2012**, *106*, 479.

[66] J. Koch, F. Korte, T. Bauer, C. Fallnich, A. Ostendorf, B.N. Chichkov, *Appl. Phys. A* **2005**, *81*, 325.

[67] A.C. Tien, Z.S. Sacks, F.J. Mayer, *Microelectron. Eng.* **2001**, *56*, 273.

[68] A.I. Kuznetsov, J. Koch, B.N. Chichkov, *Opt. Express* **2009**, *17*, 18820.

[69] A.I. Kuznetsov, A.B. Evlyukhin, C. Reinhardt, A. Seidel, R. Kiyan, W. Cheng, A. Ovsianikov, B.N. Chichkov, *J. Opt. Soc. Am. B* **2009**, *26*, B130.

[70] F. Korte, J. Koch, B.N. Chichkov, *Appl. Phys. A* **2004**, *79*, 879.

[71] A.I. Kuznetsov, J. Koch, B.N. Chichkov, *Appl. Phys. A* **2009**, *94*, 221.

[72] U. Zywietz, T. Fischer, A. Evlyukhin, Ca. Reinhardt, B. Chichkov, in *Laser Printing of Functional Materials: Electronics, 3D Microfabrication and Biomedicine* (Eds. A. Piqué, P. Serra), Wiley-VCH, Weinheim, **2018**, Ch 11.

[73] M.P. Giesbers, M.B. Hoppenbrouwers, E.C.P. Smits, R. Mandamparambil, *Proc. SPIE* **2014**, *9135*, 91350Z.

[74] R. Pohl, C.W. Visser, G.R.B.E. Römer, C. Sun, B. Huis in‘t Veld, D. Lohse, *J. Laser Micro/Nanoeng.* **2015**, *10*, 154.

[75] G. Oosterhuis, A. Prenen, A.J. Huis in’t Veld, *ECS Trans.* **2012**, *41*, 81.

[76] C.W. Visser, R. Pohl, C. Sun, B. Huis in ’t Veld, G.W. Römer, D. Lohse, *Adv. Mater.* **2015**, *27*, 4087.

[77] M. Zenou, A. Sa’ar, Z. Kotler, *Sci. Rep.* **2015**, *5*, 17265.

[78] M. Zenou, A. Sa'ar, Z. Kotler, *Small* **2015**, *11*, 4082.

[79] A.I. Kuznetsov, A.B. Evlyukhin, M.R. Gonçalves, C. Reinhardt, A. Koroleva, M.I. Arnedillo, R. Kiyan, O. Marti, B.N. Chichkov, *ACS Nano* **2011**, *5*, 4843.

[80] U. Zywietz, C. Reinhardt, A.B. Evlyukhin, T. Birr, B.N. Chichkov, *Appl. Phys. A* **2014**, *114*, 45.

[81] U. Zywietz, A.B. Evlyukhin, C. Reinhardt, B.N. Chichkov, *Nat. Commun.* **2014**, *5*, 3402.

[82] D.P. Banks, C. Grivas, I. Zergioti, R.W. Eason, *Opt. Express* **2008**, *16*, 3249.

[83] K.S. Kaur, M. Feinaeugle, D.P. Banks, J.Y. Ou, F. Di Pietrantonio, E. Verona, C.L. Sones, R.W. Eason, *Appl. Surf. Sci.* **2011**, *257*, 6650.

[84] C.L. Sones, M. Feinaeugle, A. Sposito, B. Gholipour, R.W. Eason, *Opt. Express* **2012**, *20*, 15171.

[85] M. Feinaeugle, A.P. Alloncle, Ph. Delaporte, C.L. Sones, R.W. Eason, *Appl. Surf. Sci.* **2012**, *258*, 8475.

[86] M. Feinaeugle, C.L. Sones, E. Koukharenko, B. Gholipour, D.W. Hewak, R.W. Eason, *Appl. Phys. A* **2013**, *112*, 1073.

[87] L. Rapp, C. Constantinescu, Y. Larmande, A.P. Alloncle, P. Delaporte, *Appl. Phys. A* **2014**, *117*, 333.

[88] A.J. Birnbaum, H. Kim, N.A. Charipar, A. Piqué, *Appl. Phys. A* **2010**, *99*, 711.

[89] J.M. Fitz-Gerald, A. Pique, D.B. Chrisey, P.D. Rack, M. Zeleznik, R.C.Y. Auyeung, S. Lakeou, *Appl. Phys. Lett.* **2000**, *76*, 1386.

[90] T. Lippert, A. Wokaun, J. Stebani, O. Nuyken, J. Ihlemann, *Angew. Makromol. Chem.* **1993**, *206*, 97.

[91] J. Stebani, O. Nuyken, T. Lippert, A. Wokaun, Makromol. *Chem. Rapid Commun.* **1993**, *14*, 365.

[92] T. Lippert, J.T. Dickinson, *Chem. Rev.* **2003**, *103*, 453.

[93]T. Lippert, T. Nakamura, H. Niino, A. Yabe, *Appl. Surf. Sci.* **1997**, *110*, 227.

[94] R. Fardel, M. Nagel, F. Nuesch, T. Lippert, A. Wokaun, *Appl. Surf. Sci.* **2007**, *254*, 1322.

[95] R. Fardel, M. Nagel, F. Nuesch, T. Lippert, A. Wokaun, *Appl. Phys. Lett.* **2007**, *91*, 061103.

[96] J. Xu, J. Liu, D. Cui, M. Gerhold, A.Y. Wang, M. Nagel, T. Lippert, *Nanotechnology* **2007**, *18*, 025403.

[97] L. Rapp, C. Cibert, S. Nenon, A.P. Alloncle, M. Nagel, T. Lippert, C. Videlot-Ackermann, F. Fages, P. Delaporte, *Appl. Surf. Sci.* **2011**, *257*, 5245.

[98] R. Fardel, M. Nagel, F. Nuesch, T. Lippert, A. Wokaun, *J. Phys. Chem. C* **2010**, *114*, 5617.

[99] T. Mattle, J. Shaw-Stewart, C.W. Schneider, T. Lippert, A. Wokaun, *Appl. Surf. Sci.* **2012**, *258*, 9352.

[100] J. Shaw-Stewart, T. Lippert M. Nagel, F. Nuesch, A. Wokaun, *AIP Conference Proceedings* **2010**, *1278*, 789.

[101] J. Shaw-Stewart, B. Chu, T. Lippert, Y. Maniglio, M. Nagel, F. Nüesch, A. Wokaun, *Appl. Phys. A* **2011**, *105*, 713.

[102] M. Hauer, D. Funk, T. Lippert, A. Wokaun, *Appl. Surf. Sci.* **2003**, *208–209*, 107.

[103] M. Hauer, D. Funk, T. Lippert, A. Wokaun, *Opt. Lasers Eng.* **2005**, *43*, 545.

[104] R. Fardel, M. Nagel, F. Nuesch, T. Lippert, A. Wokaun, B. Luk'yanchuk, *Appl. Phys. A* **2008**, *90*, 661.

[105] R. Fardel, M. Nagel, F. Nuesch, T. Lippert, A. Wokaun, *J. Phys. Chem. C* **2009**, *113*, 11628.

[106] D.P. Banks, K. Kaur, R. Gazia, R. Fardel, M. Nagel, T. Lippert, R. Eason, *Europhys. Lett.* **2008**, *83*, 38003.

[107] J. Chen, A. Palla-Papavlu, Y. Li, L. Chen, M. Dobeli, D. Stender, S. Populoh, A. Weidenkaff, C.W. Schenider, A. Wokaun, T. Lippert, *Appl. Phys. Lett.* **2014**, *104*, 231907.

[108] V. Dinca, A. Palla-Papavlu, M. Dinescu, J. Shaw Stewart, T.K. Lippert, F. Di Pietrantonio, D. Cannata, M. Benetti, E. Verona, *Appl. Phys. A* **2010**, *101*, 559.

[109] V. Dinca, A. Palla-Papavlu, A. Matei, C. Luculescu, M. Dinescu, T. Lippert, F. Di Pietrantonio, D. Cannata, M. Benetti, E. Verona, *Appl. Phys. A* **2010**, *101*, 429.

[110] V. Dinca, T. Mattle, A. Palla-Papavlu, L. Rusen, C. Luculescu, T. Lippert, M. Dinescu, *Appl. Surf. Sci.* **2013**, *278*, 190.

[111] F. Di Pietrantonio, M. Benetti, D. Cannata, E. Verona, A. Palla-Papavlu, V. Dinca, M. Dinescu, T. Mattle, T. Lippert, *Sens. Actuators B* **2012**, *174*, 158.

[112] A. Palla-Papavlu, V. Dinca, I. Paraico, A. Moldovan, J. Shaw-Stewart, C.W. Schneider, E. Kovacs, T. Lippert, M. Dinescu, *J. Appl. Phys.* **2010**, *108*, 033111.

[113] A. Palla-Papavlu, V. Dinca, C. Luculescu, J. Shaw-Stewart, M. Nagel, M. Dinescu, *J. Opt.* **2010**, *12*, 124114.

[114] A. Piqué A, J. Fitz-Gerald J, D.B. Chrisey, R.C.Y. Auyeung, H.D. Wu, S. Lakeou, R.A. McGill, *Proc SPIE* **2000**, *3933*, 105.

[115] B.R. Ringeisen, P.K. Wu, H. Kim, A. Piqué, R.Y.C. Auyeung, H.D.Young, D.B. Chrisey, D.B. Krizman, *Biotechnol. Progr.* **2002**, *18*, 1126.

[116] P.K. Wu, B.R. Ringeisen, D.B. Krizman, C.G. Frondoza, M. Brooks, D.M. Bubb, R.C.Y. Auyeung, A. Piqué, B. Spargo, R.A. McGill, D.B. Chrisey, *Rev. Sci. Instrum.* **2003**, *74*, 2546.

[117] J.A. Barron, H.D. Young, D.D. Dlott, M.M. Darfler, D.B. Krizman, B.R. Ringeisen, *Proteomics* **2005**, *5*, 4138.

[118] M. Colina, M. Duocastella, J.M. Fernández-Pradas, P. Serra, J.L. Morenza, *J. Appl. Phys.* **2006**, *99*, 084909.

[119] M. Duocastella, M. Colina, J.M. Fernández-Pradas, P. Serra, J.L. Morenza, *Appl. Surf. Sci.* **2007**, *253*, 7855.

[120] L. Rapp, J. Ailuno, A.P. Alloncle, P. Delaporte, *Opt. Express* **2011**, *19*, 21563.

[121] M. Makrygianni, I. Kalpyris, C. Boutopoulos, I. Zergioti, *Appl. Surf. Sci.* **2014**, *297*, 40.

[122] M. Duocastella, C. Florian, P. Serra, A. Diaspro, *Sci. Rep.* **2015**, *5*, 16199.

[123] V. Dinca, A. Patrascioiu, J.M. Fernández-Pradas, J.L. Morenza, P. Serra, *Appl. Surf. Sci.* **2012**, *258*, 9379.

[124] J. M. Fernández‐Pradas, P. Sopeña, S. Gonzalez‐Torres, J. Arrese, A. Cirera, P. Serra, *Appl. Phys. A* **2018**, *124*, 214.

[125] T. Inui, R. Mandamparambil, T. Araki, R. Abbel, H. Koga, M. Nogia, K. Suganuma, *RSC Adv.* **2015**, *5*, 77942.

[126] R. Xiong, Z. Zhang, Y. Huang, *J. Manuf. Processes* **2015**, *20*, 450.

[127] R. Xiong, Z. Zhang, J. Shen, Y. Lin, Y. Huang, D.B. Chrisey, *J. Micro Nano-Manuf.* **2015**, *3*, 011004.

[128] R. Xiong, Z. Zhang, W. Chai, Y. Huang, D.B. Chrisey, *Biofabrication* **2015**, *7*, 045011.

[129] D. Muñoz-Martín, C.F. Brasz, Y. Chen, M. Morales, C.B. Arnold, C. Molpeceres, *App. Surf. Sci.* **2016**, *366*, 389.

[130] Z. Zhang, R. Xiong, R. Mei, Y. Huang, D.B. Chrisey, *Langmuir* **2015**, *31*, 6447.

[131] T. Araki, R. Mandamparambil, D.M.P. van Bragt, J. Jiu, H. Koga, J. van den Brand, T. Sekitani, J.M.J. den Toonder, K. Suganuma, *Nanotechnology* **2016**, *27*, 45LT02.

[132] S. Papazoglou, V. Tsouti, S. Chatzandroulis, I. Zergioti, *Opt. Laser Technol.* **2016**, *82*, 163.

[133] P. Sopeña, J. Arrese, S. González-Torres, J.M. Fernández-Pradas, A. Cirera, P. Serra, ACS *Appl. Mater. Interfaces* **2017**, *9*, 29412.

[134] M. Gruene, C. Unger, L. Koch, A. Deiwick, B.N. Chichkov, *Biomed. Eng. Online* **2011**, *10*, 19.

[135] D. Young, R.C.Y. Auyeung, A. Piqué, D.B. Chrisey, D.D. Dlott, *Appl. Phys. Lett.* **2001**, *78*, 3169.

[136] D. Young, R.C.Y. Auyeung, A. Piqué, D.B. Chrisey, D.D. Dlott, *Appl. Surf. Sci.* **2002**, *197–198*, 181.

[137] B. Hopp, T. Smausz, N. Barna, Cs. Vass, Zs. Antal, L. Kredics, D. Chrisey, *J. Phys. D: Appl. Phys.* **2005**, *38*, 833.

[138] M. Duocastella, J.M. Fernández-Pradas, P. Serra, J.L. Morenza, *Appl. Phys. A* **2008**, *93*, 453.

[139] M. Duocastella, J.M. Fernández-Pradas, J.L. Morenza, P. Serra, *J. Appl. Phys.* **2009**, *106*, 084907.

[140] M. Duocastella, J.M. Fernández-Pradas, J.L. Morenza, P. Serra, *Thin Solid Films* **2010**, *518*, 5321.

[141] C. Unger, M. Gruene, L. Koch, J. Koch, B.N. Chichkov, *Appl. Phys. A* **2011**, *103*, 271.

[142] C. Boutopoulos, I. Kalpyris, E. Serpetzoglou, I. Zergioti, *Microfluid. Nanofluid.* **2014**, *16*, 493.

[143] P.B. Robinson, J.R. Blake, T. Kodama, A. Shima, Y. Tomita, *J. Appl. Phys.* **2001**, *89*, 8225.

[144] A. Patrascioiu, J. M. Fernández-Pradas, A. Palla-Papavlu, J. L. Morenza, P. Serra, *Microfluid. Nanofluid.* **2014**, *16*, 55.

[145] J.M. Fernández-Pradas, C. Florian, F. Caballero-Lucas, P. Sopeña, J.L. Morenza, P. Serra, *Appl. Surf. Sci.* **2017**, *418*, 559.

[146] A. Pearson, E. Cox, J.R. Blake, S.R. Otto, *Eng. Anal. Boundary Elem.* **2004**, *28*, 295.

[147] P. Koukouvinis, M. Gavaises, O. Supponen, M. Farhat, *Phys. Fluids* **2016**, *28*, 051203.

[148] M.S. Brown, N.T. Kattamis, C.B. Arnold, *Microfluid. Nanofluid.* **2011**, *11*, 199.

[149] E.A. Brujan, G.S. Keen, A. Vogel, J.R. Blake, *Phys. Fluids* **2002**, *14*, 85.

[150] J. Yan, Y. Huang, C. Xu, D.B. Chrisey, *J. Appl. Phys.* **2012**, *112*, 083105.

[151] M. Duocastella, J.M. Fernández-Pradas, J.L. Morenza, P. Serra, *Appl. Surf. Sci.* **2011**, *257*, 2825.

[152] P. Sopeña, J.M. Fernández-Pradas, P. Serra, *Appl. Surf. Sci.* **2017**, *418*, 530.

[153] N.T. Kattamis, P.E. Purnick, R. Weiss, C.B. Arnold, *Appl. Phys. Lett.* **2007**, *91*, 171120.

[154] M. Duocastella, J.M. Fernández-Pradas, J. Domínguez, P. Serra, J.L. Morenza, *Appl. Phys. A* **2008**, *93*, 941.

[155] P. Serra, M. Duocastella, J.M. Fernández-Pradas, J.L. Morenza, *Appl. Surf. Sci.* **2009**, *255*, 5342.

[156] M. Duocastella, A. Patrascioiu, V. Dinca, J.M. Fernández-Pradas, J.L. Morenza, P. Serra, *Appl. Surf. Sci.* **2011**, *257*, 5255.

[157] M. Duocastella, A. Patrascioiu, J.M. Fernández-Pradas, J.L. Morenza, P. Serra, *Appl. Phys. A* **2012**, *109*, 5.

[158] C. Florian, S. Piazza, A. Diaspro, P. Serra, M. Duocastella, ACS *Appl. Mater. Interfaces* **2016**, *8*, 17028.

[159] E. Biver, L. Rapp, A.P. Alloncle, P. Delaporte, *Appl. Surf. Sci.* **2014**, *302*, 153.

[160] E. Biver, L. Rapp, A.P. Alloncle, P. Serra, P. Delaporte, *Opt. Express* **2014**, *22*, 17122.

[161] A. Patrascioiu, C. Florian, J.M. Fernández-Pradas, J.L. Morenza, G. Hennig, P. Delaporte, P. Serra, *Appl. Phys. Lett.* **2014**, *105*, 014101.

[162] C. F. Brasz, J.H. Yang, C.B. Arnold, *Microfluid. Nanofluid.* **2015**, *18*, 185.

[163] D. Puerto, E. Biver, A.P. Alloncle, P. Delaporte, *Appl. Surf. Sci.* **2016**, *374*, 183.

[164] E. Turkoz, R. Fardel, C.B. Arnold, in *Laser Printing of Functional Materials: Electronics, 3D Microfabrication and Biomedicine* (Eds. A. Piqué, P. Serra), Wiley-VCH, Weinheim, **2018**, Ch 5.

[165] J.M. Fernández-Pradas, M. Colina, P. Serra, J. Domínguez, J.L. Morenza, *Thin Solid Films* **2004**, *453-454*, 27.

[166] P. Serra, J.M. Fernández-Pradas, F.X. Berthet, M. Colina, J. Elvira, J.L. Morenza, *Appl. Phys. A Mater.* **2004**, *79*, 949.

[167] P. Serra, M. Colina, J.M. Fernández-Pradas, L. Sevilla, L., J.L. Morenza, *Appl. Phys. Lett.* **2004**, *85*, 1639.

[168] B. Hopp, T. Smausz, Z .Antal, N. Kresz, Z. Bor, D. Chrisey, *J. Appl. Phys.* **2004**, *96*, 3478.

[169] T. Smausz, B. Hopp, G. Kecskeméti, Z. Bor, *Appl. Surf. Sci.* **2006**, *252*, 4738.

[170] A. Doraiswamy, R. Narayan, T. Lippert, L. Urech, A. Wokaun, M. Nagel, B. Hopp, M. Dinescu, R. Modi, R. Auyeung, D. Chrisey, *Appl. Surf. Sci.* **2006**, *252*, 4743.

[171] A. Palla-Papavlu, I. Paraico, J. Shaw-Stewart, V. Dinca, T. Savopol, E. Kovacs, T. Lippert, A. Wokaun, M. Dinescu, *Appl. Phys. A* **2011**, *102*, 651.

[172] N.T. Kattamis, N.D. McDaniel, S. Bernhard, C.B. Arnold, *Appl. Phys. Lett.* **2009**, *94*, 103306.

[173] E. Turkoz, L. Deike, C.B. Arnold, *Appl. Phys. A* **2017**, *123*, 652.

[174] N.T. Kattamis, M.S. Brown, C.B. Arnold, J. *Mater. Res.* **2011**, *26*, 2438.

[175] M.S. Brown, C. F. Brasz, Y. Ventikos, C.B. Arnold, *J. Fluid Mech.* **2012**, *709*, 341.

[176] C.F. Brasz, C.B. Arnold, H.A. Stone, J.R. Lister, *J. Fluid Mech.* **2015**, *767*, 811.

[177] M. Duocastella, J.M. Fernández-Pradas, J.L. Morenza, D. Zafra, P. Serra, *Sens. Actuators B* **2010**, *145*, 596.

[178] A. Patrascioiu, M. Duocastella, J.M. Fernández-Pradas, J.L. Morenza, P. Serra, *Appl. Surf. Sci.* **2011**, *257*, 5190.

[179] A. Patrascioiu, J.M. Fernández-Pradas, J.L. Morenza, P. Serra, *Appl. Surf. Sci.* **2012**, *258*, 9412.

[180] A. Patrascioiu, J.M. Fernández-Pradas, J.L. Morenza, P. Serra, *Appl. Surf. Sci.* **2014**, *302*, 303.

[181] P. Serra, A. Patrascioiu, J.M. Fernández-Pradas, J.L. Morenza, *Proc. of SPIE* **2013**, *8607* 86070Y.

[182] A. Vogel, K. Nahen, D. Theisen, J. Noack, *IEEE J. Sel. Top. Quantum Electron.* **1996**, *2*, 847.

[183] A. Vogel, *J. Acoust. Soc. Am.* **1996**, *100*, 148.

[184] A. Vogel, J. Noack, K. Nahen, D. Theisen, S. Busch, U. Parlitz, D.X. Hammer, G.D. Noojin, B.A. Rockwell, R. Birngruber, *Appl. Phys. B* **1999**, *68*, 271.

[185] C. B. Schaffer, N. Nishimura, E. N. Glezer, A. M. T. Kim, E. Mazur, *Opt. Express* **2002**, *10*, 196.

[186] J. Zhang, B. Hartmann, G. Marchi, H. Clausen-Schaumann, H. Huber, S. Sudhop, presented at CLEO Europe 2017, Munich, June **2017**.

[187] S. Surdo, R. Carzino, A. Diaspro, M. Duocastella, Adv. Optical Mater. **2018**, 1701190.

[188] S.A. Mathews, N.A. Charipar, R.C.Y. Auyeung, H. Kim, A. Piqué, *Proc. SPIE* **2015**, *9351*, 93510Y.

[189] H. Kim, T.E. Sutto, A. Piqué, *J. Photonics Energy* **2014**, *4*, 040992.

[190] C. Zhang, D. Liu, S.A. Mathews, J. Graves, T.M. Schaefer, B.K. Gilbert, R. Modi, H.D. Wu, D.B. Chrisey, *Microelectron. Eng.* **2003**, *70*, 41.

[191] M. I. Sánchez-Aniorte, B. Mouhamadou, A.P. Alloncle, T. Sarnet, P. Delaporte, *Appl. Phys. A* **2016**, *122*, 595.

[192] R. Wartena, A.E. Curtright, C.B. Arnold, A. Piqué, K.E. Swider-Lyons, *J. Power Sources* **2004**, *126*, 193.

[193] A. Piqué, R.Y.C. Auyeung, H. Kim, K.M. Metkus, S.A. Matthews, *J. Laser Micro/Nanoeng.* **2008**, *3*, 163.

[194] A. Piqué, R.Y.C. Auyeung, K.M. Metkus, H. Kim, S.A. Matthews, T. Bailey, X. Chen, L. J. Young, *Proc. SPIE* **2008**, *6879*, 687911.

[195] D. Soltman, B. Smith, H. Kang, S. J. S. Morris, V. Subramanian, *Langmuir* **2010**, *26*, 15686.

[196] H. Kim, J. S. Melinger, A. Khachatrian, N.A. Charipar, R.C.Y. Auyeung, A. Piqué, *Opt. Lett.* **2010**, *35*, 4039.

[197] A.P. Alloncle, J. Ailuno, L. Rapp and P. Delaporte, *AIP Conf. Proc.* **2012**, *1464*, 358.

[198] Harima Chemicals Inc. Nano Paste® Series. Retrieved from https://www.harima.co.jp/en/randd/products/new_materials.html (accessed 25 January **2018**).

[199] A. Piqué, H. Kim, R.Y.C. Auyeung, *J. Imaging Sci. Technol.* **2013**, *57*, 040404.

[200] S.A. Mathews, R.C.Y. Auyeung, H. Kim, N.A. Charipar, A. Piqué, *J. Appl. Phys.* **2013**, *114*, 064910.

[201] C. Boutopoulos, A.P. Alloncle, I. Zergioti, P. Delaporte, *Appl. Surf. Sci.* **2013**, *278*, 71.

[202] K. S. Kaur, R. Fardel, T. C. May-Smith, M. Nagel, D. P. Banks, C. Grivas, T. Lippert, R. W. Eason, *J. Appl. Phys.* **2009**, *105*, 113119.

[203] M.S. Brown, N.T. Kattamis, C.B. Arnold, *J. Appl. Phys.* **2010**, *107*, 083103.

[204] J. Wang, R. C. Y. Auyeung, H. Kim, N. A. Charipar, A. Piqué, *Adv. Mater.* **2010**, *22*, 4462.

[205] R. C. Y. Auyeung, H. Kim, A. J. Birnbaum, M. Zalalutdinov, S. A. Mathews, A. Piqué, *Appl. Phys. A* **2009**, *97*, 513.

[206] A.J. Birnbaum, M.K. Zalalutdinov, K.J. Wahl, A. Piqué, *J. Microelectromech. Sys.* **2011**, *20*, 36.

[207] R.C.Y. Auyeung, H. Kim, S. Mathews, A. Piqué, *Appl. Opt.* **2015**, *54*, F70.

[208] R.C.Y. Auyeung, H. Kim, S. Mathews, A. Piqué, *Opt. Express* **2015**, *23*, 422.

[209] L. Rapp, A.K. Diallo, A.P. Alloncle, C. Videlot-Ackerman, F. Fages, P. Delaporte, *Appl. Phys. Lett.* **2009**, *95*, 171109.

[210] L. Rapp, A.K. Diallo, S. Nénon, A.P. Alloncle, C. Videlot-Ackerman, F. Fages, M. Nagel, T. Lippert, P. Delaporte, *Thin Solid Films* **2012**, *520*, 3043.

[211] A.K. Diallo, C. Videlot-Ackermann, P. Marsal, H. Brisset, F. Fages, A. Kumagai, N. Yoshimoto, F. Serein-Spirau, J.P. Lere-Porte, *Phys. Chem. Chem. Phys.* **2010**, *12*, 3845.

[212] L. Rapp, F. Serein-Spirau, J.P. Lère-Porte, A.P. Alloncle, P. Delaporte, F. Fages, C. Videlot-Ackermann, *Org. Electron.* **2012**, *13*, 2035.

[213] A.K. Diallo, L. Rapp, S. Nénon, A.P. Alloncle, P. Delaporte, F. Fages, C. Videlot-Ackermann, *Synth. Met.* **2011**, *161*, 888–893.

[214] I. Zergioti, M. Makrygianni, P. Dimitrakis, P. Normand, S. Chatzandroulis, *Appl. Surf. Sci.* **2011**, *257*, 5148.

[215] M. Makrygianni, E. Verrelli, N. Boukos, S. Chatzandroulis, D. Tsoukalas, I. Zergioti, *Appl. Phys. A* **2013**, *110*, 559.

[216] H. Kim, R.C.Y. Auyeung, S.H. Lee, A.L. Huston, A. Piqué, *Appl. Phys. A* **2009**, *96*, 441.

[217] H. Kim, R.C.Y. Auyeung, S.H. Lee, A.L. Huston, A. Piqué, *J. Phys. D: Appl. Phys.* **2010**, *43*, 085101.

[218] L. Rapp, C. Constantinescu, P. Delaporte, A.P. Alloncle, *Org. Electron.* **2014**, *15*, 1868.

[219] C. Constantinescu, A.K. Diallo, L. Rapp, P. Cremillieu, R. Mazurczyk, F. Serein-Spirau, J.P. Lere-Porte, P. Delaporte, A.P. Alloncle, C. Videlot-Ackermann, *Appl. Surf. Sci.* **2015**, *336*, 11.

[220] S.T. Lee, M.C. Suh, T.M. Kang, Y.G. Kwon, J.H. Lee, H.D. Kim, H.K. Chung, *SID Int. Symp. Digest Tech. Pap.* **2007**, *38*, 1588.

[221] S.H. Ko, H. Pan, D. Lee, C.P. Grigoropoulos, H.K. Park, *Jpn. J. Appl. Phys.* **2010**, *49*, 05EC03.

[222] J. Shaw-Stewart, T. Lippert, M. Nagel, F. Nuesch, A. Wokaun, *ACS Appl. Mater. Interfaces* **2011**, *3*, 309.

[223] J. Shaw-Stewart, T. Lippert, M. Nagel, F. Nüesch, A. Wokaun, *Appl. Phys. Lett.* **2012**, *100*, 203303.

[224] N.T. Kattamis, N.D. McDaniel, S. Bernhard, C.B. Arnold, *Org. Electron.* **2011**, *12*, 1152.

[225] D.B. Chrisey, A. Pique, J. Fitz-Gerald, R.C.Y. Auyeung, R.A. McGill, H.D. Wu, M. Duignan, *Appl. Surf. Sci.* **2000**, *154–155*, 593.

[226] M. Duocastella, H. Kim, P. Serra, A. Piqué, *Appl.Phys. A* **2012**, *106*, 471.

[227] A. Palla-Papavlu, C. Córdoba, A. Patrascioiu, J. M. Fernández-Pradas, J. L. Morenza, P. Serra, *Appl. Phys. A* **2013**, *110*, 751.

[228] P.C. Duineveld, *J. Fluid Mech.* **2003**, *477*, 75.

[229] C. Florian, F. Caballero-Lucas, J.M. Fernández-Pradas, R. Artigas, S. Ogier,D. Karnakis, P. Serra, *Appl. Surf. Sci.* **2015**, *336*, 304.

[230] C. Florian, F. Caballero-Lucas, J.M. Fernández-Pradas, S. Ogier, L. Winchester, D. Karnakis, R. Geremia, R. Artigas, P. Serra, *Appl. Surf. Sci.* **2016**, *374*, 265.

[231] J. Chung, S. Ko, N.R. Bieri, C.P. Grigoropoulos, D. Poulikakos, *Appl. Phys. Lett.* **2004**, *84*, 801.

[232] M. Joo, B. Lee, S. Jeong, M. Lee, *Thin Solid Films* **2012**, *520*, 2878.

[233] A. Sridhar, S.M. Perinchery, E.C.P. Smits, R. Mandamparambil, J. van den Brand, *Microelectron. Reliab.* **2015**, *55*, 2324.

[234] R.C.Y. Auyeung, H. Kim, N.A. Charipar, A.J. Birnbaum, S.A. Mathews, A. Piqué, *Appl. Phys. A* **2011**, *102*, 21.

[235] E. Breckenfeld, H. Kim, R.Y.C. Auyeung, N.A. Charipar, P. Serra, A. Piqué, *Appl. Surf. Sci.* **2015**, *331*, 254.

[236] K.S. Kaur, J. Missinne, G. Van Steenberge, *Appl. Phys. Lett.* **2014**, *104*, 061102.

[237] K.S. Kaur, A.Z. Subramanian, P. Cardile, R. Verplancke, J. Van Kerrebrouck, S. Spiga, R. Meyer, J. Bauwelinck, R. Baets, G. Van Steenberge, *Opt. Express* **2015**, *23*, 28264.

[238] K.S. Kaur, G. Van Steenberge, *J. Vis. Exp.* **2015**, *97*, e52623.

[239] C. Constantinescu, L. Rapp, A.K. Diallo, C. Videlot-Ackermann, P. Delaporte, A.P. Alloncle, *Org. Electron.* **2015**, *20*, 1.

[240] C. Constantinescu, L. Rapp, P. Delaporte, A.P. Alloncle, *Appl. Surf. Sci.* **2016**, *374*, 90.

[241] C. Constantinescu, L. Rapp, P. Rotaru, P. Delaporte, A.P. Alloncle, *J. Phys. D: Appl. Phys.* **2016**, *49*, 155301.

[242] C. Visser, R. Pohl, C. Sun, G.W. Römer, B. Huis in't Veld, D. Lohse, *Adv. Mater.* **2015**, *27*, 4087.

[243] J.A. Grant-Jacob, B. Mills, M. Feinaeugle, C.L. Sones, G. Oosterhuis, M.B. Hoppenbrouwers, R.W. Eason, *Opt. Mater. Express* **2013**, *3*, 747.

[244] S. Winter, M. Zenou, Z. Kotler, *J. Phys. D: Appl. Phys.* **2016**, *49*, 165310.

[245] M. Zenou, Z. Kotler, *Opt. Express* **2016**, *24*, 1431.

[246] M. Zenou, A. Sa'ar, Z. Kotler, *Nanotechnology* **2016**, *27*, 015203.

[247] J. Voldman, M.L. Gray, M.A. Schmidt, *Annu. Rev. Biomed. Eng.* **1999**, *1*, 401.

[248] A. Karaiskou, I. Zergioti, C. Fotakis, M. Kapsetaki, D. Kafetzopoulos, *Appl. Surf. Sci.* **2003**, *208-209*, 245.

[249] I. Zergioti, D.G. Papazoglou, A. Karaiskou, C. Fotakis, E. Kapsetaki, D. Kafetzopoulos, *Appl. Phys. Lett.* **2005**, *86*, 163902.

[250] M. Colina, P. Serra, J.M. Fernández-Pradas, L. Sevilla, J.L. Morenza, *Biosens. Bioelectron.* **2005**, *20*, 1638.

[251] V. Dinca, A. Ranella, M. Farsari, D. Kafetzopoulous, M. Dinescu, A. Popescu, C. Fotakis, *Biomed. Microdevices* **2008**, *10*, 719.

[252] V. Dinca, A. Ranella, A. Popescu, M. Dinescu, M. Farsari, C. Fotakis, *Appl. Surf. Sci.* **2007**, *254*, 1164.

[253] D. B. Chrisey, A. Piqué, R.A. McGill, J.S. Horwitz, B.R. Ringeisen, D.M. Bubb, P.K. Wu, *Chem. Rev.* **2003**, *103*, 553.

[254] C.Z. Dinu, V. Dinca, J. Howard, D.B. Chrisey, *Appl. Surf. Sci.* **2007**, *253*, 8119.

[255] M. Farsari, V. Dinca, M. Dinescu, S. Georgiou, C. Fotakis, *Int. J. Nanomanuf.* **2007**, *1*, 762.

[256] V. Dinca, M. Farsari, D. Kafetzopoulous, A. Popescu, M. Dinescu, C. Fotakis, *Thin Solid Films* **2008**, *516*, 6504.

[257] I.N Katis, J.A. Holloway, J. Madsen, S.N. Faust, S.D. Garbis, P.J.S. Smith, D. Voegeli, D.L. Bader, R.W. Eason, C.L. Sones, *Biomicrofluidics* **2014**, *8*, 036502.

[258] V. Dinca, E. Kasotakis, J. Catherine, A. Mourka, A. Ranella, A. Ovsianikov, B.N. Chichkov, M. Farsari, A. Mitraki, C. Fotakis, *Nano Lett.* **2008**, *8*, 538.

[259] V. Dinca, E. Kasotakis, A. Mourka, A. Ranella, M. Farsari, A. Mitraki, C. Fotakis, *Phys. Stat. Sol. (c)* **2008**, *5*, 3576.

[260] G. Tsekenis, M. Chatzipetrou, J. Tanner, S. Chatzandroulis, D. Thanos, D. Tsoukalas, I. Zergioti, *Sens. Actuators B* **2012**, *175*,123.

[261] A. Palla-Papavlu, A. Patrascioiu, F. Di Pietrantonio, J.M. Fernandez-Pradas, D. Cannata, M. Benetti, S. D'Auria, E. Verona, P. Serra, *Sens. Actuators B* **2014**, *192*, 369.

[262] F. Di Pietrantonio, M. Benetti, D. Cannatà, E. Verona, A. Palla-Papavlu, J.M. Fernández-Pradas, P. Serra, M. Staiano, A. Varriale, S. D'Auria, *Biosens. Bioelectron.* **2015**, *67*, 516.

[263] E. Touloupakis, M. Chatzipetrou, C. Boutopoulos, A. Gkouzou, I. Zergioti, I. *Sens. Actuators B* **2014**, *193*, 301.

[264] G. Tsekenis, M.K. Filippidou, M. Chatzipetrou, V. Tsouti, I. Zergioti, S. Chatzandroulis, *Sens. Actuators B* **2015**, *208*, 628.

[265] A. Piqué, R.C.Y. Auyeung, J.L. Stepnowiski, D.W. Weir, C.B. Arnold, R.A. McGill, D.B. Chrisey, *Surf. Coat. Technol.* **2003**, *163–164*, 293.

[266] C. Boutopoulos, C. Pandis, K. Giannakopoulos, P. Pissis, I. Zergioti, *Appl. Phys. Lett.* **2010**, *96*, 041104.

[267] T. Mattle, A. Hintennach, T. Lippert, A. Wokaun, *Appl. Phys. A* **2013**, *110*, 309.

[268] V. Tsouti, C. Boutopoulos, D. Goustouridis, I. Zergioti, P. Normand, D. Tsoukalas, S. Chatzandroulis, *Sens. Actuators B* **2010**, *150*, 148.

[269] V. Dinca, R. Fardel, F. Di Pietrantonio, D. Cannatà, M. Benetti, E. Verona, A. Palla-Papavlu, M. Dinescu, T. Lippert, *Sens.Lett.* **2010**, *8*, 436.

[270] D. Cannata, M. Benetti, F. Di Pietrantonio, E. Verona, A. Palla-Papavlu, V. Dinca, M. Dinescu, T. Lippert, *Sens. Actuators B* **2012**, *173*, 32.

[271] A. Palla-Papavlu, T. Mattle, S. Temmel, U. Lehmann, A. Hintennach, A. Grisel, A. Wokaun, T. Lippert, *Sci. Rep.* **2016**, *6*, 25144.

[272] Y. Lin, Y. Huang, *J. Appl. Phys.* **2011**, *109*, 083107.

[273] J.A. Barron, D.B. Krizman, B.R. Ringeisen, *Ann. Biomed. Eng.* **2005**, *33*, 121.

[274] F. Guillemot, A. Souquet, S. Catros, B. Guillotin, J. Lopez, M. Faucon, B. Pippenger, R. Bareille, M. Rémy, S. Bellance, P. Chabassier, J.C. Fricain, J. Amédée, *Acta Biomater.* **2010**, *6*, 2494.

[275] F. Guillemot, A. Souquet, S. Catros, B. Guillotin, *Nanomedicine* **2010**, *5*, 507.

[276] L. Koch, M. Gruene, C. Unger, B. Chichkov, *Curr. Pharm. Biotechnol.* **2013**, *14*, 91.

[277] D.J. Odde, M.J. Renn, *Trends Biotechnol.* **1999**, *17*, 385.

[278] J.A. Barron, B.R. Ringeisen, H. Kim, B.J. Spargo, D.B. Chrisey, *Thin Solid Films* **2004**, *453–454*, 383.

[279] J.A. Barron, B.J. Spargo, B.R. Ringeisen, *Appl. Phys. A* **2004**, *79*, 1027.

[280] T. M. Patz, A. Doraiswamy, R. J. Narayan, W. He, Y. Zhong, R. Bellamkonda, R. Modi, D. B. Chrisey, *Biomed. Mater. Res. B Appl. Biomater.* **2006**, *78B*, 124.

[281] C.Y. Chen, J.A. Barron, B.R. Ringeisen, *Appl. Surf. Sci.* **2006**, *252*, 8641.

[282] T. Kaji, S. Ito, H. Miyasaka, Y. Hosokawa, H. Masuhara, C. Shukunami, Y. Hiraki, *Appl. Phys. Lett.* **2007**, *91*, 023904.

[283] C.M. Othon, X. Wu, J.J. Anders, B.R. Ringeisen, *Biomed. Mater.* **2008**, *3*, 34101.

[284] Y. Lin, G. Huang, Y. Huang, T.R.J. Tzeng, D.B. Chrisey, *Rapid Prototyp. J.* **2010**, *16*, 202.

[285] M. Gruene, M. Pflaum, A. Deiwick, L. Koch, S. Schlie, C. Unger, M. Wilhelmi, A. Haverich, B.N. Chichkov, *Biofabrication* **2011**, *3*, 15005.

[286] J.A. Barron, R. Rosen, J. Jones-Meehan, B.J. Spargo, S. Belkin, B.R. Ringeisen, *Biosens. Bioelectron.* **2004**, *20*, 246.

[287] J.A. Barron, P. Wu, H.D. Ladouceur, B.R. Ringeisen, *Biomed. Microdevices* **2004**, *6*, 139.

[288] B.R. Ringeisen, H. Kim, J.A. Barron, D.B. Krizman, D.B. Chrisey, S. Jackman, R.Y.C. Auyeung, B.J. Spargo. *Tissue Engineering* **2004**, *10*, 483.

[289] B.R. Ringeisen, C.M. Othon, J.A. Barron, D. Young, B.J. Spargo, *Biotechnol. J.* **2006**, *1*, 930.

[290] B. Hopp, T. Smausz, N. Kresz, N. Barna, Z. Bor, L. Kolozsvári, D.B. Chrisey, A. Szabó, A. Nógrádi. *Tissue Engineering* **2006**, *11*, 1817.

[291] N.R. Schiele, R.A. Koppes, D.T. Corr, K.S. Ellison, D.M. Thompson, L.A. Ligon, T.K.M. Lippert, D.B. Chrisey, *Appl. Surf. Sci.* **2009**, *255*, 5444.

[292] N.R. Schiele, D.T. Corr, Y. Huang, N.A. Raof, Y. Xie, D.B. Chrisey, *Biofabrication* **2010**, *2*, 32001.

[293] S. Catros, B. Guillotin, M. Bacáková, J.C. Fricain, F. Guillemot, *Appl. Surf. Sci.* **2011**, *257*, 5142.

[294] Y. Lin, Y. Huang, D.B. Chrisey, *J. Biomech. Eng.* **2011**, *133*, 025001.

[295] N.A. Raof, N.R. Schiele, Y. Xie, D.B. Chrisey, D.T. Corr, *Biomaterials* **2011**, *32*, 1802.

[296] M. Gruene, M. Pflaum, C. Hess, S.s Diamantouros, S. Schlie, A. Deiwick, L. Koch, M. Wilhelmi, S. Jockenhoevel, A. Haverich, B. Chichkov, *Tissue Eng. Part C Methods* **2011**, *17*, 973.

[297] L. Koch, S. Kuhn, H. Sorg, M. Gruene, S. Schlie, R. Gaebel, B. Polchow, K. Reimers, S. Stoelting, N. Ma, P.M. Vogt, G. Steinhoff, B. Chichkov, *Tissue Eng. Part C Methods* **2009**, *16*, 847.

[298] Y. Lin, Y. Huang, G. Wuang, T.R.J. Tzeng, D.B. Chrisey, *J. Appl. Phys.* **2009**, *106*, 43106.

[299] L. Koch, A. Deiwick, S. Schlie, S. Michael, M. Gruene, V. Coger, D. Zychlinski, A. Schambach, K. Reimers, P.M. Vogt, B. Chichkov, *Biotechnol. Bioeng.* **2012**, *109*, 1855.

[300] S. Michael, H. Sorg, C.T. Peck, L. Koch, A. Deiwick, B. Chichkov, P.M. Vogt, K. Reimers, *PLoS ONE* **2013**, *8*, e57741.

[301] P.K. Wu, B.R. Ringeisen, *Biofabrication* **2010**, *2*, 14111.

[302] R.K. Pirlo, P.K. Wu, J. Liu, B.R. Ringeisen, *Biotechnol. Bioeng.* **2012**, *109*, 262.

[303] R. Gaebel, N. Ma, J. Liu, J. Guan, L. Koch, C. Klopsch, M. Gruene, A. Toelk, W. Wang, P. Mark, F. Wang, B. Chichkov, W. Li, G. Steinhoff, *Biomaterials* **2011**, *32*, 9218.

[304] A. Doraiswamy, R.J. Narayan, M.L. Harris, S.B. Qadri, R. Modi, D.B. Chrisey, *J. Biomed. Mater. Res. A* **2007**, *80A*, 635.

[305] S. Catros, J.C. Fricain, B. Guillotin, B. Pippenger, R. Bareille, M. Remy, E. Lebraud, B. Desbat, J. Amédée, F. Guillemot, *Biofabrication* **2011**, *3*, 25001.

[306] V. Keriquel, F. Guillemot, I. Arnault, B. Guillotin, S. Miraux, J. Amédée, J.C. Fricain, S. Catros, *Biofabrication* **2010**, *2*, 14101.

[307] M. Gruene, M. Pflaum, A. Deiwick, L. Koch, S. Schlie, C. Unger, N. Hofmann, I. Bernemann, B. Glasmacher, B. Chichkov, *Tissue Eng. Part C Methods* **2010**, *17*, 79.

[308] J.L. Curley, S.C. Sklare, D.A. Bowser, J. Saksena, M.J. Moore, D.B. Chrisey, *Biofabrication* **2016**, *8*, 15013.

[309] J. Yan, Y. Huang, D.B. Chrisey, *Biofabrication* **2013**, *5*, 015002.

[310] W. Wang, G. Li, Y. Huang, *J. Manuf. Sci. Eng.* **2009**, *131*, 051013.

[311] W. Wang, Y. Lin, Y. Huang, *J. Manuf. Sci. Eng.* **2011**, *133*, 024502.

[312] H. Kim, M. Duocastella, N.A. Charipar, R.C.Y. Auyeung, A. Piqué, *Appl. Phys. A* **2013**, *113*, 5.

[313] A. Piqué, R.C.Y. Auyeung, H. Kim, N.A. Charipar, S.A. Mathews, *J. Phys. D: Appl. Phys*. **2016**, *49*, 223001.

[314] D. A. McKeown, P. L. Hagans, L. P. L. Carette, A. E. Russell, K. E. Swider, D. R. Rolison, *J. Phys. Chem. B* **1999**, *103*, 4825.

[315] C. B. Arnold, R.C. Wartena, B. Pratap, K.E. Swider-Lyons, A. Piqué, *Proc. SPIE* **2002**, *4637*, 353.

[316] C. B. Arnold, R.C. Wartena, K.E. Swider-Lyons, A. Piqué, *J. Electrochem. Soc.* **2003**, *150*, A571.

[317] H. Kim, R.C.Y. Auyeung, A. Piqué, *J. Power Sources* **2007**, *165*, 413.

[318] J. Bates, N.J. Dudney, B. Neudecker, A. Ueda, C.D. Evans, *J. Electrochem. Soc.* **2000**, *147*, 59.

[319] H. Kim, G.P. Kushto, C.B. Arnold, Z.H. Kafafi, A. Piqué, *Appl. Phys. Lett.* **2004**, *85*, 464.

[320] H. Kim, R.C.Y. Auyeung, M. Ollinger, G.P. Kushto, Z.H. Kafafi, A. Piqué, *Appl. Phys. A* **2006**, *83*, 73.

[321] M. Feinaeugle, C. L. Sones, E. Koukharenko, R. W. Eason, *Smart Mater. Struct.* **2013**, *22*, 115023.

[322] A.S. Holmes, S.M. Saidam, *J. Microelectromech. Syst.* **1998**, *7*, 416.

[323] A.S. Holmes, *SPIE Proc.* **2002**, *4426*, 203.

[324] N.S. Karlitskaya, D.F.D. Lange, R. Sanders, J. Meijer, *SPIE Proc.* **2004**, *5448*, 935.

[325] N.S. Karlitskaya, J. Meijer, D.F.D. Lange, H. Kettelarij, *SPIE Proc.* **2006**, *6261*, 62612P.

[326] S.A. Mathews, R.C.Y. Auyeung, A. Piqué, *J. Laser Micro/Nanoeng.* **2007**, *2*, 103.

[327] A. Piqué, N.A. Charipar, R.C.Y. Auyeung, H. Kim, S.A. Matthews, *Proc. SPIE* **2007**, *6458*, 645802.

[328] S.A. Mathews, N.A. Charipar, K. Metkus, A. Piqué, *Photonics Spectra* **2007**, *41*, 70.

[329] A. Piqué, N.A. Charipar, H. Kim, R.C.Y. Auyeung, S.A. Matthews, *Proc. SPIE* **2007**, 6606, 66060R.

[330] V. Marinov, O. Swenson, Y. Atanasov, N. Schneck, *Microelectron. Eng.* **2013**, *101* 23.

[331] E.E. Kuran, Y. Berg, M. Tichem, Z. Kotler, *J. Micromech. Microeng.* **2015**, *25*, 045008.

[332] A. Piqué, N.A. Charipar, R.C.Y. Auyeung, S. A. Mathews, H. Kim, "Laser Transfer of Entire Structures and Functional Devices," Chapter 18 in Laser Printing of Functional Materials: Electronics, 3D Microfabrication and Biomedicine, Edited by A. Piqué and P. Serra, Wiley-VCH Verlag GmbH & Co., Weinheim, pages 427 - 444, (**2018**). ISBN 9783527342129

[333] I. Beniam, S. Mathews, N. Charipar, R. Auyeung, A. Piqué, *SPIE Proc.* **2016**, *9738*, 97380I.

[334] Orbotech, Inc., Flat Panel Display – FPD / Repair, retrieved from https://www.orbotech.com/products/categories/fpd/array-repair-systems (accessed 16 February **2018**).

[335] High Performance Laser Additive Manufacturing. Retrieved from https://www.hiperlam.eu (accessed 16 February **2018**).

[336] Poietis, Inc., Laser assisted bioprinting of living tissue, retrieved from http://poietis.com/en/index.php#frontPage (accessed 16 February **2018**).

Figure captions

Figure 1. Schematic (not to scale) illustrating the main elements in a system for laser-induced forward transfer or LIFT.

Figure 2. SEM images illustrating the wide range of morphologies generated by LIFT of metals undergoing phase change, i.e. melting and vaporization, during the transfer process. a) Transfers onto glass substrates from an Al donor film, 0.8 μm thick with a 40 ns laser pulse. Reproduced with permission. [27] Copyright 1991, Elsevier. b), c) LIFT of Cu dots deposited on quartz substrate by fs LIFT with a laser pulse energy of 11 J and 6.5 J, respectively. Reproduced with permission. [61] Copyright 2006, American Institute of Physics. d) LIFT of a 60 nm gold donor film using a 30 fs laser pulse (image taken at an angle of 45°). Reproduced with permission. [63] Copyright 2010, Optical Society of America. e) Laser-induced jet formation on Al donor film after laser pulse. Reproduced with permission. [62] Copyright 2005, American Institute of Physics. f) Laser-induced nanobump/nanojet structure, slightly etched by an ion beam, revealing a counterjet underneath the nanobump. Reproduced with permission. [71] Copyright 2010, Springer.

Figure 3. LIFT of nanoparticles corresponding to four different materials: Au, Cu, Ge and Si on insulator. The SEM images on the left side show the donor surface after transfer at increasing laser fluence (from left to right), while the image on the right side shows nanoparticles transferred on the receiving substrate. Jets resolidified during transfer are apparent in the donor surface for Au and Cu. Reproduced with permission. [72] Copyright 2018, Wiley-VCH.

Figure 4. a) Schematic diagram of an LDT multilayered stack. The functional release layer is a 2 μm thick Ag nanopaste layer spin-coated with a 1.8 μm thick photoresist layer. SEM image of b) a cross section of a transferred multilayer stack (cured at 200 °C) on Si, part of which is exposed by focused ion beam (FIB) milling. SEM image c) of Ag/polymer stacks with various planar areas transferred onto silicon. d) Capacitance versus area/dielectric thickness for a Ag/photoresist (1818) stack. Reproduced with permission. [88] Copyright 2010, Springer.

Figure 5. LIFT with a DRL. a) Sketch of the transfer process. The DRL vaporizes or decomposes after laser irradiation and only the irradiated portion of the donor film is transferred. b) Optical microscopy image of a polystyrene microbeads pixel transferred on a Thermanox coverslip by using a TP-DRL. The pixel reproduces well the squared shape of the laser spot on the donor film. The scale bar corresponds to 100 μm. The red arrow indicates an isolated microbead. c) Stop-action movie of an ejection event. Images acquisition delays after the laser pulse are indicated in the lower part of the frames. The laser beam impinges from the right, and both the ejected shock wave and flyer are perfectly visible. Reproduced with permission. [112] Copyright 2010, AIP Publishing LLC.

Figure 6. Sketch of the LIFT of liquid films illustrating the jetting dynamics. The donor/receiver system is translated from left to right while circular droplets are being printed.

Figure 7. Optical microscopy image of an array of droplets of a water/glycerol solution printed through LIFT on a glass substrate at constant laser fluence and varying gap between donor and receiving substrate. This result shows that it is possible to print uniform droplets for gaps as large as 2 mm. Reproduced with permission. [155] Copyright 2009, Elsevier.

Figure 8. a) Optical microscopy images of droplets of a water/glycerol solution printed through LIFT on a glass substrate at constant laser fluence and varying spacing between them. It is shown that there is a range of overlaps between consecutive droplets allowing to print continuous lines. Very large overlaps lead to undesired bulging. Scale bar corresponds to 100 µm. b) Optical microscopy image of an entire area of a water/glycerol solution containing an odorant-binding protein printed through LIFT on a surface acoustic wave resonator. As in the previous example, the right droplet overlap allows printing areas. Scale bar corresponds to 200 µm. Reproduced with permission. [227] Copyright 2013, Springer Nature.

Figure 9. Stop-action movie displaying the characteristic jetting dynamics corresponding to the LIFT of liquid donor films. The donor film is located in the upper part of the images and the laser beam is impinging from above. The images acquisition delay after the laser pulse are indicated in the upper part of the frames. The donor liquid is a water/glycerol solution and the receiving substrate is glass. The movie shows that the sessile droplet is generated through contact of the laser-induced jet with the receiving substrate.

Figure 10. a) Sketch of bubble expansion and jet formation in the LIFT of liquid donor films. Red arrows indicate pressure exerted by the bubble on the liquid film. Black arrows indicate liquid flow induced by pressure gradients. b) Detail of a snapshot displaying the re-entrant jet inside the expanding bubble. Reproduced with permission. [148] Copyright 2011, Springer Nature.

Figure 11. Stop-action movie of LIFT printing from liquid donor films in bubble contact mode. As in Figure 4.2.1, the donor film is located in the upper part of the images and the laser beam is impinging from above. The images acquisition delay after the laser pulse is indicated in the upper part of the frames. The donor liquid is a commercially available Ag ink and the receiving substrate is glass. It can be appreciated that the sessile droplet is generated through contact of the expanding bubble with the receiving substrate. The relatively poor quality of the images is due to the small gap between donor and receiver required for the bubble contact mode. Reproduced with permission. [152] Copyright 2017, Elsevier.

Figure 12. Evolution of the droplets morphology with laser fluence during LIFT of a commercially available Ag ink on a silicon dioxide on silicon substrate a) with no DRL and b) with a Ti-DRL. It is observed that more consistent results are obtained when LIFT is carried out with a Ti-DRL. Reproduced with permission. [121] Copyright 2014, Elsevier.

Figure 13. Plot of the LIFTed droplet volume versus laser fluence for three different donor film thicknesses (indicated in the plot legend). The donor liquid is a water/glycerol solution, the receiving substrate is glass, and LIFT was carried out by using a Ti-DRL. A linear dependence between volume and laser fluence is observed. The three thicknesses present the same fluence threshold for deposition. Reproduced with permission. [156] Copyright 2011, Elsevier.

Figure 14. Sketch of the laser absorption process during the LIFT of liquid donor films for a) direct absorption within the ink, b) absorption within a metallic DRL through vaporization of the adjacent ink and c) absorption in BA-LIFT through production of a rapidly-expanding, sealed blister. Reproduced with permission. [164] Copyright 2018, Wiley-VCH.

Figure 15. Sketch of FF-LIFT in a) backward and b) forward configuration. c) Stop-action movie of liquid ejection during FF-LIFT of a water/glycerol solution in the absence of receiving substrate. The images acquisition delay after the laser pulse is indicated below each

frame. The movie allows tracking the evolution of both laser-generated bubble and jet. After a first expansion and collapse, the bubble splits into two daughter bubbles that expand again while sinking inside the bulk liquid. Reproduced with permission. [144] Copyright 2013, Springer Nature.

Figure 16. Comparison of laser transfers of low-viscosity Ag ink and high-viscosity Ag nanopaste on Si. SEM images of laser transfers of a) nanoink and d) nanopaste with a square laser beam profile (insets). AFM height profiles of laser transfers of b) nanoink and e) nanopaste with a rectangular beam profile. SEM images of a grid, laser printed with multiple voxels of c) nanoink and with a single (gridded) voxel of f) nanopaste. Reproduced with permission. [199] Copyright 2013, Society for Imaging Science and Technology.

Figure 17. a) Sketch of single-step laser printing of multi-stack OLEDs through a DRL. b) Optical microscopy image of three operating OLEDs of different colors printed through LIFT. The respective blue, green and red emission proves the functionality of the devices. c) Electro-luminescence spectra of the printed OLEDs (dots) compared to those of others fabricated through spin-coating (solid line). Reproduced with permission. [223] Copyright 2012, AIP Publishing LLC.

Figure 18. Fluorescence image obtained after hybridization of a laser printed microarray containing two human DNA strands (MAPK3 (columns 1, 4, 7) and ETS2 (columns 3, 6, 9)) and a DNA-free control solution (columns 2, 5, 8). The red and green emission in the positions where the DNAs were printed, as well as the absence of emission in the control positions, prove the functionality of the device. Reproduced with permission. [167] Copyright 2004, AIP Publishing LLC.

Figure 19. a) Sketch of the LIFT setup for the layer-by-layer approach for the printing of cells. b) Grid structure of fibroblasts (green) and keratinocytes (red) printed through LIFT. c) Seven-layer construct of red and green keratinocytes printed in the same way. d) Detail of the previous structure. Scale bars correspond to 500 μm. Reproduced with permission. [299] Copyright 2012, John Wiley and Sons.

Figure 20. Y-shaped tubes printed through LIFT by using a sodium alginate solution. The insets show different views of the printed tubes. This result represents a remarkable step forward for laser printing towards solving vascularization problems in tissue engineering applications. Reproduced with permission. [128] Copyright 2015, IOP Publishing.

Figure 21. SEM images corresponding to examples of 3D microfabricated structures made by LIFT. a) Printed pyramid stacks. b) Printed vertical interconnects generated by repeated transfers over the same region on the receiving substrate. c) Cross-over interconnects made by combining the printing of vertical stacks capped with free-standing cross-overs. d) Folded interconnects. Reproduced with permission. [313] Copyright 2016, IOP Publishing.

Figure 22. a) Schematic of the LIFT of metal droplets with ultra-short laser pulses ($\lambda = 515$, $\tau = 6.7$ ps). b) Sample copper pillar with a cross section of 5 μm and height up to 2 mm. c–e) Close-up showing the uniform cross-section along the length of one such pillar. f) SEM images of copper voxels deposited over a copper film at fluences of (i) 0.38, (ii) 0.44, (iii) 0.63 and (iv) 0.82 mJ/cm^2 showing the change in morphology after solidification as a function of the laser energy. Reproduced with permission. [76] Copyright 2015, John Wiley and Sons.

Figure 23. a) Cross-sectional schematic diagram (not to scale) of a typical Li- ion microbattery printed by LIFT. b) Cross-sectional SEM micrograph of a packaged thick-film Li-ion microbattery. The layers visible (from top to bottom) are: (1) Cu current collector, (2) carbon anode, (3) gel-polymer electrolyte (GPE) soaked separator, (4) LiCoO2 cathode, and (5) Al current collector. The GPE soaked separator is marked by black dashed lines. Reproduced with permission. [317] Copyright 2007, Elsevier.

Figure 24. a) Schematic cross section illustrating a dye-sensitized solar cell. b) Photograph of a packaged dye-sensitized solar cell fabricated with a laser-transferred nc-TiO2 electrode. SEM micrographs showing c) the cross section and d) the surface of a 12-μm thick nc-TiO2 layer printed by LIFT on fluorine-doped tin-oxide coated glass. The film was sintered at 450 °C for 30 min. Reproduced with permission. [189] Copyright 2014, SPIE.

Figure 25. a) Schematic (not to scale) illustrating the laser-mediated steps to produce embedded electronics by (i) laser machining a pocket, (ii) LIFT a device into the pocket, and (iii) LIFT the interconnects. b) Example of a LED array made with bare die LED using lase-and-place, with the insert showing the LEDs emitting blue light when the circuit is powered. c) Embedded blinker circuit made by lase-and-place with inset showing the bare die timing chip. Reproduced with permission. [313] Copyright 2016, IOP Publishing.

Figure 26. Images of representative structures transferred by lase-and-place. a) SEM of nickel nanorod (200 nm dia. and 10 μm long) across silicon pods. b) SEM of a copper film (10 μm wide, 50 μm long and 500 nm thick) over SU-8 pads. c) Optical micrograph of a copper foil (150 μm wide, 1 mm long and 25 μm thick) connecting two capacitors using silver paste. d) Similar to (c) this time the copper foil was laser-shaped prior to being transferred. Reproduced with permission. [332] Copyright 2018, Wiley-VCH.

Figure 27. Four-color Lasersonic® printing machine with unwinder and rewinder unit of the substrate, ink mixing and supply tanks, printing units, and human interfaces. The inking modules on top can be exchanged within a few minutes to vary between different inks or ink sequences. Reproduced with permission. [44] Copyright 2012, Japanese Laser Society.

Biographies

Pere Serra is professor at the Department of Applied Physics of the University of Barcelona. He received his Ph.D. from that university in 1997. His research has been devoted to multiple topics in the laser materials processing area, from pulsed laser deposition to laser surface treatments. In the last years he has focused his activity on laser microfabrication, with special attention to laser printing technologies for the fabrication of biomedical and printed electronics devices.

Alberto Piqué is Head of the Materials and Systems Branch at the U.S. Naval Research Laboratory He holds a B.S. and M.S. in Physics from Rutgers University and a Ph.D. in Materials Science and Engineering from the University of Maryland. His research focuses on the study and applications of laser-material interactions. He and his group have pioneered the use of laser-based direct-write techniques for additive manufacturing of electronic, sensor and micro-power generation devices.

Table of contents

Printing materials with light. This review paper aims to be a complete review of laser-induced forward transfer, a direct-writing technique allowing to print a broad range of materials in both solid and liquid state. The review encompasses the fundamental aspects of the technique, as well as the applications, which range from printed electronics to tissue engineering.

Figure 1

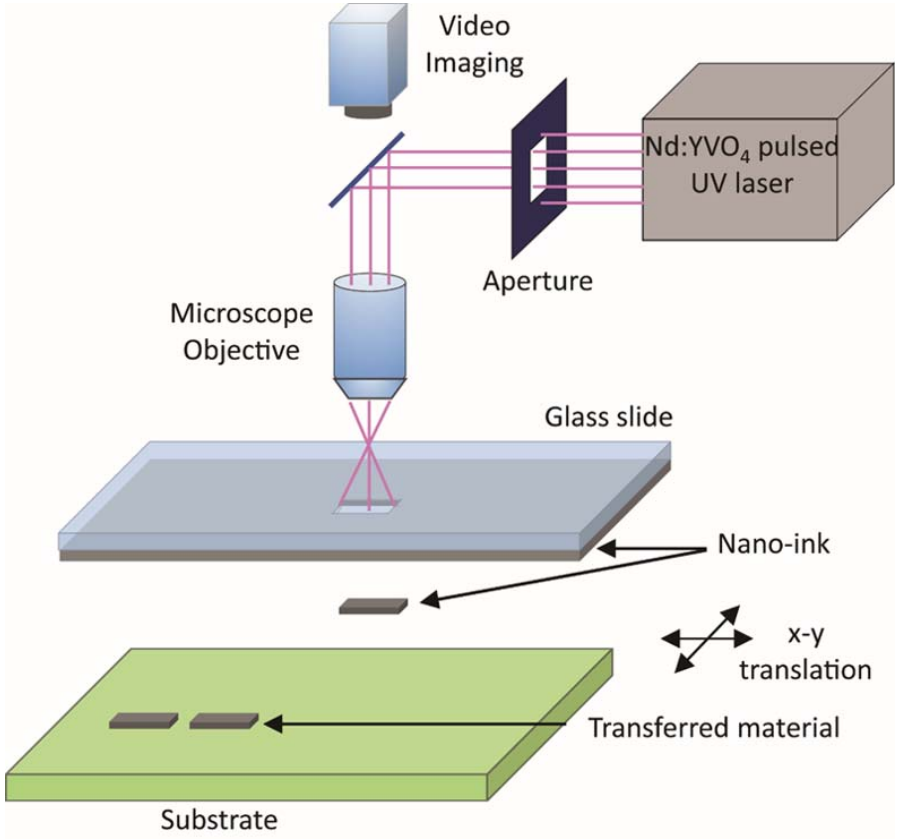
Video
Imaging
Nd:YVO4 pulsed
UV laser
Aperture
Microscope
Objective
Glass slide
Nano-ink
x-y
translation
Transferred material
Substrate

Figure 2

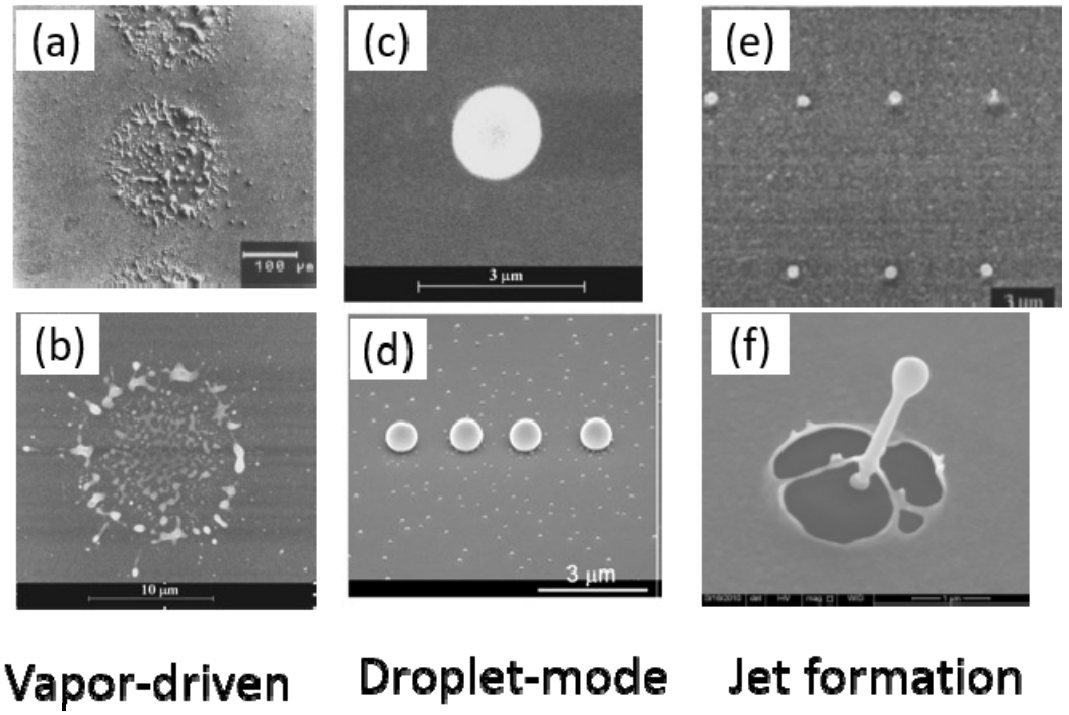
(a)
(c)
(e)
(b)
(d)
(f)
3 µm
10 µm
3 µm
Vapor-driven
Droplet-mode
Jet formation

Figure 3

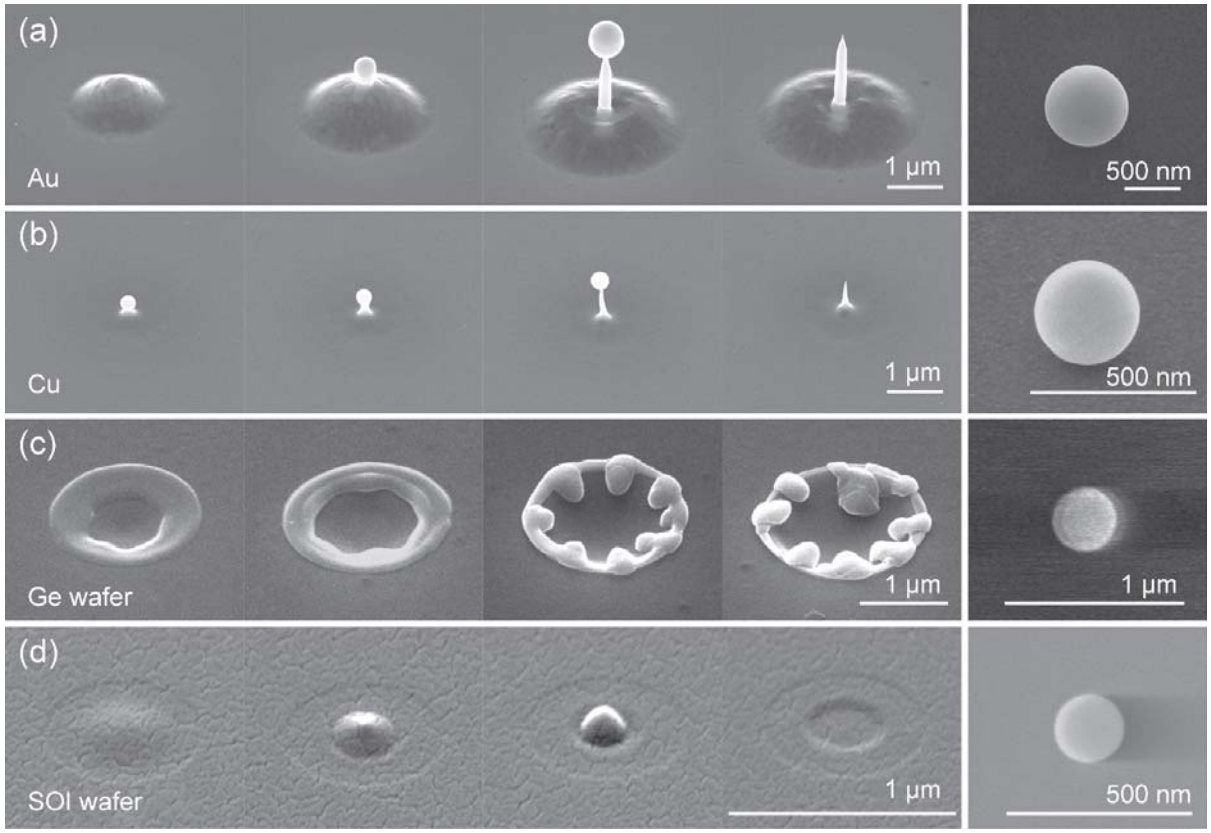
(a)
Au
1 μm
500 nm
(b)
Cu
1 μm
500 nm
(c)
Ge wafer
1 μm
1 μm
(d)
SOI wafer
1 μm
500 nm

Figure 4

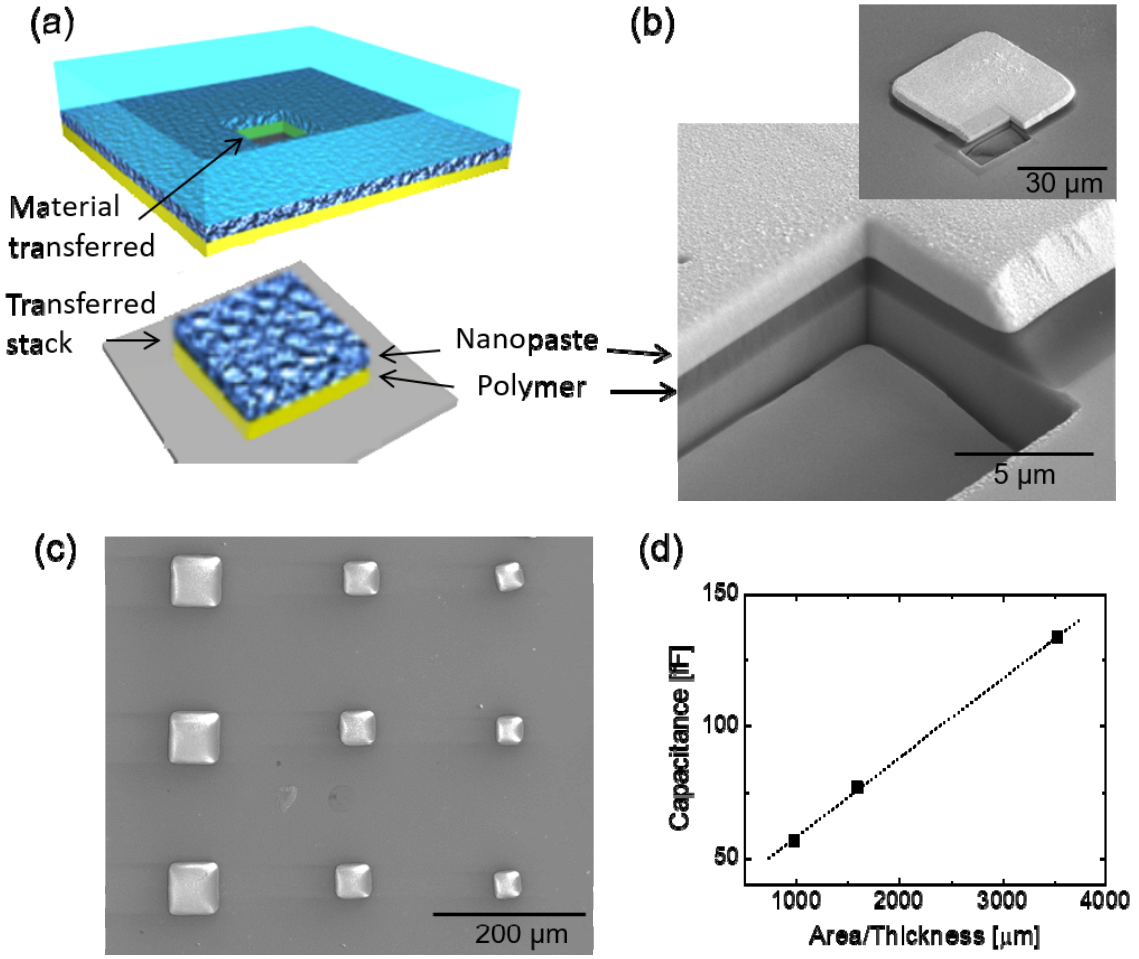
(a)
Material transferred
Transferred stack
Nanopaste
Polymer
(b)
30 µm
5 µm
(c)
200 µm
(d)
Capacitance [fF]
150
100
50
1000
2000
3000
4000
Area/Thickness [µm]

Figure 5

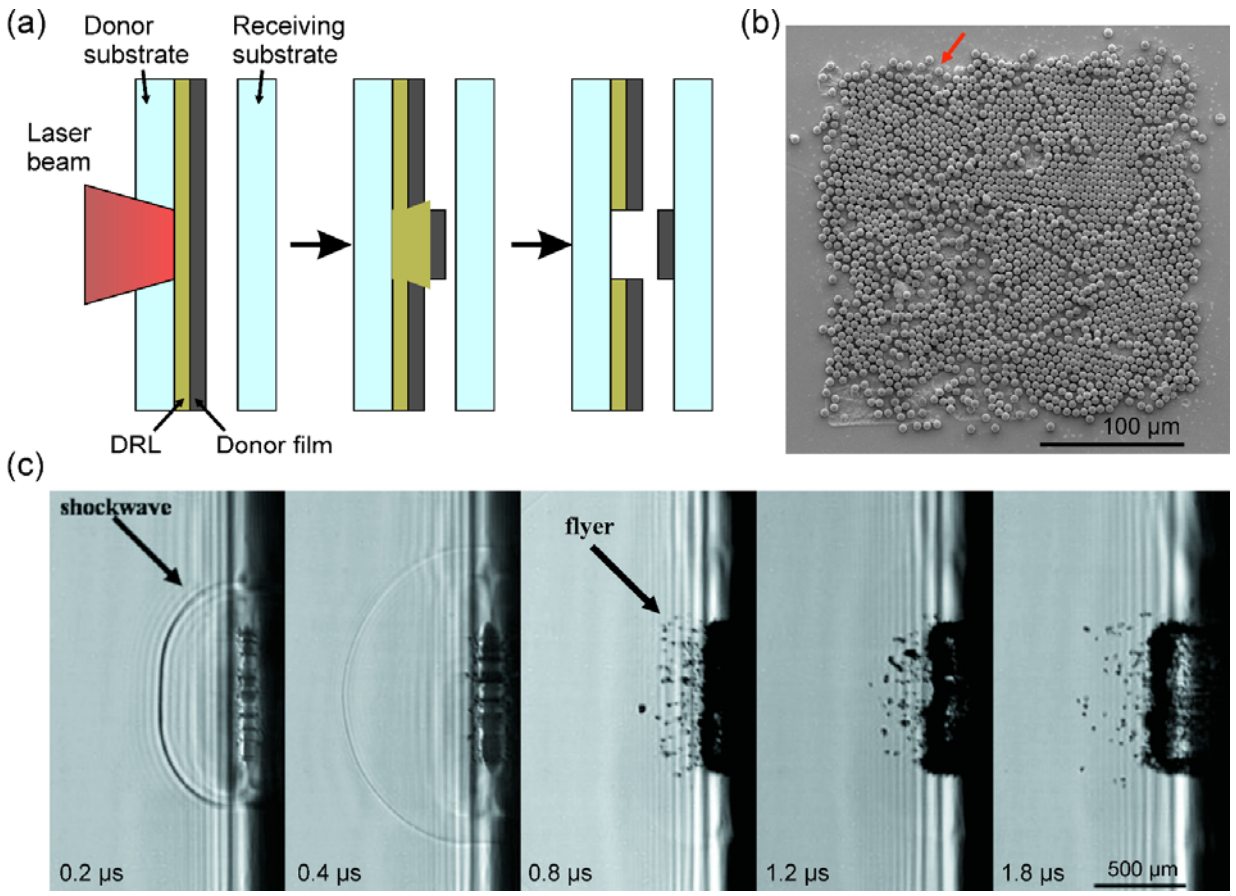
(a)
Donor substrate
Receiving substrate
Laser beam
DRL
Donor film
(b)
100 μm
(c)
shockwave
flyer
0.2 μs
0.4 μs
0.8 μs
1.2 μs
1.8 μs
500 μm

Figure 6

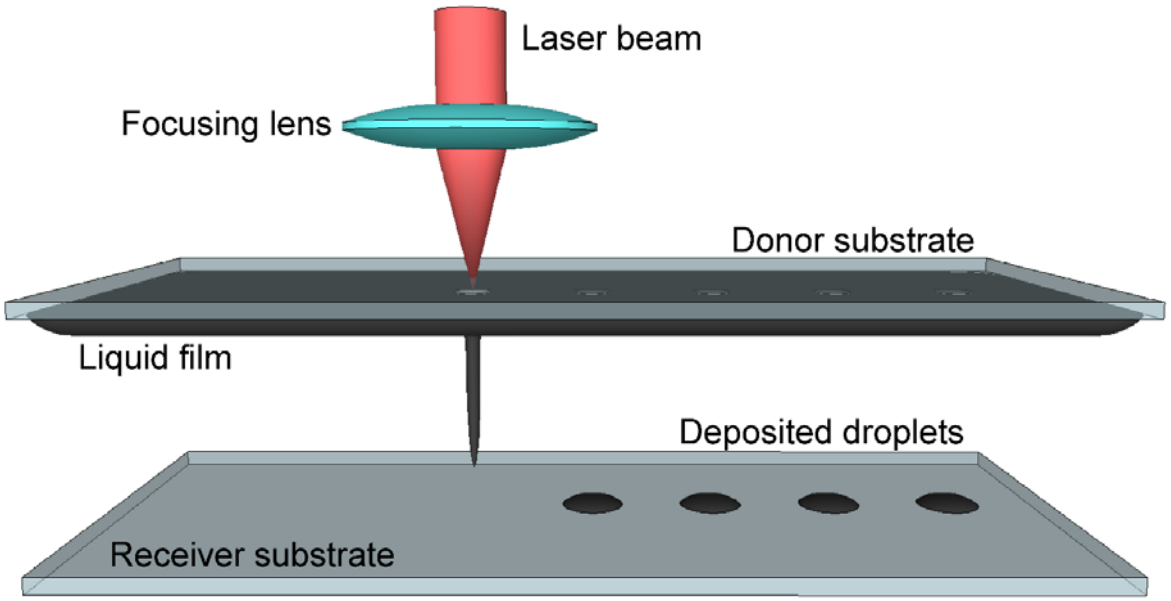
Laser beam
Focusing lens
Donor substrate
Liquid film
Deposited droplets
Receiver substrate

Figure 7

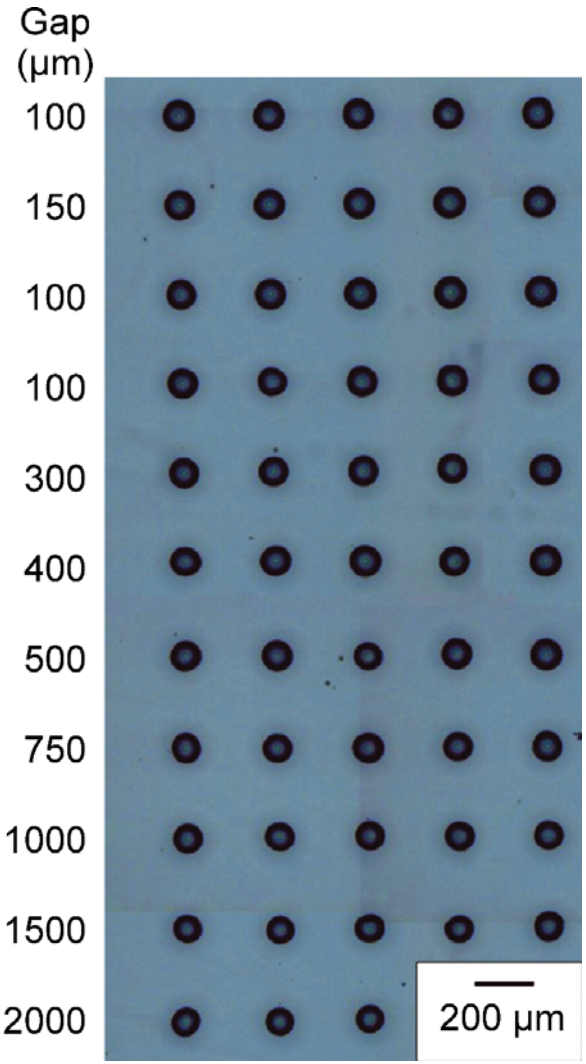

Figure 8

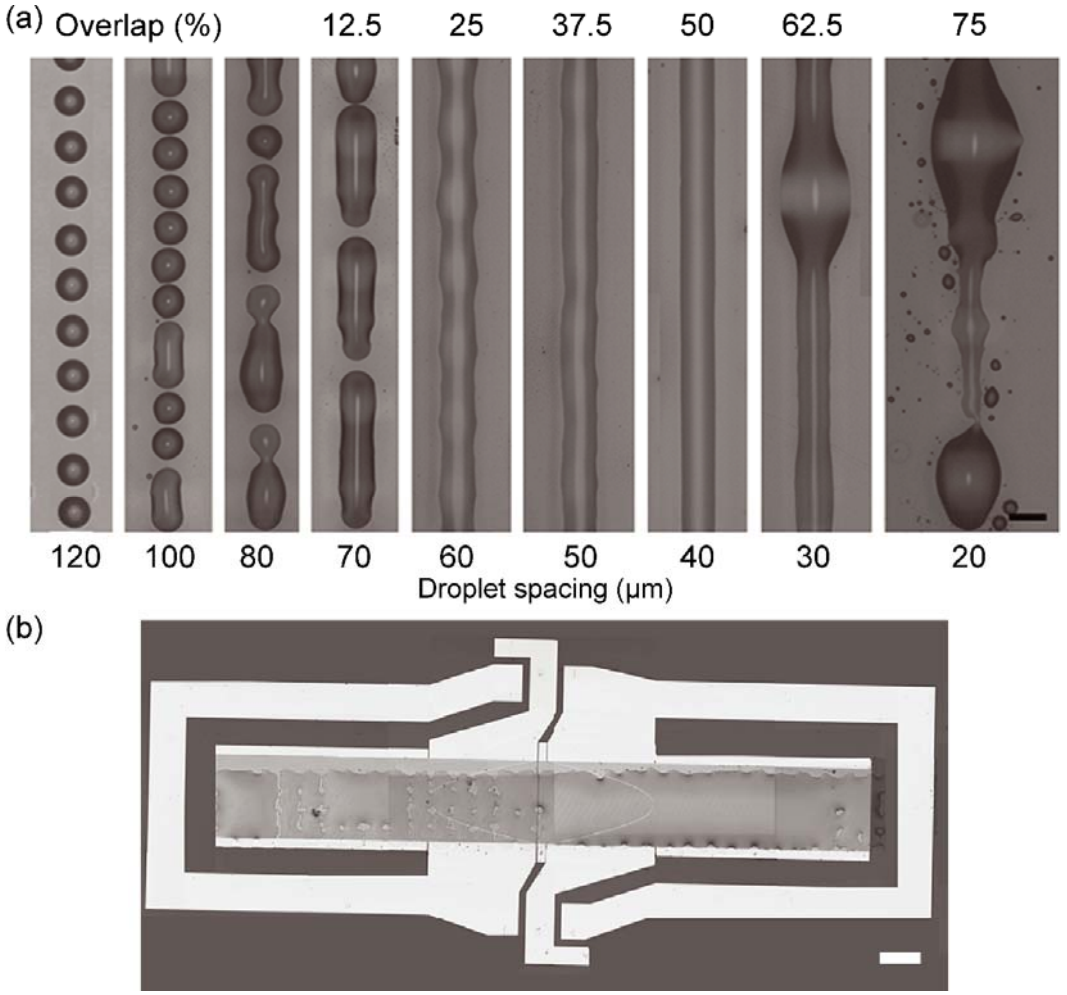
(a)
Overlap (%)
12.5
25
37.5
50
62.5
75
120
100
80
70
60
50
40
30
20
Droplet spacing (μm)
(b)

Figure 9

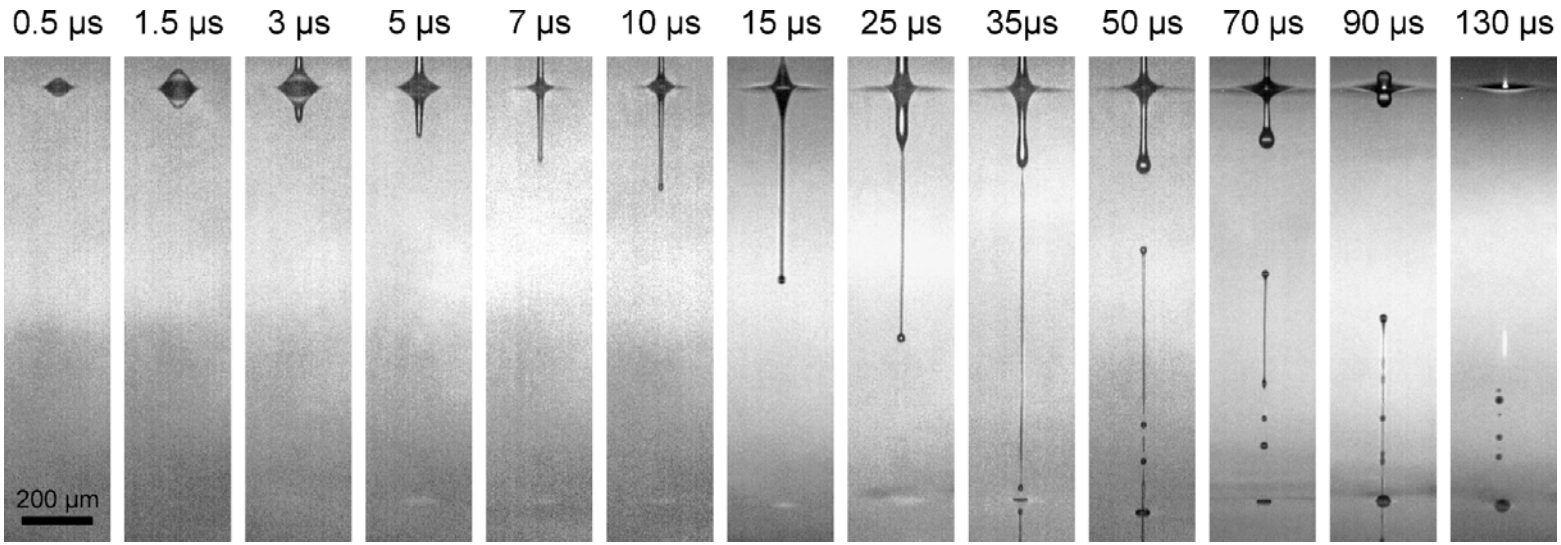
0.5 µs
1.5 µs
3 µs
5 µs
7 µs
10 µs
15 µs
25 µs
35µs
50 µs
70 µs
90 µs
130 µs
200 µm

Figure 10

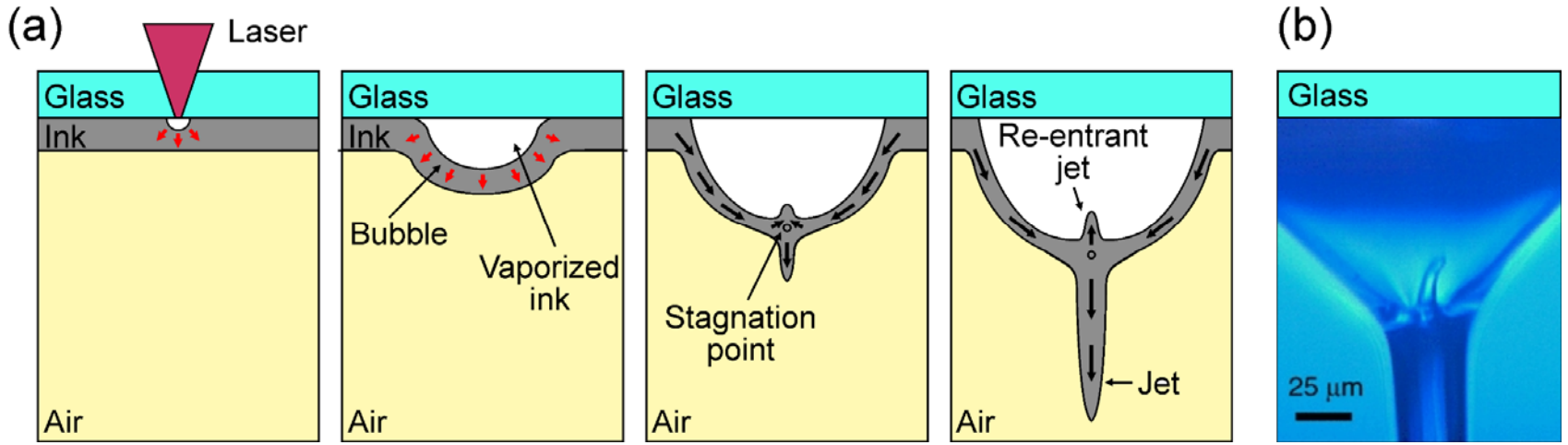
(a)
Laser
Glass
Ink
Air
Glass
Ink
Bubble
Vaporized ink
Air
Glass
Stagnation point
Air
Glass
Re-entrant jet
Jet
Air
(b)
Glass
25 μm

Figure 11

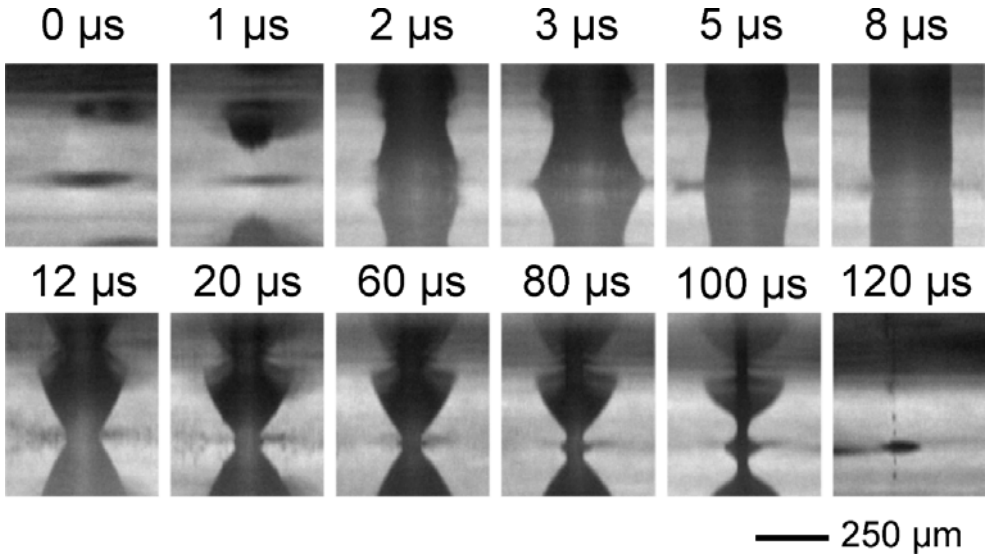

Figure 12

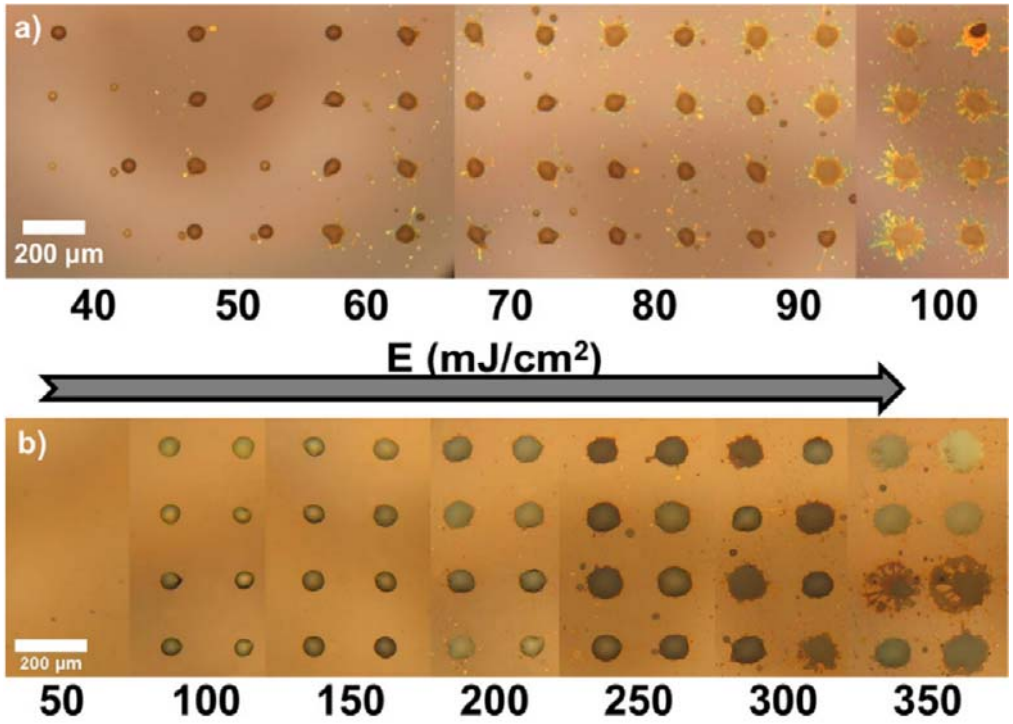
a)
200 µm
40
50
60
70
80
90
100
E (mJ/cm²)
b)
200 µm
50
100
150
200
250
300
350

Figure 13

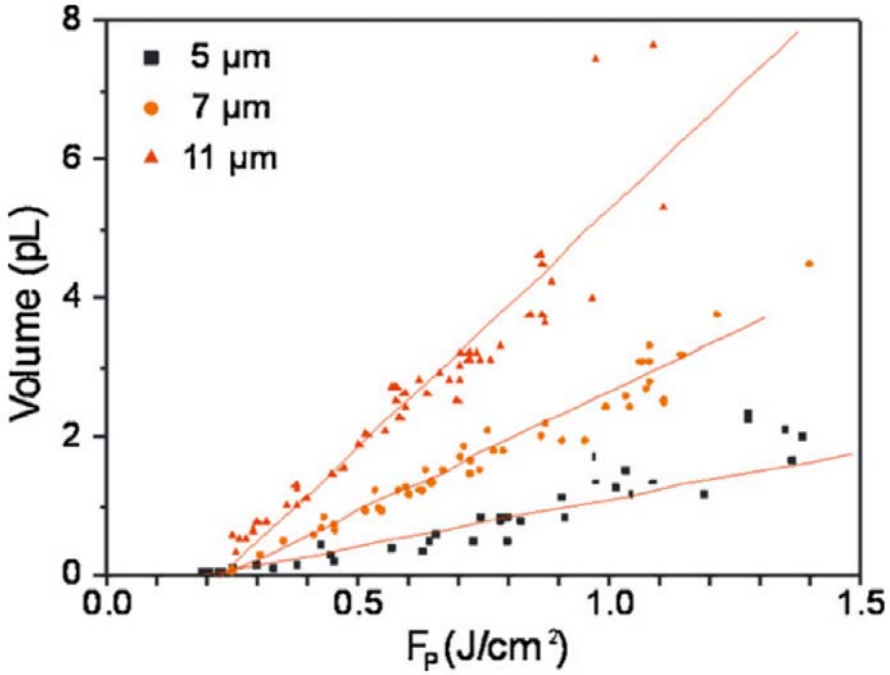

Figure 14

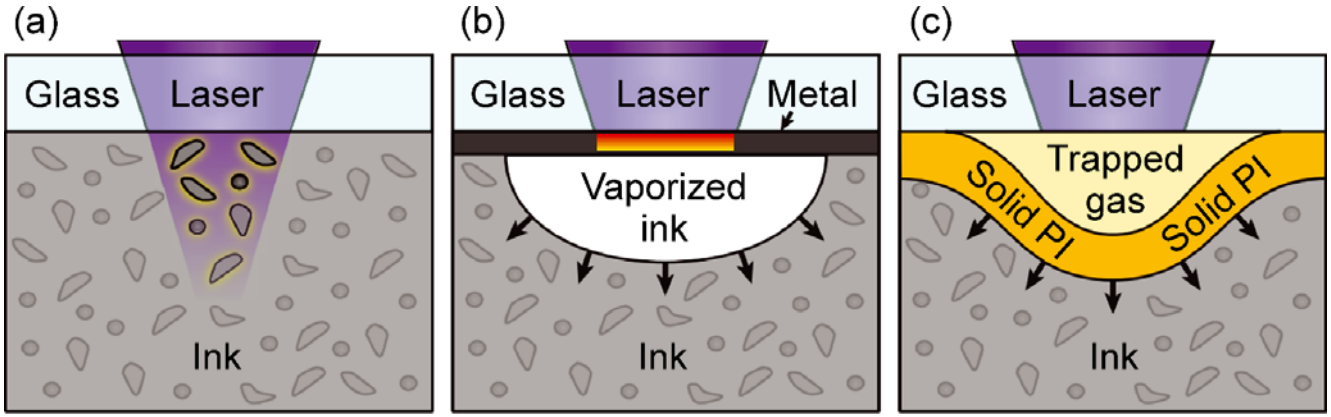
(a)
Glass
Laser
Ink
(b)
Glass
Laser
Metal
Vaporized
ink
Ink
(c)
Glass
Laser
Trapped
gas
Solid PI
Solid PI
Ink

Figure 15

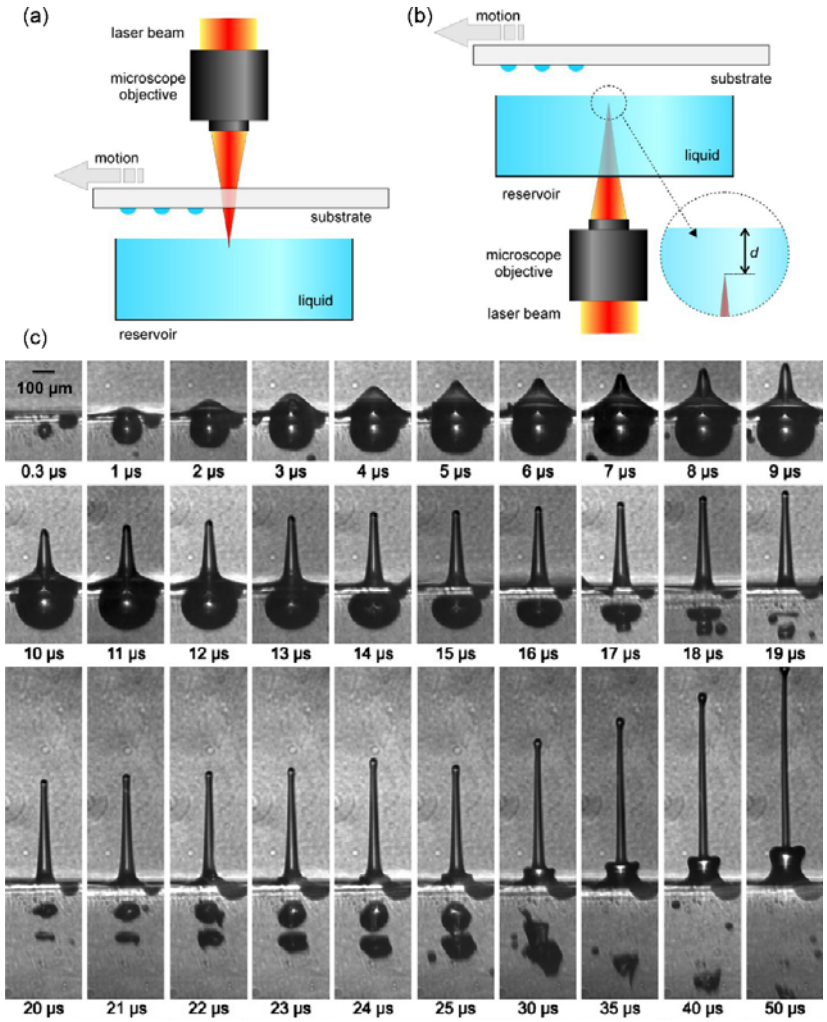
(a)
laser beam
microscope objective
motion
substrate
liquid
reservoir
(b)
motion
substrate
liquid
reservoir
microscope objective
laser beam
d
(c)
100 µm
0.3 µs
1 µs
2 µs
3 µs
4 µs
5 µs
6 µs
7 µs
8 µs
9 µs
10 µs
11 µs
12 µs
13 µs
14 µs
15 µs
16 µs
17 µs
18 µs
19 µs
20 µs
21 µs
22 µs
23 µs
24 µs
25 µs
30 µs
35 µs
40 µs
50 µs

Figure 16

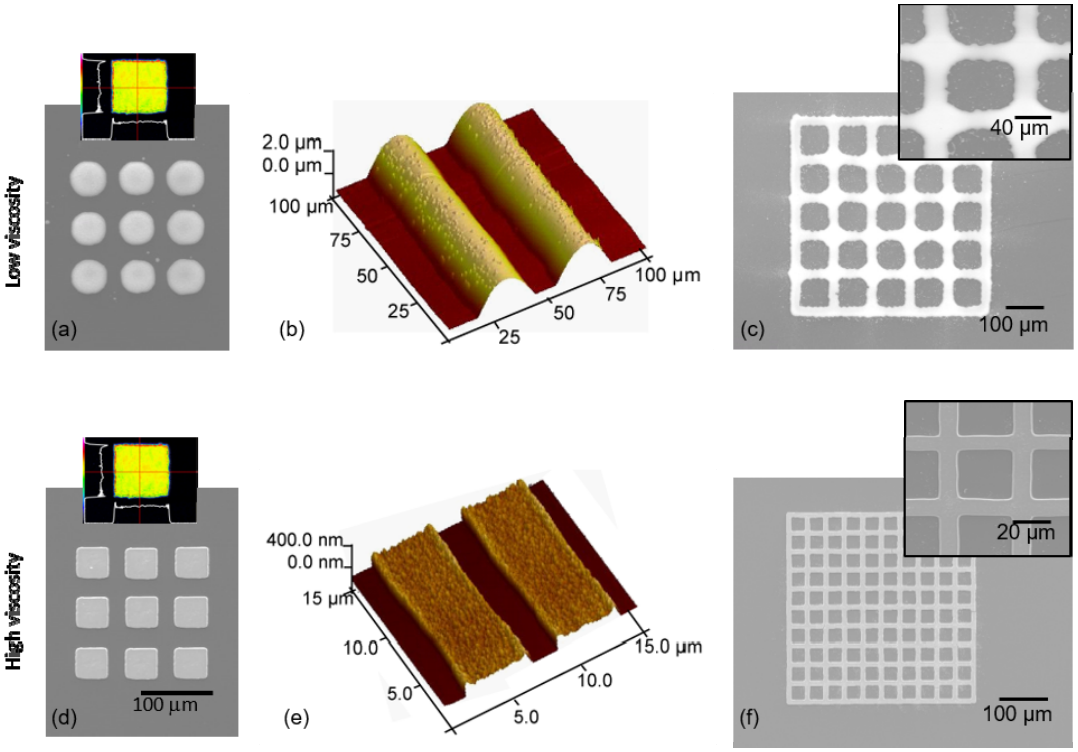
Low viscosity
(a)
2.0 µm
0.0 µm
100 µm
75
50
25
25
50
75
100 µm
(b)
40 µm
100 µm
(c)
High viscosity
100 µm
(d)
400.0 nm
0.0 nm
15 µm
10.0
5.0
5.0
10.0
15.0 µm
(e)
20 µm
100 µm
(f)

Figure 17

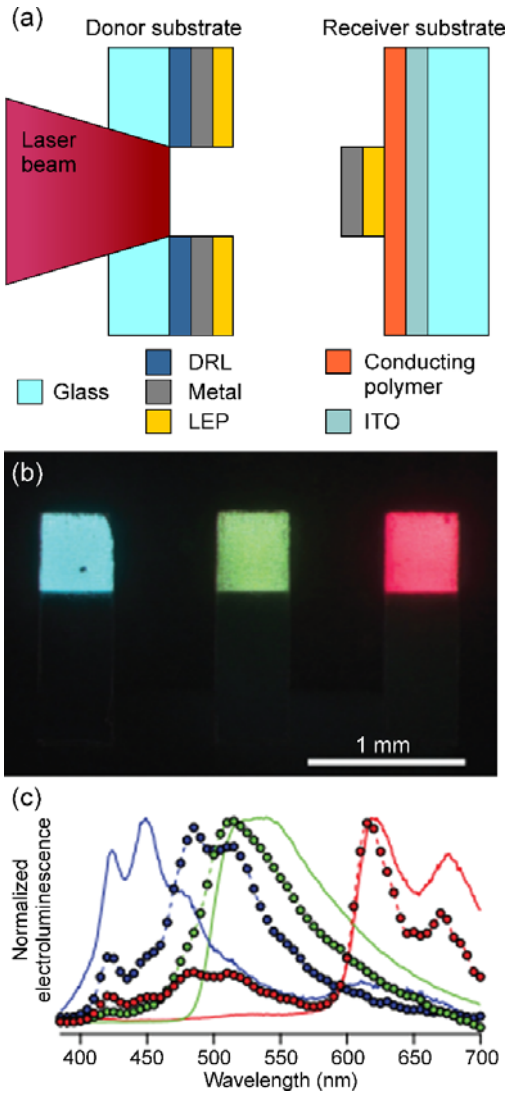
(a)
Donor substrate
Receiver substrate
Laser beam
Glass
DRL
Metal
LEP
Conducting polymer
ITO
(b)
1 mm
(c)
Normalized electroluminescence
400
450
500
550
600
650
700
Wavelength (nm)

Figure 18

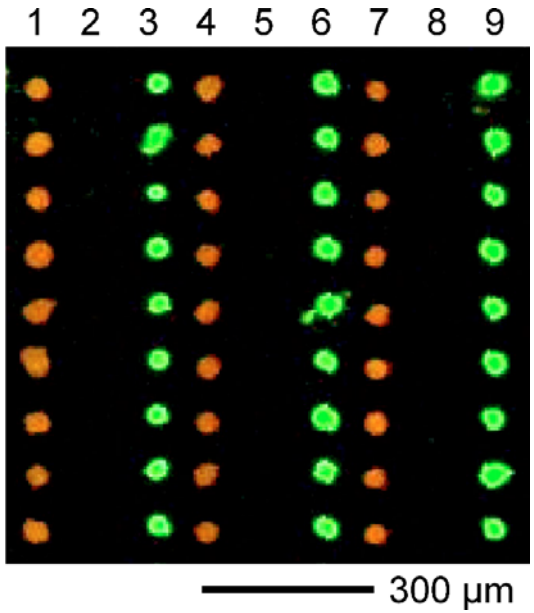

Figure 19

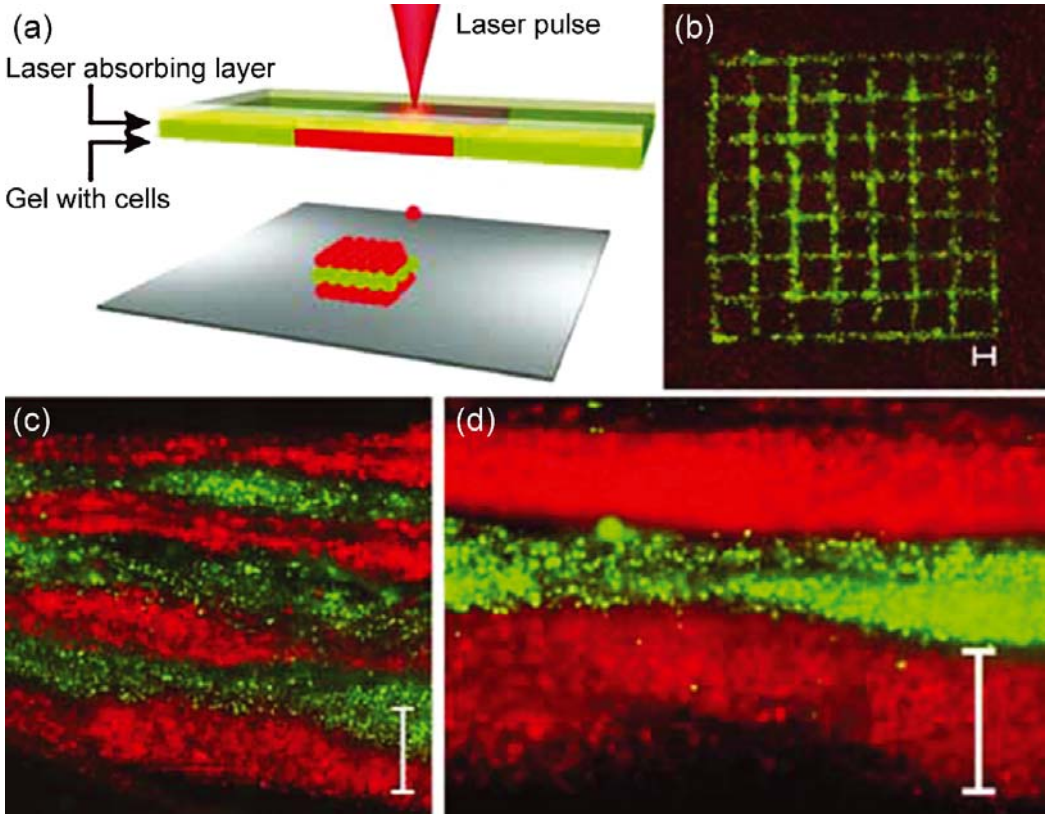

Figure 20

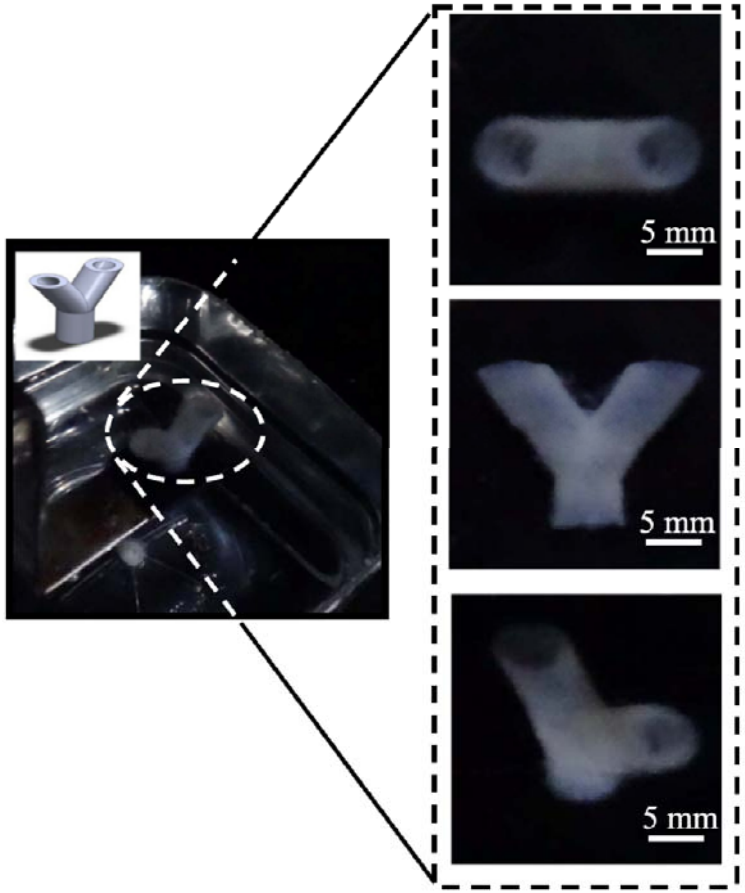

Figure 21

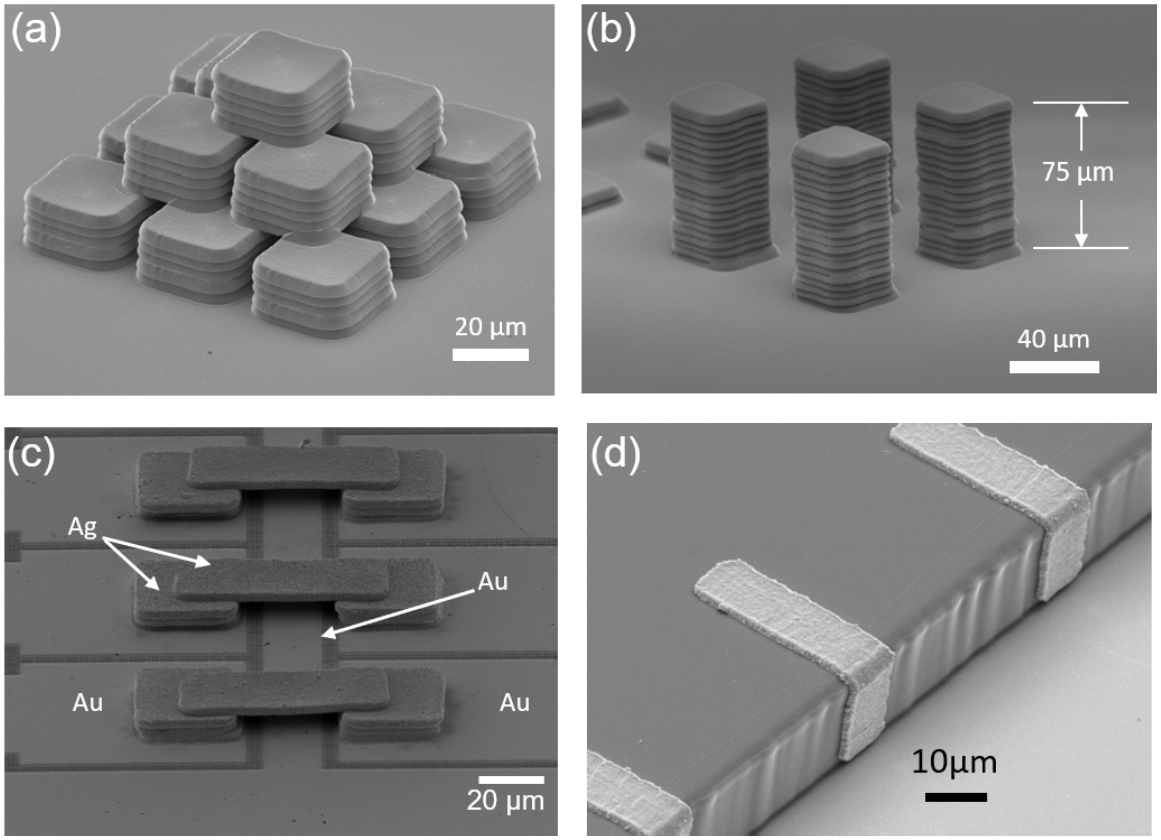

Figure 22

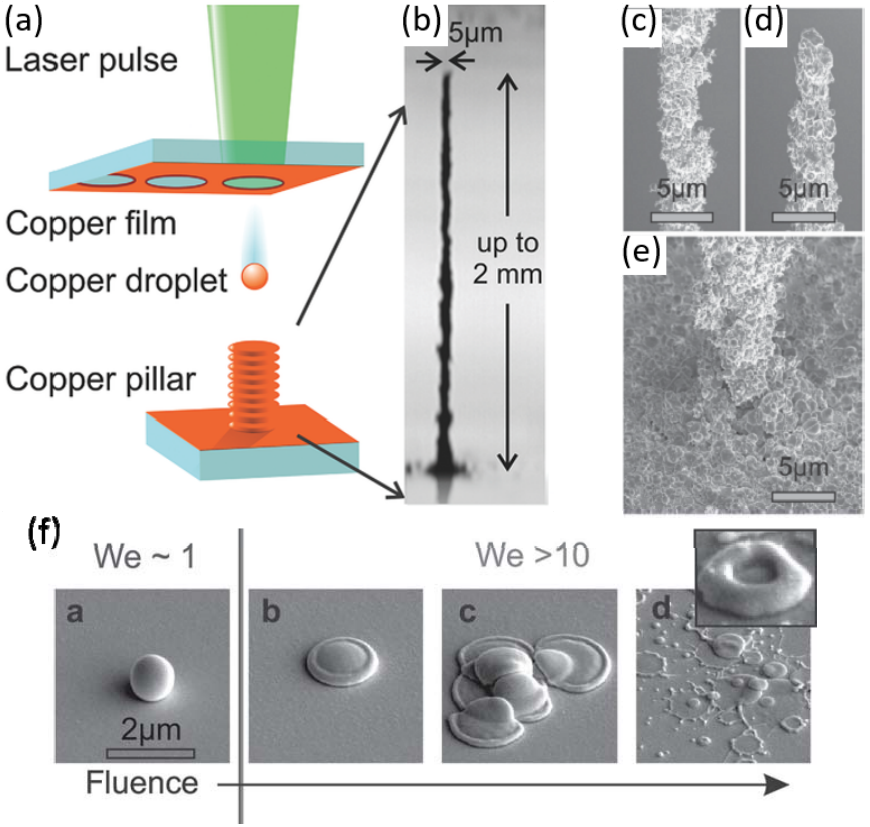
(a)
Laser pulse
Copper film
Copper droplet
Copper pillar
(b)
5μm
up to
2 mm
(c)
5μm
(d)
5μm
(e)
5μm
(f)
We ~ 1
We >10
a
2μm
b
c
d
Fluence

Figure 23

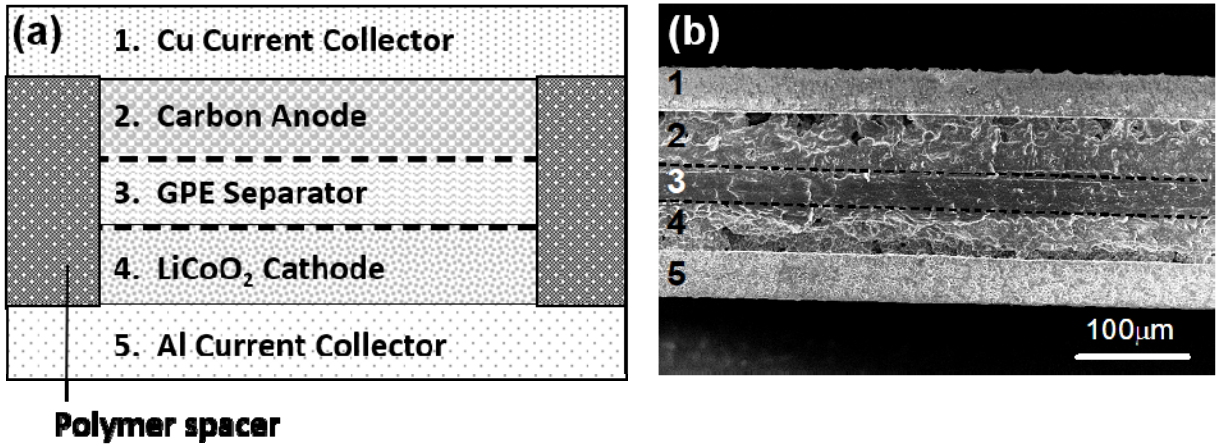
(a)
1. Cu Current Collector
2. Carbon Anode
3. GPE Separator
4. LiCoO2 Cathode
5. Al Current Collector
Polymer spacer
(b)
1
2
3
4
5
100μm

Figure 24

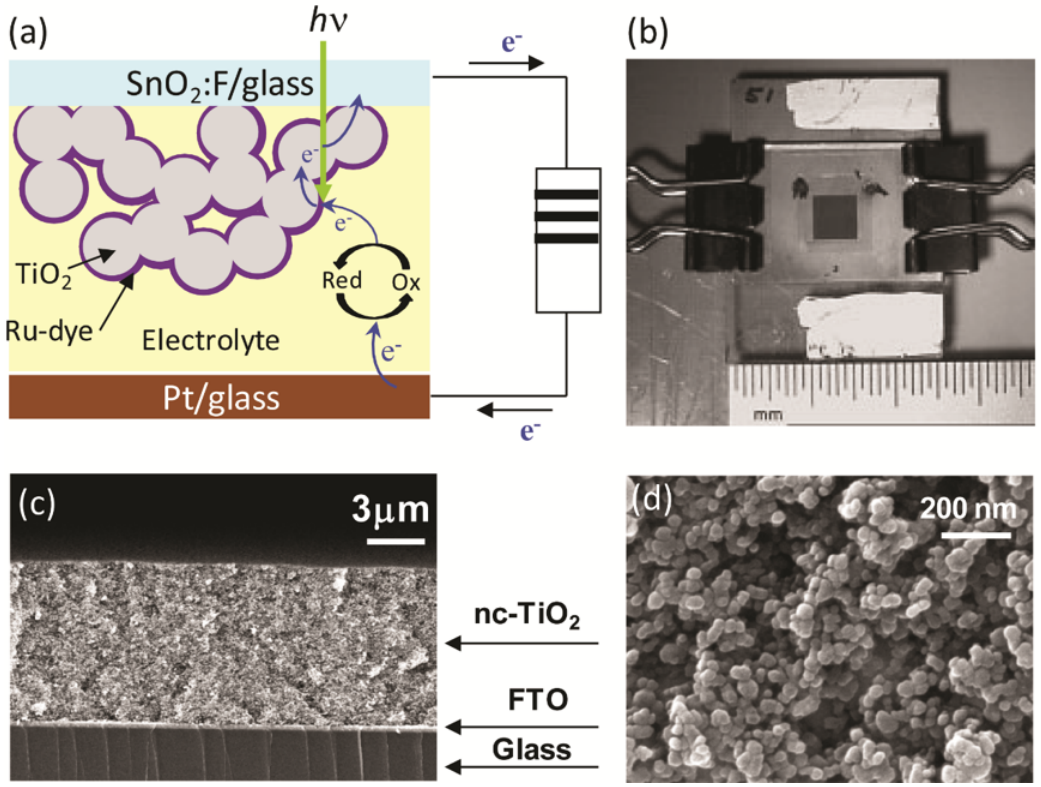
(a)
hν
e⁻
SnO2:F/glass
e⁻
e⁻
TiO2
Red
Ox
Ru-dye
Electrolyte
e⁻
Pt/glass
e⁻
(b)
(c)
3μm
nc-TiO2
FTO
Glass
(d)
200 nm

Figure 25

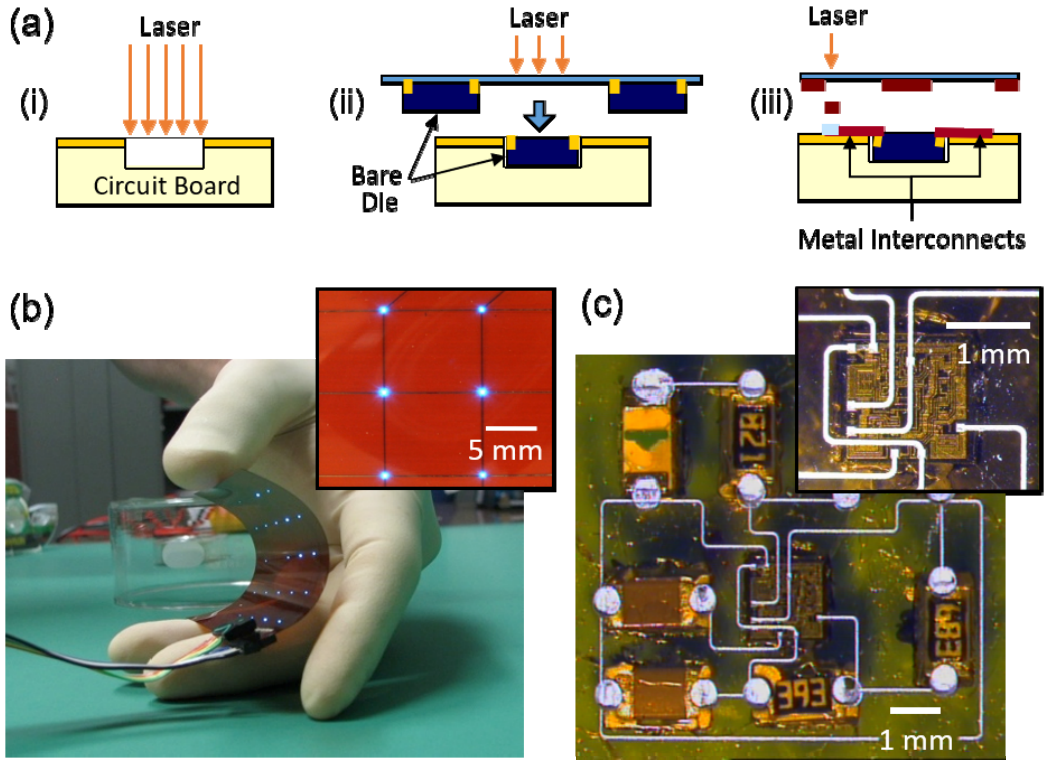
(a)
(i)
Laser
Circuit Board
(ii)
Laser
Bare
Die
(iii)
Laser
Metal Interconnects
(b)
5 mm
(c)
1 mm
1 mm

Figure 26

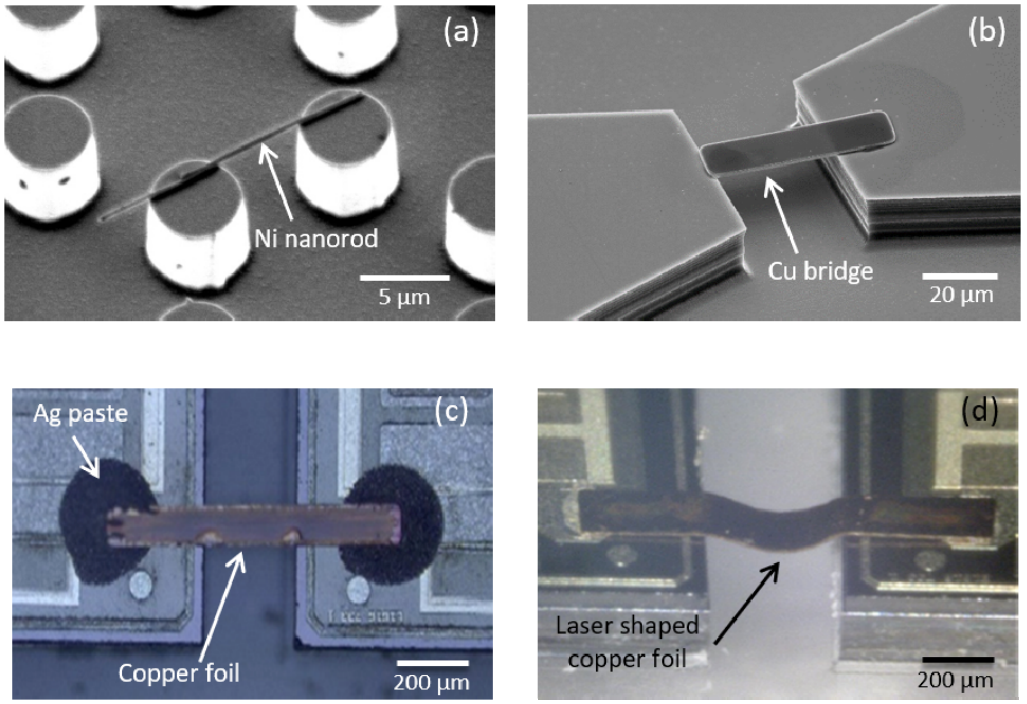
(a)
Ni nanorod
5 µm
(b)
Cu bridge
20 µm
Ag paste
(c)
Copper foil
200 µm
(d)
Laser shaped
copper foil
200 µm

Figure 27

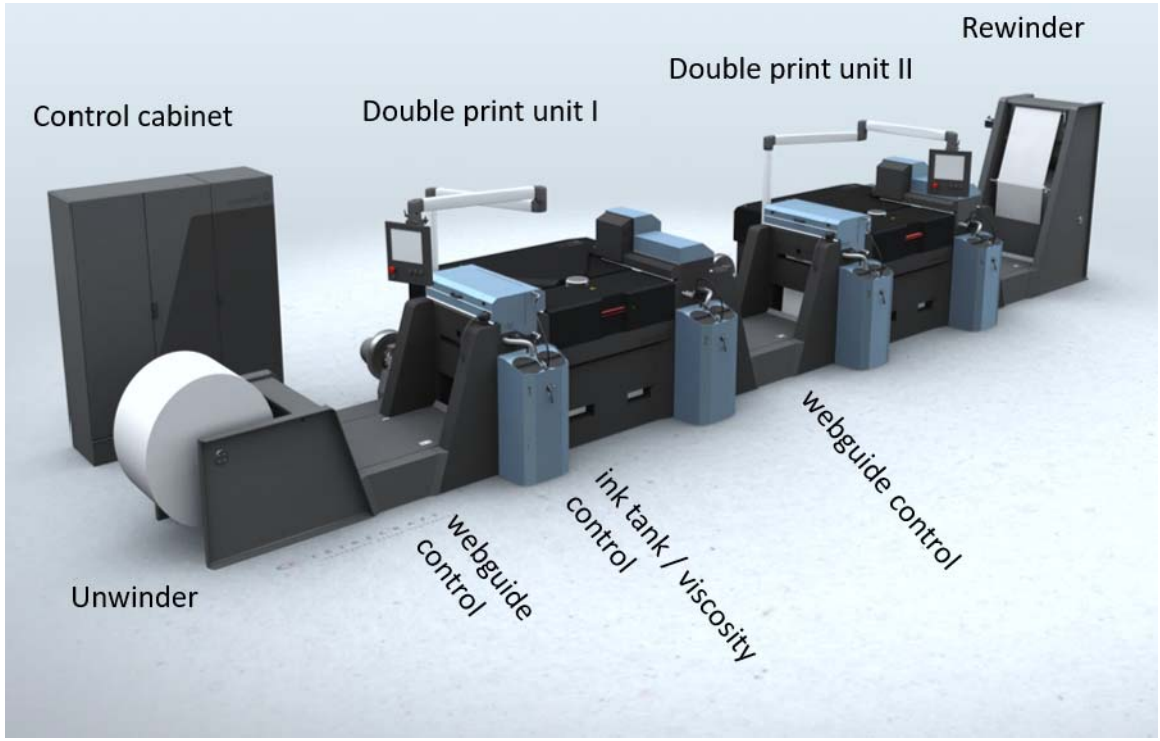
Rewinder
Double print unit II
Control cabinet
Double print unit I
webguide control
ink tank / viscosity control
webguide control
Unwinder